Università degli Studi di Ferrara

DOTTORATO DI RICERCA IN

SCIENZE FARMACEUTICHE

CICLO XXIV

COORDINATORE Prof. Stefano Manfredini

FOCUS ON NANOSTRUCTURED LIPID CARRIERS AND MONOOLEIN AQUEOUS DISPERSIONS

Settore Scientifico Disciplinare CHIM/09

Dottorando
Dott. Ravani Laura

(firma)

Tutore
Prof. Cortesi Rita

(firma)

Cotutore
Dott. Esposito Elisabetta

(firma)

Anni 2009/2011

“Imagination is more important than knowledge.
For knowledge is limited to all we now know and understand,
while imagination embraces the entire world,
and all there ever will be to know and understand.”

Albert Einstein

INDEX OF CONTENTS

1. INTRODUCTION

Modern nanotechnology is a dynamic field, multidisciplinary in nature. Even if the interest in nano-scale products has increased more and more especially in recent years, *Mother Nature* was the first scientist offering nano-materials. For example, Ayurveda, the ancient traditional system of medicine in India, has described and used several “bhasmas”, which were characterized by nanoparticles.

The first definition of modern nanotechnology was explained in 1959 by Richard Feynman at the annual meeting of the American Physical Society: “There’s plenty of room at the bottom”. However, the actual term nanotechnology was defined only in 1974 by Norio Taniguchi from Japan in a paper in which he declared: "Nano-technology mainly consists of the processing of separation, consolidation, and deformation of materials by one atom or by one molecule."

The interest in interface and colloid science together with the development of analytical tools, such as the scanning tunnelling microscope in 1981 and the atomic force microscope in 1986, fed the impetus for modern nanotechnology.

Nowadays, everyone feels the impact of nanotechnology in his life. There is a trend that urges people to revisit many research areas with a nano-view, in order to understand how the same thing can work at nano- level. This phenomenon is revolutionizing pharmaceutical sciences and many drugs are being reformulated for possibilities of delivering as a nanosystem.

1.1 NANOCARRIERS AND DRUG DELIVERY

The concept of nanoparticles and drug targeting was inspired by a visit of Paul Erlich to Karl Maria von Weber's opera "Der Freishütz" [1]. In this opera, a so-called "Freikugeln" or flying bullets, made by calling the spirit of the devil, play a central role. Ehrlich after attending this opera thought that this concept of targeted delivery could greatly improve drug therapy. He called the delivery system that would be used in therapy "Magic Bullets". Notwithstanding Erlich as a medical doctor, with a great interest in bacteriology and immunology, had something like antibodies in mind, this idea lead to the concept of nanoparticles and of drug targeting.

The nanoscopic era of targeted nano-carriers, linked to the concept of "Magic bullet", began with systems proposed in the 1970s and presently is evolving into many exciting and clinically successful products in the 2000s [2].

In fact, especially in recent years, studies have revealed that an increasing number of new molecular entities (NMEs) suffer from undesirable physicochemical and biopharmaceutical properties, even if they have been selected for full scale development thanks to their safety and pharmacological data. Poor water solubility, insufficient bioavailability, high food dependency or fluctuating plasma levels are the main and common problems. Thus, it becomes evident that the development of new drugs alone is not sufficient to ensure progress in drug therapy.

In this field, colloidal carriers have attracted the main interest because they fulfil the characteristics of non-toxicity, sufficient drug-loading capacity, possibility of drug targeting, chemical and physical storage stability, controlled release characteristics and feasibility of scaling up production [3-5].

Among colloidal carriers, nanosized systems have a preeminent position because of their capability in increasing the solubility and therefore the bioavailability of poorly water-soluble substances [6-8].

The field of drug delivery has also attracted the attention of pharmaceutical industry because it offers a strategic tool to expand current drug markets; new delivery technologies could repackage classic drugs, thus providing a competitive edge after the expiration of patents and

preclude completion from generics. Targeted drug systems can convey drugs more effectively and conveniently than those of the past, increase patient compliance, extend the product life cycle, provide product differentiation and reduce healthcare costs [9].

In addition, novel drug delivery systems would offer protection and improvement of the pharmacokinetics of easily degradable molecules, such as peptides and proteins often displaying short half-lives in vivo [10,11]. Therefore, the development of techniques that could selectively deliver drugs to the pathological sites is currently one of the most important areas of drug research. The emergence of nanotechnology is likely to have a significant impact on the drug delivery sector and nanoparticles (NPs) are at the leading edge, with many potential applications in clinical medicine and research [12]. NPs can be correctly considered as the future of drug delivery technology as they have the potential to become useful therapeutic and diagnostic tools in the near future.

Nanometric carriers might differ in composition, materials, application spectrum and drug loading and concerning their different characteristics, they should be employed for various administration routes. Parenteral [13], dermal [14-16], oral [17,18], ocular [19] and pulmonary [20] applications have been widely studied for NPs. In all cases, one of the major advantages that nanotechnology offers is targeted drug delivery to the site of disease. This can be achieved either through passive targeting of drugs to the site of action or by active targeting of the drug (Fig. 1).

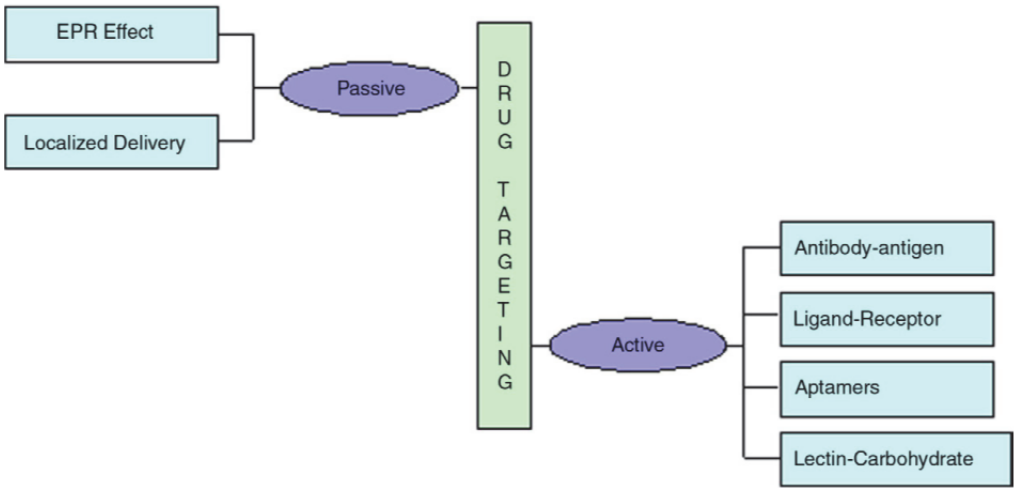

Figure 1. Schematic representation of different drug-targeting approaches.

1.1.1 *Passive tageting*

Passive targeting can be divided in EPR effect and localized delivery.

In the first case, targeting exploits the anatomical differences between normal and diseased tissues to deliver the drugs to the required site. In fact, the physiology of diseased tissues may be altered in a variety of physiological conditions through the enhanced permeability and retention (EPR) effect [21,22]. This phenomenon occurs because tumour vasculature is leaky and as consequence, circulating NPs can accumulate more in the tumour tissues than in normal tissues. Besides exploiting the structural framework of cancerous tissues, the EPR effect is also observed at the site of inflammation.

In the second case, the approach is the direct intratumour delivery of anticancer agents using NPs, which can be used in the treatment of local cancers (prostate, head, neck). Recently it has been demonstrated that transferrin conjugated anticancer drug loaded biodegradable NPs are more effective in demonstrating the antiproliferative effect of the drug than its solution or with unconjugated NPs [23]. The better efficacy of conjugated NPs was due to their greater cellular uptake and sustained intracellular retention than unconjugated NPs or the drug in solution.

1.1.2 *Active targeting*

Active targeting, on the other hand, requires the conjugation of receptor specific ligands that can promote site specific targeting [24,25]. The success of drug targeting depends on the selection of the targeting moiety, which should be abundant, have high affinity and specificity of binding to cell surface receptors and should be well suited to chemical modification by conjugation. The active targeting depends on molecular recognition of the diseased cells by various signature molecules overexpressed at the diseased site either via ligand-receptor, antigen-antibody interactions or by targeting through aptamers.

Conjugating the carrier with a cell or tissue-specific ligand, thereby allowing a preferential accumulation of the drug at the diseased site, can actively target the therapeutic agent.

Thus, the submicron size range of nanosystems as well as the ability to couple/conjugate different targeting ligands offer excellent opportunities to pass the physiological barriers and access different tissues followed by an efficient cellular uptake and intracellular internalization; various nanosystems can be accumulated at higher concentrations than normal drug.

1.2 APPLICATIONS OF NANOPARTICLES IN MEDICINE

The use of NPs in medicine is widespread. Especially in recent years, nanoparticulate systems are used not only for therapeutic applications, but also in diagnostics and imaging fields.

1.2.1 *Therapeutics*

The therapeutic applications of NPs are different, ranging from cancer therapeutics, antimicrobial actions, vaccine delivery, gene delivery and site-specific targeting to avoid the undesirable side effects of the current therapies. Many chemotherapeutic agents such as carboplatin, paclitaxel, doxorubicin and etoposide, etc., have been successfully loaded to NPs and the obtained nanopaticulate systems resulted very potent against various cancers [26].

In addition, NPs with surface-functionalised biomolecules have also been synthesized and are

studied as potential therapeutic agents. Functionalised NPs have also been used for targeted gene silencing or as therapeutics due to their antimicrobial properties.

1.2.2 *Diagnostics*

Nanomaterials and nanotechnology combined with modern instrumentation have the potential to understand biology and medicine at the molecular level with accurate quantification. These analyses can be possible with the aid of a variety of nanomaterials for multiplex diagnostics and thus can offer sensitive, rapid and cost effective solutions for the modern clinical laboratory. NPs are being increasingly applied to molecular diagnostics and several technologies are in development. NPs, such as gold (Au) NPs or quantum dots (QDs), are the most widely used but different other nanotechnology devices, as well as nanobiosensors, are also promising for clinical applications.

1.2.3 *Imaging*

The development of the effective carrier system does not only mean the execution of the delivery, but also the positive confirmation of the site-specific delivery of the drug. Consequently, the ability to track and image the fate of any nanomedicine from the systemic to the subcellular level becomes essential. NPs can be successfully exploited to improve the utility of fluorescent markers for medical imaging and diagnostic purposes.

Although various fluorescent markers are widely used in research and clinical diagnostic applications, current techniques have several disadvantages, such as the requirement of color-matched lasers, fluorescence bleaching and lack of discriminatory capacity of multiple dyes. Fluorescent NPs can greatly overcome these problems, enhancing their use to image tumours and other diseases in vivo.

1.3 ADVANTAGES OF NANOPARTICLES AS DRUG DELIVERY SYSTEMS

NPs are colloidal particles with sizes ranging from 10 to 1000 nm in diameter [27,28]. Many types of NPs can be formulated from diverse materials with the aim to serve as a possible drug delivery vehicle to treat a particular disease.

Drugs can be loaded onto NPs by various methods, such as encapsulation, surface attachment or entrapment [29]. NPs, due to their small size, can efficiently penetrate across barriers through small capillaries into individual cells, thus allowing efficient drug accumulation at target site. Therefore, the unwanted side effects and the toxicity of the therapeutic agent are reduced and the therapeutic efficacy is enhanced [30].

NPs in pharmaceutical and biotechnological sectors are useful for improving the therapeutic index of drugs and provide solutions to future delivery problems for new and upcoming classes of biotechnological products, such as recombinant proteins and oligonucleotides.

Various advantages can be ascribed to NPs:

- Increase of the aqueous solubility of the drug;
- Drug protection from degradation;
- Improvement of drug bioavailability;
- Production of a prolonged release;
- Provision of a targeted delivery of the drug;
- Decrement of drug toxic effects;
- Possibility of an appropriate form for all routes of administration;
- Rapid formulation development.

Thanks to these advantages, NPs can be used to deliver the active therapeutics to the site of action. However, despite widespread applications of these NPs, colloid stability has received little attention. To improve the stability of NPs, polymeric surfactants or other modifiers are often adsorbed or grafted to particles, forming a layer that generates an effective repulsive force between NPs that prevents flocculation.

Concerning the choice of a drug formulation, it should be remembered that no delivery system

per se meets all desired requirements for overall/general problem solution. Moreover, optimal formulations have to be chosen carefully for each drug, according to the feature of the nanocarriers. The aim is to achieve desired drug release profiles in vivo by minimizing side effects.

Concerning the materials used for the production, a possible classification of NPs is between non-lipid and lipid-based nanocarriers. Next paragraphs are dedicated to an analysis of these different systems.

1.4 NON-LIPID COLLOIDAL DRUG CARRIER SYSTEMS

1.4.1 *Polymeric NPs*

Polymeric NPs are nanoparticles prepared from polymers. Depending on the desired properties different types of polymers, in term of chain length, type and number can be used.

Polymers suitable for the preparation of nanoparticles include cellulose derivatives, poly(alkylcyanoacrylates), poly(methylidene malonate), polyorthoesters, polyanhydrides and polyesters such as poly(lactid acid), poly(glycolic acid) and poly (ε-caprolactone) and their copolymers [4]. Various procedures can be applied, such as the coacervation technique, the solvent evaporation [31] and solvent diffusion methods, the interfacial polymerization [32], the denaturation or desolvation of natural proteins or carbohydrates [32], and the degradation by high-shear forces (i.e. by high pressure homogenization [33] or by micro fluidization [34]).

Colloidal particles are either left as aqueous dispersion or they are converted into solid form, usually by lyophilisation [35].

They also exhibit a good potential for surface modification and functionalization with different ligands, moreover they provide excellent pharmacokinetic control and are suitable to encapsulate and deliver a plethora of therapeutic agents. Depending on the type of process used for their preparation, these can be NPs, nanospheres or nanocapsules (Fig. 2).

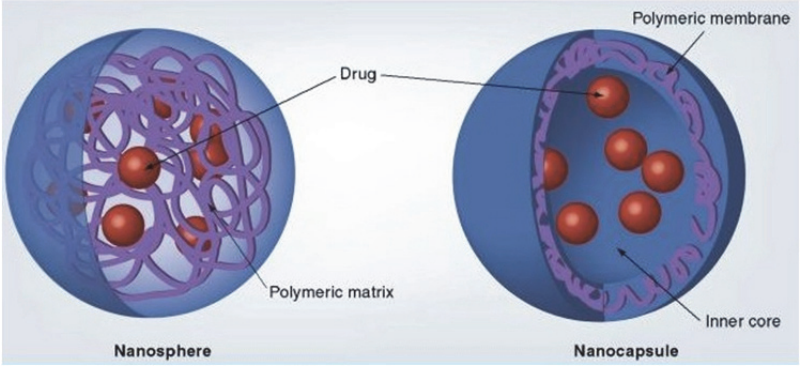

Figure 2. Schematic representation of nanospheres and nanocapsules.

Nanospheres have a matrix-like structure where active compounds can be firmly adsorbed at their surface, entrapped or dissolved in the matrix. Nanocapsules have a polymeric shell and an inner core. In that case, an active substance is usually dissolved in the core but can also be adsorbed at their surface [27,36]. The drug is dissolved, entrapped, encapsulated or attached to a nanoparticle.

The main advantage of using NPs for drug-delivery applications is their small size when taken up by cells, which could allow efficient drug accumulation at the target sites [37]. Biodegradable materials used for the formulation of NPs allow sustained drug release within the target site over a period of days or even weeks. Biodegradable NPs formulated from poly D, L-lactide co-glycolide (PLGA) and polylactide (PLA) have been investigated for sustained drug delivery [36,38].

The main interest of the researchers is to study their intracellular trafficking and determine the parameters that are critical to their efficient cellular uptake and retention. Recently, studies have demonstrated rapid escape of NPs from the endo-lysosomal compartment to the cytoplasmic compartment [38].

Multidrug resistance (MDR) is one of the major causes of treatment failure in cancer therapy, which may be attributed to the decreased accumulation of drug in the tumour site together with the activity of membrane glycoprotein (P-gp)-dependent accelerated drug efflux [39,40]. The performed studies suggest that the use of targeted, antisense agent NPs would be a potential

approach to overcome tumour drug resistance [41].

Another characteristic of NPs is their ability to deliver drugs to the target sites across biological barriers such as the blood-brain barrier (BBB) [42,43]. The brain delivery of a wide variety of drugs, such as antineoplastic and anti-HIV drugs, is markedly hindered because they have great difficulty in crossing the BBB [44]. Thus, by using the nanotechnological approaches, researchers have tried to improve the pharmacokinetics of drugs for the treatment of central nervous system (CNS) diseases. The application of NPs to brain delivery is a promising way to overcome this barrier. Although not fully elucidated, the most likely transport mechanism for these particles is via endocytosis across the endothelial cell lining of the BBB. Moreover, by packaging therapeutic molecules inside a liposome and decorating the surface of the liposome using molecular “Trojan horse” technology, researchers have obtained promising results [45].

Recently many surface-modified NPs have been used to treat various diseases. Surface modification of PLGA NPs with polyethyleneimine (PEI) utilizing a cetyl-derivative was used to improve surface functionalization and aid siRNA delivery [46].

1.4.2 *Ceramic NPs*

The use of inorganic (ceramic) particles for drug delivery, especially biomacromolecular therapeutics, is emerging as a new area [47], because of their ultra-low size (less than 50 nm) and porous nature. It is well documented that smaller-sized drug-carrier systems are more effective in evading the uptake by the RES [48]. Silica and other materials such as alumina, titania, etc., which are highly compatible with biological systems because of their inert nature, are widely being used for the formulation of NPs [49,50].

1.4.3 *Magnetic NPs*

Magnetic NPs (MNPs) are a class of nanoparticle that can be manipulated using magnetic field. Such particles commonly consist of magnetic elements such as iron, nickel and cobalt and their chemical compounds.

MNPs are increasingly being being widely used for biotechnological and biomedical applications. Drug delivery may be benefited by the use of MNPs because these particles can be addressed to a specific site, such as a tumour, thereby reducing the systemic distribution of cytotoxic compounds in vivo, result in effective treatment at lower doses [51].

1.4.4 *Metal-based NPs*

Metal NPs can be synthesized in extremely small sizes of around 50 nm and thus the large surface area provides the ability to carry a relatively higher dose of drugs.

AuNPs are the most commonly used as they offer manifest advantages. It is easy to synthesize a range of sizes of Au NPs by changing few parameters by simple, cheap and reliable methods.

Other common metal-based NPs are silver NPs and amphiphilic TiO_2 nanotube.

Silver NPs have wound-healing properties improving cosmetic appearance in a dose-dependent manner after topical delivery. These NPs also exert positive effects through their antimicrobial properties, reduction in wound inflammation and modulation of fibrogenic cytokines [52].

Amphiphilic TiO_2 nanotube arrays can serve as an actively controllable drug delivery system by utilising the photocatalytic ability of TiO_2 [53].

1.4.5 *Polymeric micelles*

Polymeric micelles represent a class of colloidal system formed of block copolymers consisting of hydrophilic and hydrophobic monomer units [54]. These micelles are composed of a core of hydrophobic blocks stabilized by a corona of hydrophilic polymeric chains. Although a variety of hydrophilic polymers can be used, in majority of cases, PEG blocks with a molecular weight ranging from 1 to 15 kDa are used as corona-forming blocks and the length of a hydrophobic core-forming block is close or somewhat lower than that of a hydrophilic block. Enhancing drugs' solubility using micelle-forming surfactants results in increased water solubility of a poorly soluble drug. They also improve drugs' bioavailability by enhancing their permeability across physiological barriers. Thus, they bring about substantial changes in drug biodistribution.

1.4.6 *Dendrimers*

Dendrimers derive their name from the Greek word “dendra”, meaning reminiscent of a tree. They are polymeric molecules composed of multiple perfectly branched monomers that emanate radially from a central core. Though many biological applications use dendrimers based on polymers, such as polyamidoamines (PAMAMs), polyamines, polyamides (polypeptides), poly (aryl ethers), polyesters, carbohydrates and DNA, in most cases PAMAM dendrimers are used [55,56].

1.5 LIPID-BASED NANOSYSTEMS

Although within the remit of the above mentioned nanoscience initiatives, lipid-based nanosystems such as nanoemulsions, lipid-core micelles, small unilamellar vesicles, solid lipid nanoparticles, nanostructured lipid carriers, colloidal liquid crystalline structures, cubosomes and variations thereof, have long been in existence and some have long been improving patient's lives. Indeed, lipid-based nano-formulations are among the most attractive candidates for improving drug solubility and for site-specific targeting following parenteral administration.

In recent years, a particular attention has been focused on new generations of lipid nanoparticles such as nanostructured lipid carriers and monoolein aqueous dispersions, derived from the mesophases originated from the system monoolein/water/poloxamer. These nanoparticles have been analysed as possible drug delivery systems and are the object of the discussion of this doctorate project.

1.5.1 *Solid Lipid Nanoparticles (SLN) and Nanostructured Lipid Carriers (NLC)*

Solid lipid NPs (SLN) are a colloidal carrier system for controlled drug delivery developed at the beginning of the 1990s as an alternative carrier system to emulsions, liposomes and polymeric NPs [12]. These particles are delivery systems where the nanodispersed phase has a solid matrix of crystalline solid lipids (i.e. lipids solid both at room and at body temperature) and is stabilized by surfactant(s). SLN can be formulated by using highly purified triglycerides, complex glyceride mixtures or even waxes.

In comparison with other particulate carriers, SLN have many advantages for drug delivery, such as good tolerability, biodegradability [57], a high bioavailability by ocular administration [58] and a targeting effect on the brain [59]. SLN have been developed and investigated for parenteral, pulmonary and dermal application routes [60-62].

In recent years, the study of SLN has markedly increased, especially with the method of high pressure homogenization.

Because of their small sizes, SLN may be injected intravenously and used to target drugs to

particular organs. The particles, together with all intravenously injected and colloidal particulates, are cleared from the circulation by the liver and spleen. In tumour tissues, drugs can be targeted by PEG-coated polymeric NPs (stealth NPs) that helps in escaping from reticuloendothelial system (RES) [63]. This effect may be also achieved using block polyoxyethylene polypropylene copolymers like Pluronic F188 in which the hydrophobic portion of the molecule forms the NP matrix while the water soluble polyoxyethylene block forms a hydrophilic coating on the particle. Stealth SLN increases the tumour accumulation, antibacterial activity of antiparasitic and antifungal drugs, and allows brain delivery of anticancer drugs not capable of crossing the BBB [64].

Clear advantages of SLN include the use of physiological well tolerable lipids [65], the avoidance of organic solvents in some preparation processes, a wide potential application routes (dermal, oral, intravenous) and the rapid and effective preparation process allowing the possibility of large scale production [66].

Common disadvantages of SLN include particle aggregation, particle growth, unpredictable gelation tendency, unexpected dynamics of polymorphic transition, burst drug release and consequently low incorporation capacities due to the crystalline structure of the solid lipid [3,67,68].

This last mentioned drawback can be explained by the crystallization process to which SLN are subjected during the cooling process, causing a transition of lipids in higher energy modification α and β'. Triglycerides are known to crystallize mainly in three polymorphic forms which transform monotrophically from α via β′ to β [69].

During storage, SLN triglycerides are subjected to a shift into the low energy and more ordered β modification. The formed high degree of order causes a reduction of imperfections in the crystal lattice and consequently, the drug expulsion (Fig. 3).

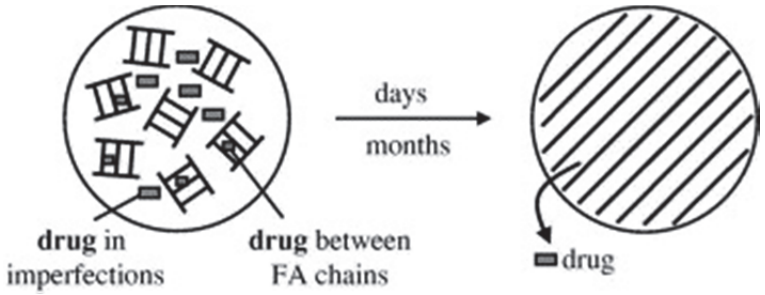

Figure 3. Mechanism of drug expulsion during storage of SLN dispersions; transition to highly ordered lipid crystal [15]

To obtain a sufficiently high drug load, the creation of a less ordered solid lipid matrix is necessary. In this case, the drug can dispose itself between the chains of the fatty acids or between the lipid layers and the imperfections. When SLN are formulated with mono acid highly purified glyceride, such as Tristearin, the drug loading is limited and very frequently drug expulsion occurs within hours or few days due to the formation of the perfect β modification [70]. The second generation of SLN, avoiding some disadvantages of classic SLN, is represented by Nanostructured Lipid Carriers (NLC), which are composed of a solid lipid matrix with a certain content of a liquid lipid phase [71].

Liquid lipids are able to better disperse lipophilic drugs than solid lipids. The liquid lipids form droplets within the solid lipid particles matrix, providing a high incorporation capacity and a control of drug release (Fig 4).

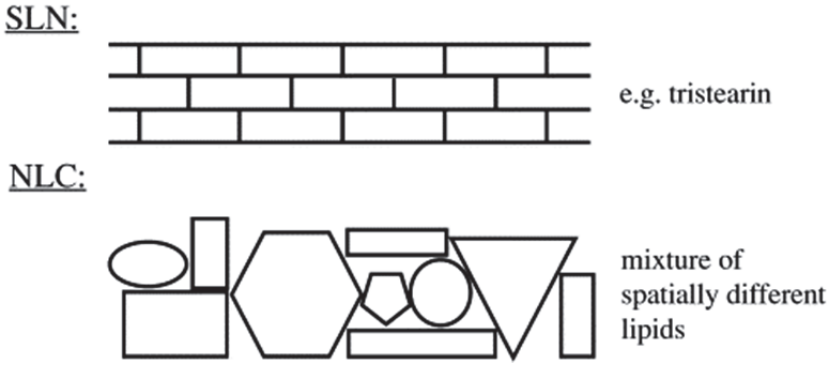

Figure 4. Perfect crystal in SLN comparable with a brick wall and structure with imperfections due to spacially very different molecules in NLC [15]

The use of different lipid molecules (solid and liquid at room temperature) in the preparation of NLC allow the building of the matrix of the wall with different types of stones leaving enough imperfections to accommodate the drugs. In this way the problem of the formation of a perfect crystal, that seems a wall made of bricks, is overcome.

Especially, as schematized in figure 5, three types of NLC can be produced:

1. Imperfect type
2. Amorphous type
3. Multiple type

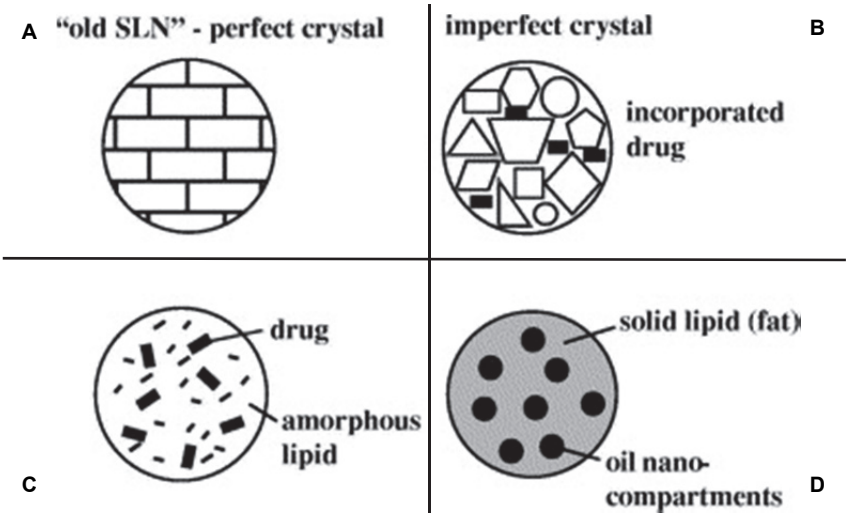

Figure 5. Different types of NLC compared to the ordered matrix of SLN (**A**); NLC types: imperfect type (**B**), amorphous type (**C**), multiple type (**D**) [15]

The process of drug loading in SLN is due to the formation of lipid crystals. The formation of a perfect crystal causes drug expulsion. Thus, by avoiding crystallization and creating more imperfections in the crystal the drug loading is higher (Fig 5A).

NLC are solid but not crystalline particles. By using special mixtures of solid lipids and liquid lipids (e.g. isopropylmyristate, hydroxyloctacosanylhydroxylstearate) the obtained nanoparticles become solid after cooling but they don't crystallize (Fig. 5C).

From the production point of view, a too high concentration of drug in the molten lipidic phase could lead to an immediate drug expulsion during the cooling process or create a dilution in the cold water. Based on these supposes, the multiple type of NLC was developed (Fig. 5D).
In this last structure, the solid matrix of the lipid nanoparticle contains tiny liquid nano-compartments of oil, in which the drug solubility is higher. It follows an increase in the total drug loading capacity. The oil nano-compartments are all surrounded by solid matrix, allowing, also in this case, a prolonged drug release.

1.5.2 *Monoolein aqueous dispersions (MAD)*

Surfactants, lipids and polymer molecules that have both polar and nonpolar components are called amphiphilic. The hydrophobic effect drives amphiphilic molecules into polar solvents to spontaneously self-assemble into a rich array to thermodynamically stable lyotropic liquid crystalline phases with characteristic lengths on the nanometer scale.
The content of water or other solvent molecules changes the self-assembled structures.
A generic progression of phases, going from low to high amphiphile concentration, is:

1. Discontinuous cubic phase (micellar cubic phase)
2. Hexagonal phase (hexagonal columnar phase) (middle phase)
3. Lamellar phase
4. Bicontinuous cubic phase
5. Reverse hexagonal columnar phase
6. Inverse cubic phase (Inverse micellar phase)

At very low amphiphile concentration, the molecules will be dispersed randomly without any ordering. At slightly higher (but still low) concentration, amphiphilic molecules will spontaneously assemble into micelles or vesicles. This is done so as to 'hide' the hydrophobic tail of the amphiphile inside the micelle core, exposing a hydrophilic (water-soluble) surface to aqueous solution. These spherical objects do not order themselves in solution and are denoted by the symbol I_1. This is a highly viscous, optically isotropic phase in which the micelles are arranges

on a cubic lattice.

At higher amphiphile concentrations the micelles fuse to form cylindrical aggregates of indefinite length, and these cylinders are arranged on a long-ranged hexagonal lattice. This lyotropic liquid crystalline phase is known as the 'hexagonal phase', or more specifically the 'normal topology' hexagonal phase and is generally denoted by the symbol H_I.

At higher concentrations of amphiphile the 'lamellar phase' is formed. This phase is denoted by the symbol L_α and consists of amphiphilic molecules arranged in bilayer sheets separated by layers of water. Each bilayer is a prototype of the arrangement of lipids in cell membranes. For most amphiphiles that consist of a single hydrocarbon chain, one or more phases having complex architectures are formed at concentrations that are intermediate between those required to form a hexagonal phase and those that lead to the formation of a lamellar phase. Often this intermediate phase is a bicontinuous cubic phase (Fig. 6).

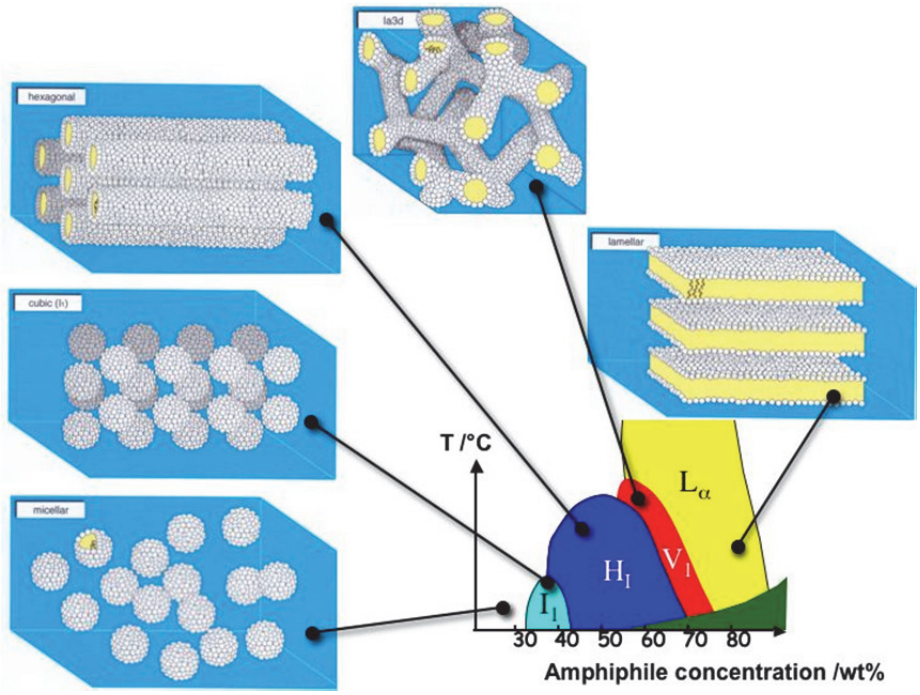

Figure 6. Schematic showing the aggregation of amphiphiles into micelles and then into lyotropic liquid crystalline phases as a function of amphiphile concentration and of temperature.

The lamellar phase is the basis of the planar lipid bilayer of the vesicle structure, while the bicontinuous phase consists of a single continuous curved bilayer that forms a complex network with 3D cubic symmetry and continuous water channels. Cubic phase surface could assume different curvatures: *Ia3d* (gyroid surface, G), Pn3m (diamond surface, D), Im3m (primitive surface, P) [72] (Fig. 7).

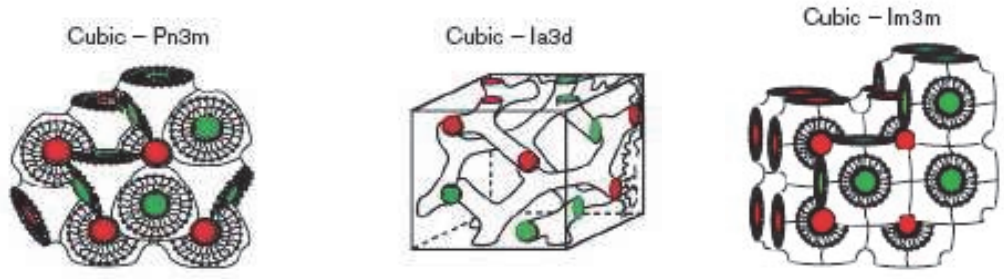

Fig.7 Cubic phase surface curvatures. Individual lipids are shown as small circles with adjoined curved lines, representing the polar headgroup and hydrophobic acyl chain respectively. The red and green regions represent water. [72]

Monoglycerides are polar lipids with poor water solubility that exhibit aqueous phase behaviour, reflecting their structural similarity to nonionic surfactants. The most studied, among aqueous monoglycerides systems, is that formed by monoolein, the unsaturated C_{18} monoglyceride.

As shown in figure 6, the formation of cubic phases is often localized in a narrow region between lamellar and hexagonal liquid crystalline phases. Differently, the monoolein-water system is the only that possesses a cubic phase region spanning large compositional and temperature ranges (Fig. 8).

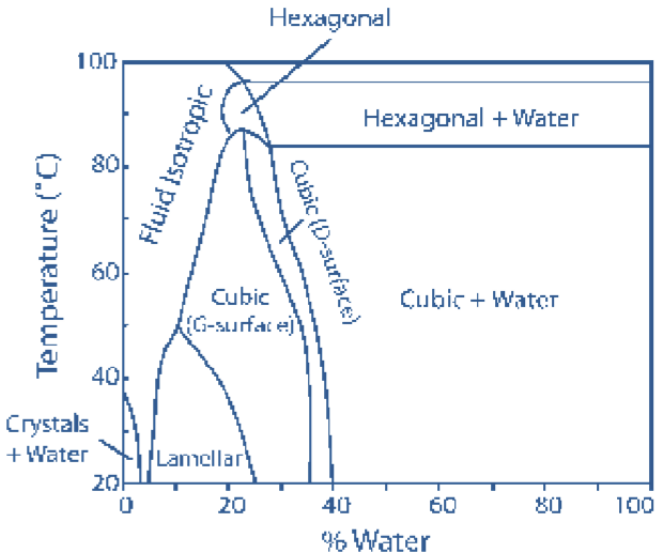

Fig.8 Aqueous phase behaviour of the monoolein-water system, evidencing the existence of two cubic phases [73].

In the cubic phase, the minimal surface is formed by the self assembled bilayer that occurs as the hydrophobic or hydrophilic portions of the surfactants molecules line up to minimize their interaction with their opposite. The three structures, P-, D- and G- surfaces, are all bicontinuous (i.e., they divide space into two continuous but nonintersecting regions); in the case of cubic phases, two separate regions of hydrophilic material (water channels) are formed.

Cubic liquid crystals are transparent, isotropic viscous phases and physically stable in excess water [74-77]. Since cubic phases are characterized by high viscosity, they are difficult to administrate by parenteral routes. For this reason some researchers have developed the emulsification of cubic lipid phases in water resulting in the production of cubosomes that can be defined as nanoparticulate disperse systems characterized by high biocompatibility and bioadhesivity [78,79].

Dispersed particles of bicontinuous cubic phases were first observed during studies of fat digestion that simulated stomach contents by combining oil with lipase and bile salts [80].

One of the first published instances of the word “cubosomes” appears in a review written by Larsson [81] in which the author discussed about implications of bicontinuous cubic phases to

biological membranes. Cubosomes structures, such as bulk cubic phases, are critical elements of some biological processes and for example, occur naturally in bacterial cells [82].

The formation of cubosomes is possible in binary and ternary systems with a sufficiently large miscibility gap between the cubic phase and the solvent. Colloidal stabilization of cubosomes is good when Poloxamer 407 is used to provide steric stabilization against aggregation and coalescence, but other suitable polymers can be used as well [83].

Concerning their applications in pharmaceutical and biotechnological fields, cubosomes have been proposed as a delivery system able to provide both a solubilization benefit (increased drug payload) and a system for controlled or sustained release [84]. In particular, cubosomes show the ability to solubilize hydrophobic, hydrophilic and amphiphilic molecules (Fig. 9) and a high biodegradability by simple enzyme action [85].

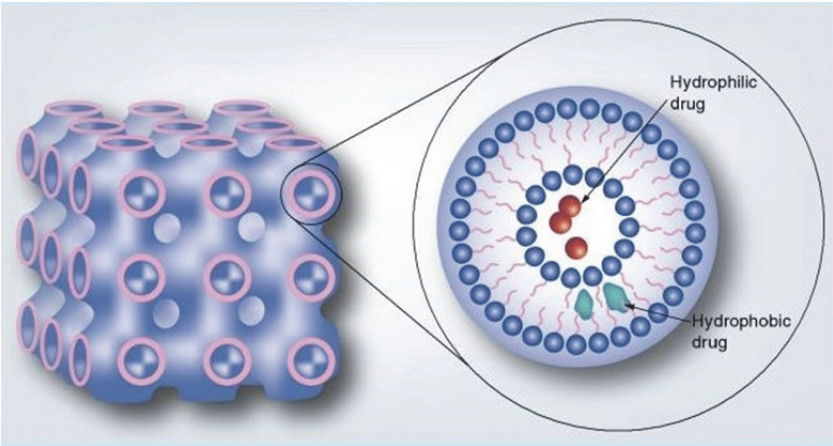

Fig.9 Cubosome exhibiting its cavernous internal and cubic structure and its membrane composition with different drug-loading modalities.

Compared to liposomes or vesicles, cubosomes possess much higher bilayer area-to-particle volume ratios as well as higher viscous resistance to rupture [84]. Because of their properties, these versatile delivery systems can be administrable by different routes (such as orally,

parenterally, or percutaneously) [86].

The methods of preparation [87,88] and the inner structure [89,90] of cubosomes have been widely studied. Nevertheless, drug release from these systems has been poorly investigated [91].

1.6 AIMS AND ORGANIZATION OF THE THESIS

In recent years, the field of lipid nanostructures shows a growing interest from the pharmaceutical technology research groups world wide. In particular, Solid Lipid Nanoparticles (SLN), Nanostructured Lipid Carriers (NLC) and Monoolein Aqueous Dispersions (MAD) have been proposed as new carrier systems for many applications.

In this thesis different NLC, SLN or MAD formulations were developed as drug delivery systems specifically for antiparkinson or antimycotic drugs, in order to prolong their action and reduce the side effects. The thesis consists of seven main chapters.

The *first chapter* contains an introduction on nanoparticulate systems, focusing the attention on properties and the differences existing between non-lipid and lipid vectors.

The *second and third chapters* describe materials and methods used in this work respectively.

From chapter four to six, the applications of lipidic nanosystems as delivery vectors are analysed in order to improve the bioavailability and controlled release of incorporated drugs.

In *chapter four,* NLC and MAD formulations containing Bromocriptine are described and compared. In particular, characterization of morphology, size, inner structure and drug distribution of nanosystems have been made. Finally, *in vitro* and *in vivo* analyses have been performed.

In *chapter five*, four different new L-dopa derivatives are studied as model drugs for NLC and SLN formulations. After the inclusion in nanoparticulate systems, the derivatives have been analysed in dimensions, morphology, L-dopa release by time and *in vitro* release tests.

In *chapter six*, NLC and MAD are described as possible drug delivery systems for Clotrimazole, an antimycotic agent. After dimensional, morphology and stability studies, NLC and MAD have been viscosized in order to facilitate a mucosal application and delivery of the drug. The obtained gels have been analysed through rheological and calorimetric assays, then cytotoxic and anticandidal activities have been tested.

The *last chapter* contains the conclusions of the work considering the obtained results.

2. MATERIALS

The materials used in this work are only partially composed of individual chemical substances and their composition may differ according to the manufacturer. Therefore, the physicochemical properties and the producer details for all the materials used are given in the present section.

2.1 SOLID LIPIDS

Lipids that are solid at room temperature are saturated. The solid lipids used in this work are well tolerated, accepted for human use and they are characterized by *in vivo* biodegradability.

2.1.1 *Tristearin*

Tristearin is also known as glycerol tristearate, stearin, glyceryl tristearate, trioctadecanoin, hardened oil, stearin, tri-, spezialfett 118, stearic triglyceride.

His molecular formula is $C_{57}H_{110}O_6$ and his molecular weight is 891.4797.

Tristearin is the primary fat in beef. It is a triglyceride, a molecule of glycerine has reacted with three molecules of the fatty acid stearic acid. It is a saturated fat, solid at room temperature.

Tristearin was provided by Fluka (Buchs, Switzerland).

2.2 LIQUID LIPIDS (OILS)

Liquid lipids at room temperature are unsaturated. The oils used in this work are well tolerated and accepted for human use.

2.2.1 *Miglyol ® 812*

It is a liquid lipid at room temperature, having a density between 0.945 and 955 g/cm^3. This oil consists of medium chain triacylglycerols (C8-C10) (caprylic/capric triglycerides) and it is virtually colourless and of neutral odour and taste. It is used as skin oil and as dissolution medium for many substances. It is soluble in hexane, toluene, diethyl ether, ethyl acetate, acetone, isopropanol and ethanol 96%. It is miscible in all ratios with paraffin hydrocarbons and natural oils. The acid value is 0.1 mg KOH/g and the saponification value is between 325-345 mg KOH/g [92].

Miglyol 812 was purchased from Eigenmann & Veronelli (Rho, Milano, Italy).

2.2.2 *Monoolein*

Synonyms of monoolein are RYLO MG 19, Arlacel™ 186, D-L-alpha-monoolein, delta 9 cis monoolein, glycerol-1-monooleate, glycerol alpha-monooleate, glycerol monooleate, glyceryl monooleate, glyceryl cis-9-octadecenoate. His molecular formula is $C_{21}H_{40}O_4$ and his molecular weight is 356.54.

Monoolein is a monoacylglycerol with 9-cis-octadecenoic acid at the sn-1 position of glycerol. The mesophase propensities and structure of monoolein dispersed in water are of interest in a number of areas ranging from controlled uptake and release to cosmetic, food and pharmaceutical formulations.

RYLO MG 19 was purchased from Danisco Cultor (Grindsted, Denmark).

2.3 EMULSIFYING AGENTS

The International Union of Pure and Applied Chemistry (IUPAC) defines the properties of an emulsifying agent as a surfactant, which is positively adsorbed at interfaces and lowers the interfacial tension [93]. Surfactants have amphiphilic structures and are able to form micelles. Some polymers (i.e. poloxamers) can function in the same manner, if they have a sufficient

surface activity.

2.3.1 *Pluronic F68*

Lutrol F 68, (oxirane, methyl-, polymer with oxirane (75;30)) or poloxamer 188 is a water-soluble non-ionic polyoxyethylene-polyoxypropylene polymer. Its value in the HLB system (Hydrophile - Lipophile Balance) amounts to 29. The stabilizer and solution enhancer does not cause toxic reactions after parenteral, dermal or peroral administration [92]. Moreover, the transition time of gut is not influenced in GIT of rats [92]. Tenside micelles are not likely to occur in the concentration range of poloxamer used in this study.

Poloxamer 188 arranges only at higher concentrations and temperatures in form of micellar structures [94,95].

Lutrol F 68, was a purchased from BASF ChemTrade GmbH (Burgbernheim, Germany).

2.3.2 *Pluronic F127*

Pluronic F127 (PEO_{98}-POP_{67}-PEO_{98}) or poloxamer 407, is a hydrophilic non-ionic surfactant of the more general class of copolymers known as poloxamers. Poloxamer 407 is a triblock copolymer consisting of a central hydrophobic block of polypropylene glycol flanked by two hydrophilic blocks of polyethylene glycol. The approximate length of the two PEG blocks is 101 repeat units while the approximate length of the propylene-glycol block is 56 repeat units.

Poloxamer 407 shows thermo-reversible properties. Its fluid state at room temperature facilitates the administration while its gel state above sol-gel transition temperature promotes prolonged release of pharmacological agents. Pharmaceutical evaluation consists in determining the rheological behaviour (flow curve or oscillatory studies), sol-gel transition temperature, in vitro drug release using either synthetic or physiological membrane and (bio)adhesion characteristics. Poloxamer 407 formulations led to enhanced solubilisation of poorly water-soluble drugs and prolonged release profile for many galenic applications (e.g., oral, rectal, topical, ophthalmic, nasal and injectable preparations) but did not clearly show

relevant advantages when used alone. Combination with other excipients like poloxamer 188 or mucoadhesive polymers (i.e. xanthan gum, sodium alginate, methyl cellulose and others) promotes poloxamer 407 action by optimising sol-gel transition temperature or increasing bioadhesive properties. Inclusion of liposomes or micro(nano)particles in poloxamer 407 formulations offers interesting prospects, as well [96].

Pluronic F127 was obtained from BASF (Ludwigshafen, Germany).

2.3.3 *Soybean phosphatidylcholine*

Phosphatidylcholine (PC) is a phospholipid that incorporates choline as a head group. Phosphatidylcholine is a major constituent of cell membranes and is more commonly found in the exoplasmic or outer leaflet of a cell membrane. It is thought to be transported between membranes within the cell by phosphatidylcholine transfer protein (PCTP) [97].

Phosphatidylcholines are composed of a choline head group and glycerophosphoric acid with a variety of fatty acids, one being a saturated fatty acids and one being an unsaturated fatty acid.

The phospholipids are such a major component of lecithin that in some contexts the terms are sometimes used as synonyms. However, lecithin extract consists of a mixture of phosphatidylcholine and other compounds.

In pharmaceutical applications it acts as a wetting and stabilizing agent, it helps in emulsifications and encapsulation and it is a good dispersing agent. It can be used in manufacture of intravenous fat infusions and for therapeutic use.

Phospholipon® 90G (P 90G) is a highly purified soybean lecithin that contains at least 90% phosphatidylcholine. P 90G was supplied by Rhône-Poulenc-Rorer (Germany).

2.3.4 *Labrasol*

Labrasol ® or caprylocaproyl macrogol-8 glycerides is a non-ionic water dispersible surfactant composed of well-characterised polyethylene glycol (PEG) esters, a small glyceride fraction and free PEG.

It is able to self-emulsify on contact with aqueous media forming a fine dispersion or to act as solubilizer and wetting agent. It is also used as bioavailability enhancer.

It is obtained from coconut oil and has very low toxicity with an LD50 of 22g/kg for rats.

Labrasol® was purchased form Gattefossé (France).

2.4 WATER

The water used in all experiments was purified water by reverse osmosis and was obtained from a Milli Q Plus system (Millipore®, USA).

2.5 OTHER MATERIALS

FL-70 was used for SdFFF analyses. FL-70 is a detergent composed of water 88.8%, triethanolamine oleate 3.8%, sodium carbonate 2.7%, Alcohols, C12-14-secondary, ethoxylated 1.8%, Tetrasodium ethylenediaminetetraacetate 1.4%, Polyethylene glycol 0.9%, Sodium oleate 0.5%, Sodium bicarbonate 0.1%.

FL-70 was obtained from Fisher Scientific (Fair Lawn, NJ, USA).

2.6 DRUGS

2.6.1 *Bromocriptine*

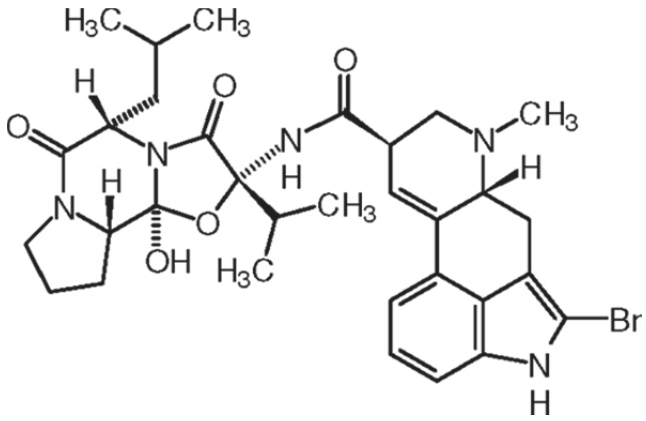

Figure 10. Chemical structure of Bromocriptine.

Bromocriptine (Fig. 10), an ergoline derivative, is a dopamine agonist that is used in the treatment of pituitary tumours, Parkinson's disease (PD), hyperprolactinemia, neuroleptic malignant syndrome and type 2 diabetes.

Bromocriptine is a dopamine receptor agonist, which activates postsynaptic dopamine receptors. The dopaminergic neurons in the tubero-infundibular process modulate the secretion of prolactin from the anterior pituitary by secreting a prolactin inhibitory factor (thought to be dopamine); in the corpus striatum the dopaminergic neurons are involved in the control of motor function. Clinically, Bromocriptine significantly reduces plasma levels of prolactin in patients with physiologically elevated prolactin as well as in patients with hyperprolactinemia. The inhibition of physiological lactation as well as galactorrhea in pathological hyperprolactinemic states is obtained at dose levels that do not affect secretion of other tropic hormones from the anterior pituitary. Experiments have demonstrated that Bromocriptine induces long lasting stereotyped behaviour in rodents and turning behaviour in rats having unilateral lesions in the substantia nigra. These actions, characteristic of those produced by dopamine, are inhibited by dopamine

antagonists and suggest a direct action of Bromocriptine on striatal dopamine receptors.

Bromocriptine is a nonhormonal, nonestrogenic agent that inhibits the secretion of prolactin in humans, with little or no effect on other pituitary hormones, except in patients with acromegaly, where it lowers elevated blood levels of growth hormone in the majority of patients.

In about 75% of cases of amenorrhea and galactorrhea, Bromocriptine therapy suppresses the galactorrhea completely, or almost completely, and reinitiates normal ovulatory menstrual cycles.

Galactorrhea may take longer to control depending on the degree of stimulation of the mammary tissue prior to therapy. At least a 75% reduction in secretion is usually observed after 8-12 weeks. Some patients may fail to respond even after 12 months of therapy.

In many acromegalic patients, Bromocriptine produces a prompt and sustained reduction in circulating levels of serum growth hormone.

Bromocriptine produces its therapeutic effect in the treatment of Parkinson's disease, a clinical condition characterized by a progressive deficiency in dopamine synthesis in the substantia nigra, by directly stimulating the dopamine receptors in the corpus striatum.

The pharmacokinetics and metabolism of Bromocriptine in human subjects were studied with the help of radioactively labelled drug. Twenty-eight percent of an oral dose was absorbed from the gastrointestinal tract. The blood levels following a 2.5 mg dose were in the range of 2-3 ng equivalents/mL. Plasma levels were in the range of 4-6 ng equivalents/mL indicating that the red blood cells did not contain appreciable amounts of drug and/or metabolites. In vitro experiments showed that the drug was 90%-96% bound to serum albumin.

Bromocriptine was completely metabolized prior to excretion. The major route of excretion of absorbed drug was via the bile. Only 2.5%-5.5% of the dose was excreted in the urine. Almost all (84.6%) of the administered dose was excreted in the faeces in 120 hours.

Bromocriptine mesylate, 2-Bromo-∝-ergocriptine methansulfonate salt (BC), amphetamine and 6-hydroxydopamine (6-OHDA) were purchased from Sigma Chemical Company (St Louis, MO, USA).

2.6.2 *L-DOPA derivatives*

L-Dopa (LD) is a direct precursor of dopamine (DA), which is deficient in the brains of patients suffering from Parkinson's disease (PD). Although LD is the treatment of choice, its metabolism generates a variety of free radicals that contribute to the progression of the disease, increasing the loss of nigrostriatal dopaminergic neurons [98]. In particular, it was demonstrated that systemic administration of LD in the rat increases the production of free radicals in the substantia nigra [99]; in addition, cell-death, both of the necrotic and the apoptotic types, was observed in neuronal and non-neuronal cell cultures treated with LD [100].

Experimental studies have also shown that LD alters cellular energy metabolism, probably by inducing oxidative damage of specific enzymes of the mitochondrial respiratory chain [101].

Miller et al. confirmed that catecholamines, including the neurotransmitter DA and its biochemical precursor LD, are subjected to autoxidation [102]. This process, which is accelerated in the presence of pro-oxidative transition metals, such as iron and copper, is enhanced by the presence of neuromelanin in dopaminergic neurons, due to its reported ability to accumulate iron and consequently acting through promotion of Fenton and Haber-Weiss reactions with production of potentially cytotoxic reactive oxygen species (ROS) [103].

These ROS have been hypothesized to play a role in the progressive and selective loss of nigrostriatal dopaminergic neurons that occurs in aging and in neurodegenerative disorders such as PD and Alzheimer disease [104]. This hypothesis suggests that inhibition of catecholamine autoxidation and the scavenging of ROS produced by such oxidation are important strategies for preventing or slowing down the progression of aging and aged-related neurodegenerative disorders. It is well known that low molecular weight natural free radical scavengers such as glutathione, vitamin E, carnosine and ascorbic acid have been extensively studied as useful neuroprotective agents [105,106].

However, the use of these natural antioxidants as therapeutic agents is limited, mainly due to the marginal efficiency of these scavengers to cross the blood-brain barrier. Conversely, antioxidant (e.g. ascorbate or R-tocopherol) interventions that do not affect iron accumulation

have shown only limited efficacy in lowering oxidant stress in the aging brain [107,108]. Thus new, nontoxic, therapeutic agents that improve both alterations in iron and antioxidant status may be needed.

Starting from these data, the synthetic study, performed by Professor Di Stefano group at the University of Chieti, was focused on providing molecular combinations obtained joining an antioxidant molecule with a therapeutic compound also able to generate a targeted antioxidant. These compounds could permit a targeted delivery of the antioxidant moiety directly to specific groups of cells, including neurons, where cellular stress is associated with pathology, including that associated with normal aging and neurodegenerative disorders [109]. With regard to PD, an analysis of the literature reveals that despite antioxidant therapy having been explored in a number of pathological conditions, the joining of an antioxidant molecule to a group capable of targeting a specific population of dying cells has not so far been considered.

In addition, another strategy adopted for the production of prodrug forms was the synthesis of dimeric derivatives, in which two identical structural molecules are linked together through a spacer and after administration are metabolized into their identical agents [110-113].

Derivative A (Der-A)

Der-A (Fig. 11) was synthesized through the interaction of 3,4-diacetyloxy-L-dopa methyl ester hydrochloride 3 with caffeic acid 4 [114-116]. Preliminary *in vitro* and *in vivo* studies evaluated chemical and enzymatic properties of this molecule and showed that Der-A is stable in aqueous solutions and improves the release of LD and dopamine in the brain [117].

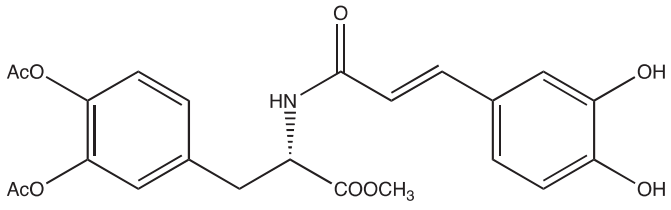

Figure 11. Chemical structure of Der-A.

Derivatives B (Der-B) and C (Der-C)

For the synthesis of Der-B and Der-C novel molecular combinations were proposed in which dopamine is linked to antioxidant and iron-chelating agents such as (R)-R-Lipoic acid.

These multifunctional codrugs, containing antioxidant molecules whose benefits have been demonstrated in several neurodegenerative disorders, could represent useful dopaminergic agents devoid of the pro-oxidant effects associated with the presence of the catecholic moiety [118].

The amides were synthesized by the classical methods through the interaction of (*R*)-R-lipoic acid with 2-(3,4-diacetoxy)-phenylethylamine (Fig. 12), and 2-(3,4- dihydroxy)-phenylethylamine (Fig. 13), respectively.

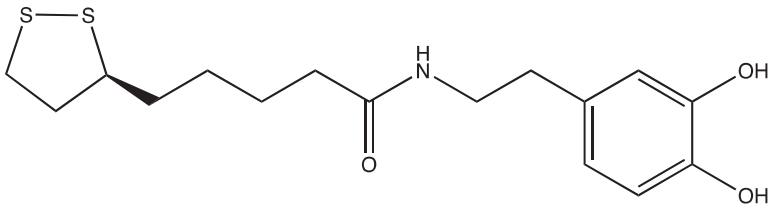

Figure 12. Chemical structure of Der-B.

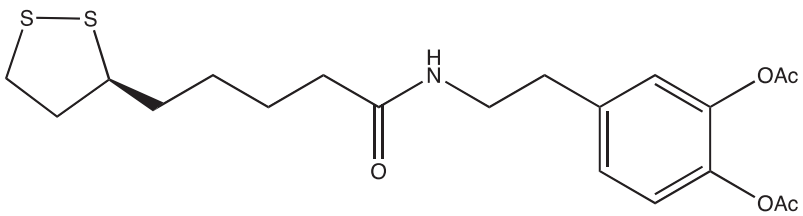

Figure 13. Chemical structure of Der-C.

Derivative D (Der-D)

Der-D (Fig. 14) was synthetized protecting all the three sensitive centres of LD (the carboxy function, the amino group and the catechol system) and following the classical methods through the interaction of 3,4-diacetyloxy-l-phenylalanine methyl ester hydrochloride with the respective dicarboxylic acid dichloride [119]. Der-D showed chemical stability in aqueous, acid and physiological solutions. Furthermore, *in vitro* studies showed a slow release of LD from Der-D in human and rat plasma.

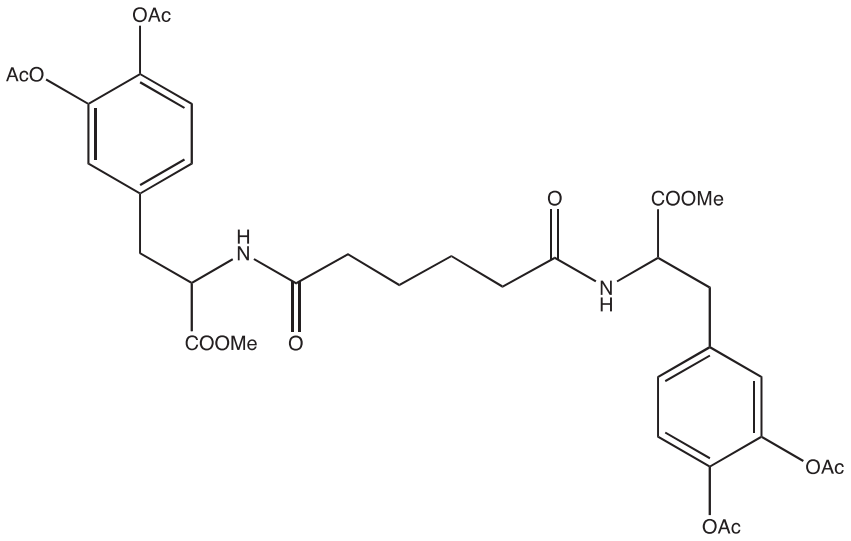

Figure 14. Chemical structure of Der-D.

The physico-chemical characteristics of LD derivatives are reported in table I.

Table I. Physico-chemical characteristics of LD derivatives.

	Molecular weight	**Melting point (°C)**	**λ (nm)**	**Colour**
Der-A	429.202	140	254	Yellow ochre
Der-B	341.332	80	282	Grey
Der-C	397.399	60	220	Yellow phosphorescent
Der-D	630.307	170	220	Grey/White

2.6.3 *Clotrimazole*

Clotrimazole (Fig. 15), an imidazole derivative, is an antifungal agent commonly used in the treatment of fungal infections (of both humans and other animals) such as vaginal yeast infections, oral thrush and ringworm.

It is commonly available as an over-the-counter substance in various dosage forms, such as a cream, and also (especially in the case of ear infection) as a combination medicine. It is also available as a troche or throat lozenge. Fungal infections can be slow to clear up, so the usual course for an anti-fungal agent is, in general, longer than the typical 3–7 days of an antibiotic.

Additionally, Clotrimazole is used to treat the sickling of cells (related to sickle cell anaemia) by blocking ion channels in the RBC (red blood cell) membrane, keeping ions and water within the cell [120,121].

The primary mechanism of action of clotrimazole is against the division and growing of fungi [122]. Clotrimazole alters the permeability of the fungal cell wall and inhibits the activity of enzymes within the cell. Studies show that minimal concentrations of clotrimazole causes leakage of intracellular phosphorus compounds into the ambient medium along with the breakdown of cellular nucleic acids and an accelerated K^+ efflux [122]. This leads eventually to the cell's death. It does not appreciably spread through the user's body but remains at the point of application [123].

Potential for drug interactions with clotrimazole oral exists, as it is a potent, specific inhibitor of cytochrome P450 oxidase and may alter the metabolism of other drugs.

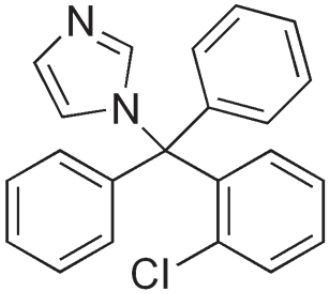

Figure 15. Chemical structure of Clotrimazole.

3. METHODS

3.1 NANOSYSTEMS PRODUCTION

3.1.1 *NLC preparation*

NLC were alternatively prepared by stirring, followed by homogenization or ultrasonication. Briefly, 1 g of lipidic mixture was melted at 70°C. The lipidic mixture concentration ranged 5% w/w (with respect to the total weight of dispersions) and was constituted of a mixture tristearin/tricaprin 2:1 w/w. The fused lipid phase was dispersed in 19 ml of an aqueous poloxamer 188 solution (2.5% w/w) at 13,500 rpm, 70°C for 1 min, using a high-speed stirrer (Ultra Turrax T25, IKA-Werke GmbH & Co. KG, Staufen, Germany). The emulsion was subjected to ultrasonication (Microson^{TM}, Ultrasonic cell Disruptor) at 6.75 kHz for 15 min and then cooled down to room temperature by placing it in a water bath at 22 °C. NLC dispersions were stored at room temperature.

In the case of BC-containing dispersions, 5 mg of the drug (0.025% w/w with respect to the total dispersions, 0.5% w/w with respect to the lipid phase) were added to the molten lipidic mixture and dissolved before adding to the aqueous solution.

LD derivatives-containing NLC were prepared by adding 5 mg of LD-derivate to the molten lipidic mixture and by adding it in the aqueous solution.

In the case of CLO-containing dispersions, 20 mg of the active were added to the lipid mixture and dissolved before addition to the aqueous solution.

3.1.2 *SLN preparation*

SLN were prepared by stirring and ultrasonication method, using the same parameters used for NLC production. Briefly, 0.8 g of tristearin and 0.005 g of soybean phosphatidylcholine were melted at 70°C. The fused lipid phase was added to 0.2 g of Labrasol and the obtained melted mixture was dispersed in 19 ml of an aqueous poloxamer 188 solution (2.5% w/w). The

emulsion was subjected to ultrasonication (Microson™, Ultrasonic cell Disruptor) at 6.75 kHz for 15 min and then cooled down to room temperature by mean of a water bath. SLN dispersions were stored at room temperature.

Alternatively 2.5 (1x), 5 (2x) or 10 mg (4x) of Der-A were added to the molten mixture of tristearin/soybean phosphatidylcholine/Labrasol, dissolved and added to the aqueous phase.

3.1.3 *MAD preparation*

Production of dispersions was based on the emulsification of monoglycerides/surfactant mixtures in water. In particular, the monoglyceride-based lipidic phase was composed of RYLO MG19.

Poloxamer 407 was used as surfactant in a concentration of 0.5% wt/wt with respect to the disperse phase. The concentration of the monoglyceride/surfactant mixture was 5% wt/wt with respect to the total weight of the dispersion. Typically, 2.25 g of RYLO MG19 plus 0.25 g poloxamer 407 were melted in a water bath (Haake FS bath, Enco sas, Karlsruhe, Germany). The obtained molten mixture was added dropwise into 47.5 mL of water at 70°C under mechanical stirring (Eurostar digital stirrer, IKA Labotechnik, Sardo, Torino, Italy) at 1500 rpm. The dispersion was maintained under stirring and was cooled to room temperature up to the solidification of lipid droplets (after 2 hours). Afterwards, the dispersion was heated to 60°C and subjected to homogenization at 13500 rpm (Ultra Turrax, Janke & Kunkel, Ika-Werk, Sardo, Italy) for 5 minutes. Then, the dispersion was cooled at room temperature and stored in glass vials at 25°C.

Twelve point five (12.5) mg of BC (0.55% w/w with respect to the monoolein, 0.025% w/w with respect to the dispersion) were added to the molten MO/poloxamer solution and dissolved before addition to the aqueous solution.

Conversely, In the case of CLO-containing MAD, 50 mg of the active were added to the molten MO/ poloxamer mixture and dissolved before addition to the aqueous solution.

3.2 NANOSYSTEMS CHARACTERIZATION

3.2.1 *Water and dispersed phase loss after NLC and MAD production*

The disperse phase that was lost on the paddle of the overhead mechanical stirrer was recovered and weighed. The dispersions were then weighed in order to evaluate the water evaporation due to high temperature and rapid stirring during production. The extent of water loss due to evaporation was calculated as shown in Equations 1 and 2, concerning MAD and NLC respectively:

$$water\ loss = W\ MO/P407/H20 - (Wdp + Wdisp) \quad (1)$$

$$water\ loss = W\ Tris/Tric/P188\ sol\ 2.5\% - (Wdp + Wdisp) \quad (2)$$

where *W MO/P407/H2O* is the weight of monoglyceride/poloxamer and water before dispersion; *W Tris/Tric/P188 sol 2.5%* is the weight of the lipidic mixture (tristearin/tricaprin 2:1 w/w) and the aqueous Poloxamer 188 solution, *Wdp* is the weight of disperse phase lost on the paddle; and *Wdisp* is the weight of dispersion after production.

MAD dispersions was then filtered through filter paper (Whatman ®, 90mm Dia, England) in order to separate big monoglyceride-poloxamer aggregates. After filtration, both dispersion and filter were weighed. Finally, the filter was left to desiccate in an oven at 70°C for 12 hours and again weighed.

3.2.2 *Particle density*

In order to measure the particle density of MAD and NLC, eight aliquots of dispersion (1 ml each) were centrifuged 4 times at 20000 g for 20 min. The precipitates were collected and suspended in 1 ml of water. 200 µl of this suspension were poured on a glass watch previously weighted and left to desiccate, afterwards the glass watch was weighted and the particles weight was calculated by difference. The particles density was calculated through the “density = mass/volume” equation.

3.2.3 *Photon correlation spectroscopy (PCS)*

Photon correlation spectroscopy (PCS) is a technique used to determine the mean particle size diameter (mean PCS diameter) and the width of the particle size distribution expressed as polydispersity index (PI) [124-127]. The measurement using PCS is based on the light scattering phenomena in which the statistical intensity fluctuations of the scattered light from the particles in the measuring cell are measured. These fluctuations are due to the random movement of the particles in the dispersion medium because of the Brownian motion of the dispersion medium molecules (e.g. water). The measuring range of PCS is approximately from 3 nm to approximately 3 µm.

Usually a PCS device consists of a laser light which is focused to illuminate a small volume of the sample, which is a dilute suspension of particles. The light scattered from these particles is collected again by a lens and its intensity is measured by a photomultiplier. The diffusion rate of the particles depends on their size (at a known fluid viscosity and temperature). Hence, the size of these particles can be calculated from the rate of fluctuation of the scattered light intensity. The lower particle size limit for a measurement is determined by the scattering intensity and the experimental noise. When the suspended particles are small, they diffuse relatively fast, and the fluctuations in the scattered light are rapid. On the other hand, if the particles are large, they move slowly, and the fluctuations in the scattered light are slow. The detected intensity signals are used to calculate the auto-correlation function G(τ), from the decay of this correlation function the diffusion coefficient *D* of the particles is obtained. Once the diffusion coefficient is known, the equivalent diffusional spherical diameter can be calculated applying the *Stokes-Einstein equation*, which relates the diffusion coefficient *D* of a spherical particle to its diameter *r*.

$$r = \frac{kT}{3\pi\rho D}$$

where *ρ* is the viscosity of the surrounding medium, *k* is Boltzmann's constant, *T* is the absolute temperature.

The apparatus consists of a laser, a temperature controlled sample cell and a photomultiplier for

the detection of the scattered light at a certain angle (e.g. 90º or 173º) [125]. The photomultiplier (or photodiode in the new apparatus) signal is transferred to a correlator for calculation of the G(τ). This G(τ) is after that sent to a microprocessor for the calculation of *D* and the correlated mean particle size.

As it was previously mentioned, small particles diffuse faster than large ones, causing a stronger fluctuation in the scattering signal and a more rapid decaying G(τ). For a monodisperse particle population G(τ) is a single exponential, but if more than one size of particles is present the function is polyexponential. Deviation from a single exponential is used to calculate the PI, which is a measure of the width of the size distribution. The PI is 0.0 when a monodisperse particles population is measured. PI values of around 0.10-0.20 indicate a relatively narrow distribution, values of 0.5 and higher are obtained in case of very broad distributions.

Submicron particle size analysis was performed using a Zetasizer 3000 PCS (Malvern Instr., Malvern, England) equipped with a 5 mW helium neon laser with a wavelength output of 633 nm. The dispersant refractive index was 1.33 and the absorbance was 0.00. Glassware was cleaned of dust by washing with detergent and rinsing twice with sterile water. Measurements were made at 25° C at an angle of 90° with a run time of at least 180 sec. Samples were diluted with bidistilled water in a 1:10 v/v ratio. Data were analysed using the “CONTIN” method [128].

3.2.4 *Sedimentation Field Flow Fractionation (SdFFF)*

Sedimentation Field-Flow Fractionation (SdFFF) is a name describing a group of separation methods constituting a subclass of general field-flow fractionation (FFF).

SdFFF technique is ideally suited for the characterization of nanoparticles with highest resolution since it can separate nanoparticles by size and density in the range of 50 nm up to several μm. In case of very dense particles, such as gold sols, particles down to 10 nm can be analysed. Two identically sized particles can be still separated by Sd-FFF into two peaks, when the density is different.

In SdFFF (Fig. 16) the separation force is established by a centrifugal field, which is generated

by spinning the complete circular SdFFF channel at a high rate. The bigger and denser particles are forced more in the direction of the bottom wall (outer wall) than the smaller particles. Thus the bigger particles are eluted later from the SdFFF channel as they are located in slower streamlines in the channel than the smaller particles which are located in faster stream lines. Typical spinning rates used in SdFFF go up to 2500 rpm. To ensure a high resolution over a broad size range, spinning gradients are used for the Sedimentation Field-Flow Fractionation separations as well.

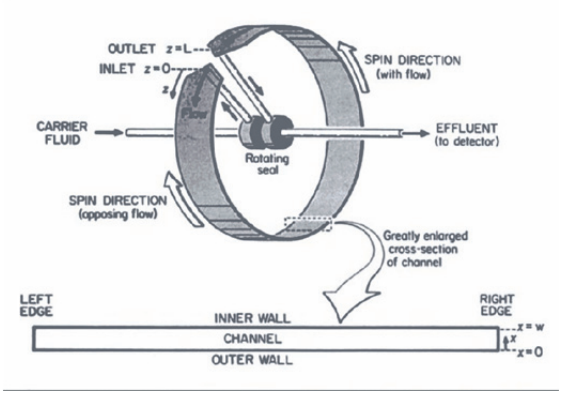

Figure 16. Schematic representation of Sd-FFF apparatus.

A SdFFF system was employed to determine the size distribution of particles (PSD) by converting the fractograms, i.e. the graphical results, assuming the particle density is known [129].

The SdFFF was a Model S101 (Postnova Analytics, Salt Lake City, UT, USA) with hastelloy C channel walls. The rotor radius *r* was 15.5 cm. Nominal channel dimensions, cut from a Mylar spacer, were 90 cm (tip-to-tip length), 2 cm (breadth) and 0.0254 cm (thickness). The void volume of 4.86 cm^3 was experimentally determined from injections of sodium benzoate. An HPLC Pump model 422 Master (Kontron Instruments, Milan, Italy) was used to deliver the carrier solution. The outlet tube from the channel was connected to a UV detector operating at 240 nm (Uvidec 100, Jasco Ltd., Tokyo, Japan).

The mobile phase was a 0.01% v/v solution of FL-70 in Milli-Q water (Millipore S.p.A.,

Vimodrone, Milan, Italy) pumped at 2.0 ml/min and monitored in each run. Fifty microliter samples were injected as they were through a 50 µL Rheodyne loop valve.

The fractions were automatically collected by a Model 2110 fraction collector positioned at the end of the SdFFF system (Bio Rad laboratories, UK) after setting a collecting time of 90 sec. The volume of each fraction was 3 ml.

The analyses were performed by Dr.Contado of the University of Ferrara.

3.2.5 *Cryogenic Transmission Electron Microscopy (Cryo-TEM)*

Cryogenic Transmission Electron Microscopy (Cryo-TEM) is an electron microscopic technique on freezed the biological samples to view the sample with the least possible distortion and the fewest possible artefacts with respect to the original sample.

In cryo-TEM, the freezing of the sample is done in ethane slush to produce vitreous, or non-crystalline, ice. The frozen sample grid is then kept at liquid nitrogen temperature in the electron microscope and digital micrographs are collected with a camera.

The advantages of cryo-TEM over traditional TEM techniques include the preservation of the sample in a near-native hydrated state without the distortions from stains or fixatives needed for traditional TEM. With image processing and averaging of multiple images, cyro-TEM provides high resolution information (below 10 angstroms).

In order to analyse the morphology of the produced nanoparticles, a Zeiss EM922 Omega (Zeiss SMT, Oberkochen, Germany) transmission electron microscope equipped with a cryoholder (CT3500, Gatan, Munich, Germany) was used.

Before the analysis, samples were vitrified [130]. In particular, a drop of the sample was put on an untreated pure copper transmission electron microscopy (TEM) grid (600 mesh, Science Services, Munich, Germany), where most of the liquid was removed with blotting paper leaving a thin film stretched over the grid holes. The specimens were instantly shock frozen by rapid immersion into liquid ethane and cooled to approximately 90K by liquid nitrogen in a temperature-controlled freezing unit (Zeiss Cryobox, Oberkochen, Germany). The temperature

was monitored and kept constant in the chamber during all the sample preparation steps. After freezing the specimens, the remaining ethane was removed using blotting paper. The specimen was then transferred in the cryo-TEM apparatus. Sample temperature was kept below 100K throughout the examination. Specimens were examined with doses of about 1000-2000 e/nm^2 at 200 kV. Images were recorded by a CCD digital camera (Ultrascan 1000, Gatan) and analyzed using a GMS 1.8 software (Gatan).

The analyses were conducted by Dr. Markus Drechsler of the University of Bayreuth (Germany).

3.2.6 *X-ray diffraction measurements*

Diffraction methods, in particular X-Ray scattering, are the most reliable way of carrying out lyotropic phase identification. Spectroscopic techniques such as NMR and freeze-fracture electron microscopy, when used in conjunction with X-ray diffraction, can yield useful complementary data. Because of the large number of phases that can be observed as a function of composition and temperature [131] the attention was focused on lipid-water systems.

A common property of lipids is the segregation of polar and paraffinic moieties into distinct regions. A direct consequence is the ability of lipids to take up a wide variety of structure when mixed with water. In the lipid diffraction, there are two regions of the diffraction pattern that are used to identify the phase. The diffraction pattern observed in the low-angle region (from several hundred Å to 10 Å) specifies the crystalline lattice, identifies the symmetry of the structures and gives information about the long range organization of the phase, whereas from the diffraction observed in the wide-angle region (centred around 4 Å) information on the molecular packing and the short-range organization of the lipids can be observed. It must be noticed that the phases considered by one parameter belong to one- (lamellar phase), two- (hexagonal phase) and three- dimensional (cubic phase) systems.

Low angle X-ray scattering experiments were performed at the DESY synchrotron facility on the A2 beamline in Hamburg, Germany. The investigated *Q*-range ($Q = 4\pi \sin\theta / \lambda$, where 2θ is the scattering angle and λ = 1.50 Å the X-ray wavelength) was 0.02-0.35 Å^{-1}. Experiments were

performed in the 20-40°C range. Scattering data were recorded on a bidimensional CCD camera of 1024 x 1024 pixels, radially averaged and corrected for the dark, detector efficiency and sample transmission [132]. A few wide-angle X-ray diffraction experiments were performed using a laboratory 3.5 kW Philips PW 1830 X-ray generator equipped with a Guinier-type focusing camera operating with a bent quartz crystal monochromator (λ = 1.54 Å). Diffraction patterns were recorded on GNR Analytical Instruments Imaging Plate system. Samples were held in a tight vacuum cylindrical cell provided with thin Mylar windows. Diffraction data were collected at 20°C.

In each experiment, a number of Bragg peaks were detected in the low angle X-ray diffraction region. The peak indexing was performed considering the different symmetries commonly observed in lipid phases [75]. From the averaged spacing of the observed peaks, the unit cell dimension, *a*, was calculated using the Bragg law. The nature of the short-range lipid conformation was derived analyzing the high-angle X-ray diffraction profiles [133].

The experiments were performed by the group of Prof. Mariani of the Marche Polytechnic University.

3.2.7 *Differential Scanning Calorimetry (DSC)*

The International Confederation of Thermal Analysis and Calorimetry (ICTAC) defines the thermal analysis as “a group of techniques in which a physical property of a substance is measured as a function of temperature whilst the substance is subjected to a controlled temperature program”. In this work Differential Scanning Calorimetry (DSC) analysis was employed to characterize the produced particles.

DSC is usually used to get information about both the physical and the energetic properties of a compound or formulation. DSC measures the heat loss or gain as a result of physical or chemical changes within a sample as a function of the temperature. There are 2 types of DSC instruments, the power compensate DSC and the heat-flux DSC [134].

The power compensate DSC consists of 2 separate ovens while the heat-flux DSC consists of

one oven that heat up both the reference and the sample pans (Figure 17). Heat is transferred through the disc (where the sample and the reference pans are placed) and through the sample pan to the contained sample and reference. The differential heat flow is monitored, as well as the sample temperature. Software linearization of the cell calibration is used to maintain calorimetric sensitivity. The cell has a volume of 2 ml and can be used with various inert atmospheres, as well as oxidizing and reducing atmospheres. Different sample pans (hermetic, open or sealed) allow sample volumes of 0.04 ml to 0.1 ml, which can be up to 100 mg depending on sample density.

Examples of endothermic (heat-absorbing) processes are fusion (melting), boiling, sublimation, vaporization, desolvation and solid-solid transitions. An important exothermic, (energy is liberated) process is crystallization. Qualitative measurements of these processes have many applications, such as materials identification, study of purity, polymorphism, solvation, degradation quantitative and qualitative analysis, aging, glass transition temperature and compatibility of substances.

Since DSC analysis allows the study of the melting and crystallization behaviour of crystalline material like lipid nanoparticles, DSC was used to determine the state and the degree of crystallinity of SLN [135-138].

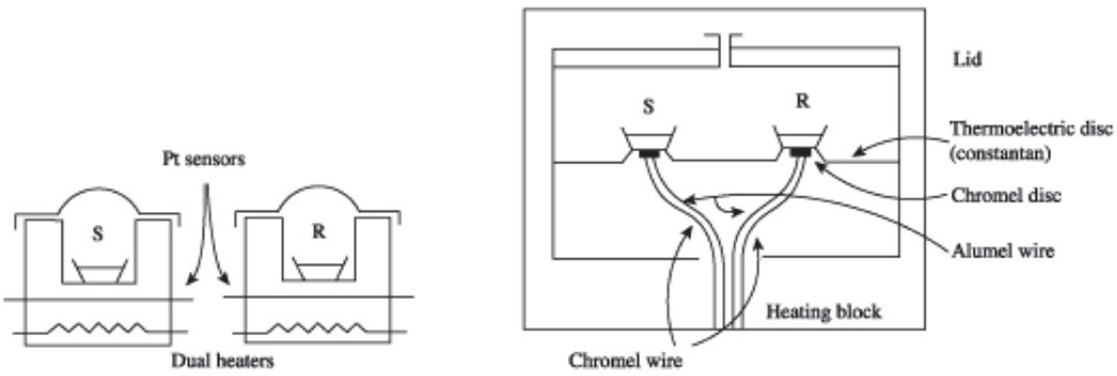

Figure 17. The two DSC types: the power compensate DSC (left) and the heat-flux DSC (right).

DSC was performed by using a Mettler TA Star^e calorimeter equipped with a DSC 822® calorimetric cell and a Mettler STAR® V 8.10 software. The reference pan was filled with bidistilled H_2O.

80 µl of SLN were taken from the bulk, put into the calorimetric pan, hermetically sealed and submitted to calorimetric analysis as follows: (i) a heating scan from 5 to 65 °C (2 °C/min); (ii) a cooling scan from 65 to 5 °C (4 °C/min); for at least three times.

The analyses were performed by the group of Prof. Maria Grazia Sarpietro of the University of Catania.

3.2.8 *Micro Differential Scanning Calorimetry (Micro-DSC)*

Micro Differential Scanning Calorimetry (micro-DSC) is a technique in which the heat flux is measured in function of time or temperature in a controlled atmosphere. The use of a three-dimensional flow meter allows to precisely measure the heat flow in all directions of space. The required sample volume is greater than in the DSC and the speed of scanning in temperature must be low (between 3°C/min. and 0.001°C/min.). Micro calorimetry uses a suite of techniques to directly measure enthalpy and heat capacity changes that arise when chemical reactions occur. In aqueous solutions, heat flux into or out of the sample almost always happens on reaction. These reactions may involve a wide variety of situations, e.g., the interaction of two molecules (such as a cyclodextrin and its guest), changes in the conformation of complex macromolecules (such as proteins or DNA), or even in the structure of very complex multi-molecular colloidal drug delivery systems (such as liposomes or nanoparticles).

The measurements of Micro-DSC were carried out with a calorimeter Micro-DSC III Setaram (Fig.18) with the aim to determine the critical micellization temperature (CMT). The cells used to deposit the sample and the reference (distilled water) were the type batch (1 mL).

Figure 18. Micro-DSC Setaram III and closed “batch” cells.

Two empty cells with the caps were weighed after complete drying, and the joints were chosen to obtain the same mass (± 0.2 mg). The sample and the reference should be introduced to the cells at room temperature and weighed for the identical mass (± 0.3 mg). After their insertions into the oven at room temperature, the temperature of the oven was reduced until 1 °C with 1 °C/min, and then it was kept at this constant temperature to equilibrate the thermal flow. The scan of temperature was performed at 0.1 °C/min until 37 °C. After this, the oven was maintained at this temperature for six hours, mimicking the body application of the formulation. Then, it was started the fusion with 0.1 °C/min to 1 °C. The analysis of the enthalpograms led to the determination of the CMT according to the previously described and well-known method [139]. The analyses were carried out in the Thermal Physics Laboratory, collaborating with Prof. Madeleine Djabourov during my visiting period at ESPCI-Paris Tech from November to December 2011.

3.3 DRUG CONTENT

3.3.1 *Drug content of dispersions*

With the aim of quantifying the total drug content (free plus bonded) of dispersions after production, an amount of dispersion was diluted in an appropriate organic solvent, selected by a

solubility test previously performed on MAD, NLC and SLN. In the case of MAD, 100 µl of filtered dispersion were diluted with 900 µl of ethanol. In the case of NLC, 100 µl of dispersion were diluted with 900 µl of methanol. The mixtures were then stirred for 3 h in order to completely extract the drug. A sample was then filtered (0.45 µm pore diameter) and analyzed by high performance liquid chromatography (HPLC) for drug content.

Drug recovery = amount of drug detected by HPLC x 100 / total amount of drug employed

All data were the mean of 8 determinations on different batches of the same type of dispersion.

For Sedimentation Field Flow Fractionation (SdFFF) and *in vivo* experiments, the amount of drug detected by HPLC after filtration was taken as reference of the total amount of drug.

BC or CLO associated with particles was quantified by HPLC analyses of several fractions collected after the separation by SdFFF.

3.3.2 *Stability studies*

Physical and chemical stability studies were conducted in triplicate at 0, 1, 2 and 3 months from production of formulations.

Physical stability studies were performed analysing macroscopic aspect (phase separation, turbidity and macroscopic viscosity) under visual inspection.

Chemical stability was evaluated on drug loaded formulations, stored at 25°C, determining CLO content by HPLC analyses. Shelf life values were calculated [87].

Log (CLO residual content, %) was plotted against time and the slopes (*m*) were calculated by linear regression.

The slopes (*m*) were then substituted into the following equation for the determination of *k* values:

$$k = m \times 2.303 \quad (1)$$

Shelf life values (the time for 10% loss, t_{90}) were then calculated by the following equation:

$$t_{90} = 0.105/k \quad (2)$$

as previously reported [140].

3.4 HIGH PERFORMANCE LIQUID CHROMATOGRAPHY (HPLC) ANALYSIS

HPLC technique is a suitable and accurate way to determine the content of a substance and/or its chemical stability.

HPLC determinations were performed using a HPLC system (1200 Series, Agilent Technologies, USA) equipped with an isocratic pump, an UV-detector and a 7125 Rheodyne injection valve with a 50 µl loop.

Only in the case of CLO ex-vivo studies, the instrument used was an HPLC apparatus (Waters®, USA) equipped with a binary pump (model 515), an autosampler (model 717 plus) and a tuneable absorbance detector (model 486).

Each injection was performed in triplicate (n=3).

Details of HPLC conditions for each drug studied are below reported in tables II to VIII.

3.4.1 *BC*

Table II. HPLC analysis method for BC

Specification	Details
COLUMN	C_{18} RP-column (Alltech® - Hypersil BDS RP18 (5 µm) 4.6 x 150 mm)
MOBILE PHASE	0.1 M ammonium formate (pH 3) and acetonitrile 55:45 v/v
FLOW	0.8 ml/min
INJECTION	40 µl
WAVE LENGHT	305 nm
RETENTION TIME	5.8 min

3.4.2 *Der-A*

Table III. HPLC analysis method for Der-A

Specification	Details
COLUMN	C_{18} RP-column (Grace® - Alltima RP18 (5 µm) 4.6 x 150 mm)
MOBILE PHASE	Methanol, Water 60:40 v/v
FLOW	0.5 ml/min
INJECTION	40 µl
WAVE LENGHT	254 nm
RETENTION TIME	5.4 min

3.4.3 *Der-B*

Table IV. HPLC analysis method for Der-B

Specification	Details
COLUMN	C_{18} RP-column (Grace® - Alltima RP18 (5 µm) 4.6 x 150 mm)
MOBILE PHASE	Methanol, Water 60:40 v/v
FLOW	1.0 ml/min
INJECTION	40 µl
WAVE LENGHT	220 nm
RETENTION TIME	11.1 min

3.4.4 *Der-C*

Table V. HPLC analysis method for Der-C

Specification	Details
COLUMN	C_{18} RP-column (Grace® - Alltima RP18 (5 µm) 4.6 x 150 mm)
MOBILE PHASE	Methanol, Water 60:40 v/v
FLOW	0.8 ml/min
INJECTION	40 µl
WAVE LENGHT	282 nm
RETENTION TIME	5.7 min

3.4.5 *Der-D*

Table VI. HPLC analysis method for Der-D

Specification	Details
COLUMN	C_{18} RP RP-column (Grace® - Alltima RP18 (5 µm) 4.6 x 150 mm)
MOBILE PHASE	Methanol, Water 70:30 v/v
FLOW	0.5 ml/min
INJECTION	40 µl
WAVE LENGHT	220 nm
RETENTION TIME	6.2 min

3.4.6 *CLO*

Table VII. HPLC analysis method for CLO, used with Agilent HPLC apparatus

Specification	Details
COLUMN	C_{18} RP-column (Agilent® - Zorbax Eclipse Plus (5 µm) 4.6 x 150 mm)
MOBILE PHASE	Methanol, Water 80:20 v/v
FLOW	0.8 ml/min
INJECTION	40 µl
WAVE LENGHT	305 nm
RETENTION TIME	6.8 min

Table VIII. HPLC analysis method for CLO, used with Waters HPLC apparatus.

Specification	Details
COLUMN	C_{18} RP-column (Waters®, XTerra (5 µm) 3.9 x 150 mm)
MOBILE PHASE	Methanol, Water 75:25 v/v
FLOW	0.5 ml/min
INJECTION	50 µl
WAVE LENGHT	233 nm
RETENTION TIME	6.2 min

3.5 GEL PRODUCTION

NLC and MAD have been respectively viscosized by the use of the polymers poloxamer 407 or carbomer.

The NLC gel was produced with two different procedures. In the first case, the gel was obtained by diluting at 0°C a poloxamer water solution (30% w/w) to NLC in order to obtain a poloxamer concentration of 24% w/w in the final mixture (NLC-D). In the second case, poloxamer 407 (24%, w/w) was directly slowly dispersed in the NLC dispersion at 0°C, under stirring until complete dispersion of the polymer (NLC-S).

For the preparation of the MAD containing gel, firstly the carbomer gel was prepared. The polymer (2.1%, w/w) was added to bidistilled water and left to swell at room temperature to obtain a homogeneous and liquefied mixture. After an overnight incubation, an equal amount of triethanolamine was added to neutralize the solution. The obtained gel was diluted with MAD (1:2, v/v), resulting in a final carbomer concentration of 0.7% w/w and 3% w/w of lipids.

3.6 PREPARATION OF SIMULATED VAGINAL FLUID

Vaginal fluid is the resultant of fluids that comes from several strains such as uterus, cervix and sometimes menstrual secretions and sperm. Noteworthy, due to the limited quantity of human vaginal fluid and its rapid degradation once collected from its source, researchers have developed a simulated vaginal fluid (SVF). SVF was prepared using the procedure previously described by Owen et al [141].

Briefly, to 900 ml of distilled water contained in a beaker, NaCl (3.51 g), KOH (1.4 g), $Ca(OH)_2$ (0.22 g), bovine serum albumin (0.018 g), lactic acid (2.00 g), acetic acid (1.00 g), glycerol (0.16 g), urea (0.4 g) and glucose (5.00 g) were added and stirred mechanically until complete dissolution.

The pH of the mixture was then adjusted to 4.5 using HCl, and the final volume was adjusted to 1 L.

3.7 RHEOLOGICAL EVALUATION OF HYDROGELS

Rheology is the branch of physics that studies the deformation and flow of matter. The rotational rheometers are commonly used for measuring the rheological properties of the material.

Rheological measurements of the gels NLC-D and NLC-S were performed on a controlled stress AR-G2 rheometer (TA Instrument Ltd., London, UK) using a cone-plate geometry (diameter 60 mm, angle 2° and gap 55 μm). A solvent trap maintained a solvent-saturated atmosphere around the cell and evaporation was not significant for the temperatures and time scales investigated (Fig.3).

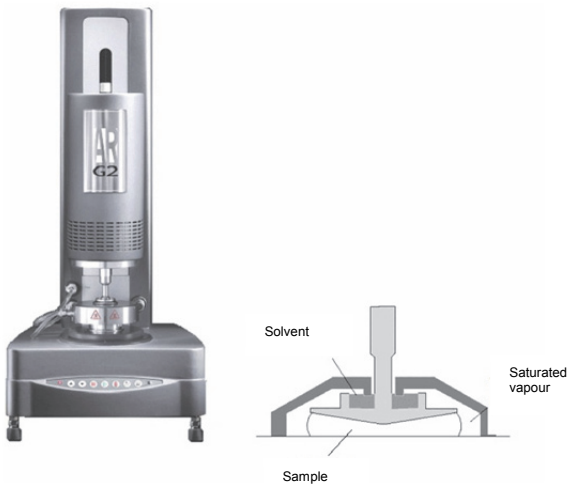

Figure 3. Ar-G2 rheometer and cone-plate geometry with solvent trap.

Elastic (or storage) (*G′*) and the viscous (or loss) moduli (*G″*) were recorded under a constant strain of 0.5 % to be in the linear viscoelastic regime in which the moduli are independent of the strain, at a frequency of 1 Hz. The presence of Pelletier diodes, placed in the lower plate, allowed to perform temperature sweeps from 5 to 70 °C with a precision of 0.1 °C. The elastic (G') and loss (G'') moduli were recorded, the temperature at which G' suddenly varied corresponded to sol-gel transition temperature.

Oscillatory (or dynamic) experiments were carried out. A sinusoidal shear was applied to the

sample, where the stress $\tau(t)$ and the strain $\gamma(t)$ were defined as follows:

$$\tau(t) = \tau_0 \cos(\omega t) \quad (1)$$

$$\gamma(t) = \gamma_0 \cos(\omega t - \delta) \quad (2)$$

τ_0 and γ_0 are, respectively, the maximal amplitudes of the stress and strain, $\omega_0 = 2\pi N$, with N the frequency and ω the shear pulsation and δ is the phase angle stress/strain.

From the phase angle, it is possible to define various dynamic viscoelastic quantities and especially the elastic (or storage) modulus G' (3) and the viscous (or loss) modulus G'' (4).

$$G' = \frac{\tau_0}{\gamma_0} \cos\delta \quad (3)$$

$$G'' = \frac{\tau_0}{\gamma_0} \sin\delta \quad (4)$$

The higher the G' value, the more pronounced the elastic character and conversely, the higher G'', the more pronounced the viscous properties. The elastic modulus is a measure of the energy stored and recovered per cycle of deformation and reflects the solid-like component of elastic behaviour.

The oscillatory experiments were used mainly in order to determine the sol-gel transition temperature, by measuring the temperature for which G' underwent a critical variation.

After the common rheology measurement, SVF was added to NLC formulations in order to simulate the vaginal application. Considering that current topical vaginal products are generally applied in volumes in the range of 2-5 mL and that the volume of fluid ambient present in the vagina (vaginal fluid transudate and mucus) is approximately 0.5 – 0.75 ml [141], to simulate the dilution of formulations that might occur after application, 2 ml of each formulation was mixed to 0.75 ml of SVF and the influence of the dilution on thermogelling and rheological properties of poloxamer-based hydrogels was tested. All rheological results are the means of n=3 experiments.

Viscosity of carbomer gels, in the absence (CLO carbomer gel) and in the presence of CLO-MAD (CLO-MAD carbomer gel), was measured using a Brookfield dial reading viscometer model RTV (Brookfield engineering laboratories, Stoughton, MA, USA). Appropriate spindles

with different speeds (0.1 - 5 rev/min) were used to obtain the correct dial readings. Three readings were taken for each sample and the mean dial reading was corrected using factors supplied by the instrument manufacturer.

The analyses were carried out in the Thermal Physics Laboratory, collaborating with Prof. Madeleine Djabourov, during my visiting period at ESPCI-Paris Tech from November to December 2011.

3.8 IN VITRO TESTS

3.8.1 *Dialysis*

D*ialysis method* was used as *in vitro* test for BC and LD derivatives containing preparations.

In the case of BC containing NLC and MAD and LD derivatives containing NLC, 5 ml of nanoparticulate dispersion were placed into a dialysis tube dipped into 100 ml of receiving phase, alternatively constituted of pure citrate buffer (50 mM, pH 3.5) or in mixture with ethanol or methanol and shaken horizontally (MS1, Minishaker, IKA, Germany) at 175 rpm and 37°C. At regular time intervals, 400 µl samples of receiving buffer were withdrawn and refilled again with fresh medium.

In the case of Der-A SLN (2x) the test was performed using the same procedure and quantities but the receiving phase was constituted of water and methanol (50:50 v/v).

3.8.2 *Reverse dialysis method*

For the *reverse dialysis method*, 5 ml of MAD were directly placed into 200 ml of a stirred solution, constituted of citrate buffer (50 mM, pH 3.5) and methanol (50:50 v/v) in which 10 dialysis sacs containing 1 ml of the same solution were previously immersed. The sacs were previously equilibrated with the solution for 30 min. At regular time intervals one dialysis bag was withdrawn and replaced with an equal volume of solution. The dialysis bag content was

assayed by HPLC for BC concentration.

3.8.3 *USP XXII paddle method*

The *USP XXII paddle method* is a procedure based on the use of an apparatus consisted of an approximately 25.4 mm × 34.92 mm stainless steel, 40-mesh paddle rotating at a constant speed of 100 rpm. The paddle was positioned inside a glass vessel placed in a water bath. 200 ml of a poloxamer 188 solution (0.1% w/v) in phosphate buffer (0.1 M, pH 7.4) was placed in the vessel and stirred by the paddle. 8 ml of NLC was poured in the vessel.

At regular time intervals, 1 ml samples were withdrawn from the vessel and refilled again with fresh medium. 200 □l of samples were filtered through nylon filters (Steriflip, pore size 0.1 □m pore size, Millipore, MA) and analysed by HPLC. The filters were validated with regard to drug adsorption.

3.8.4 *Franz-cells method*

For BC analyses, *Franz type glass diffusion cell* were assembled with a nylon membrane (GNWP, 0.2 µm pore size, Millipore, MA). The cell body was filled with a receptor phase constituted of 100 mM phosphate buffer, pH 7.4. One gram of MAD was placed into the donor cell compartment and tamped down on the membrane, previously moistened with the receptor phase. Samples of receptor phase were withdrawn after predetermined time intervals and the BC concentration was measured by using a HPLC analytical procedure. Each removed sample was replaced with an equal volume of simple receptor phase. Samples were then diluted with methanol in a 1:1 v/v ratio. The amount of drug released was determined by HPLC.

For CLO analyses, the cell body was filled with a receptor phase constituted of an ethanol:water mixture (20:80, v/v). Experiments were carried on following a protocol previously reported [142]. The calculated CLO concentrations were plotted as a function of time and the slopes of the lines were computed from the linear portion of the accumulation curve. All the obtained diffusion rates were determined six times in independent experiments and the mean values ± standard

deviations were calculated.

3.8.5 *Esterase degradation*

Der-A containing SLN were tested in order to create a degradation kinetic of the derivative and determine the amount of LD released by time.

Alternatively, Der-A SLN dispersion or LD mother solution (50 µl) were added to a 10% v/v fetal calf serum (FCS) water solution in the same quantity. Thirteen Eppendorf were prepared with this solution and placed in a thermostatic bath at 37°C. At different time intervals, comprising between 0 and 1440 minutes, samples were removed from the bath and 150 µl of pure methanol were added to the solution. Samples were filtered with 0.22 µm nylon syringe filters and analysed by HPLC.

A kinetic curve was obtained plotting the amounts of non-degraded Der-A in function of time (min.).

3.8.6 *Anticandidal activity study*

MAD and NLC samples, empty and CLO-containing, was assayed for antimicrobial activity, employing *C. albicans* ATCC 48274 as tester strain. Mother cultures of *C. albicans* strain have been set up starting from 1.5 ml of liquid nitrogen stored inoculum put in 250 ml sterile flasks containing 98.5 ml of liquid YEPD medium (yeast extract 0.5%, bactopeptone 1%, glucose 2%; Oxoid, Italy) placed at 37 °C on an orbital shaker (110 rpm). After 72 hours of culturing, *C. albicans* mother cultures reached the stationary phase of growth. For the experiment, mother cultures have been then properly diluted to have aliquots corresponding to $5 \cdot 10^4$ CFU/ml (Colony Forming Units). Fifty ml sterile flasks have been prepared with 800 µl of sterile phosphate buffer (100 mM, pH=7.4), 1000 µl of diluted *C. albicans* mother culture ($5 \cdot 10^4$ CFU/ml), and 200 µl of samples to test set up as follows, reaching a final volume of 2 ml: sterile water solutions of MAD and NLC samples with and without CLO (0.169 mg/ml); CLO solutions in DMSO (dimethyl sulfoxide, Sigma-Aldrich) at the same concentration employed for MAD and

NLC samples and at 1.69 mg/ml to test the strain sensitivity; negative controls with DMSO and sterile water have been properly processed. All the 50 ml flasks prepared as described above have been incubated for 2 hours at 37 °C and gently shaken (110 rpm). Then, 100 µl of each solution (2 ml) have been plated in Petri dishes (9 cm) previously prepared with 15 ml of YEPD agarized medium. The Petri plates have been then incubated at 37 °C and, after 72 hours, *C. albicans* colonies have been counted. The experiments have been processed in triplicate and the results expressed as CFU/plate ± standard deviation.

Relative standard deviations and statistical significance (Student's t test; P≤0.05) were given where appropriate for all bioactivity data collected. One-way ANOVA and LSD post hoc Fisher's honest significant difference test were used for comparing the bioactive effects of different samples.

The experiments were performed by Prof. Gianni Sacchetti group of the University of Ferrara.

3.8.7 *Cytotoxicity assay*

In the case of CLO forms cytotoxicity was investigated.

Cell viability was measured by trypan blue exclusion. Trypan blue is a vital stain used to selectively colour dead cells blue. Live cells with intact cell membranes are not coloured.

Since cells are very selective in the compounds that pass through the membrane, in a viable cell trypan blue is not absorbed, however, it traverses the membrane in a dead cell.

Cytotoxicity test was performed on NLC dispersions and viscosized formulations, empty and CLO-containing. In order to better investigate the toxicity of these systems, absolute Ethanol, a Clotrimazole solution (1 mg/ml) in Ethanol, a Poloxamer aqueous solution (24% w/w) and a Poloxamer gel (24% w/w) containing Clotrimazole in a dispersed form (1 mg/ml) were tested as positive and negative controls.

HeLa cells were seeded in a 24 wells plate (1 cm^2) at a concentration of 150 000 cells/ml. 1 ml of this suspension was filed in each well. Then, cells were incubated at 37°C for 48 hours.

The viability of the cells was checked after 24 hours and the medium was changed in order to

maintain a suitable environment. After 48 hours, the medium of cells was removed by aspiration. Cells were washed once with PBS 1x to remove non-adherent cells and the multiwell plate was placed on ice in order to facilitate the correct application of thermo-reversible gel formulations. 100µl of each sample were put in a well and 1 ml of cells medium was consequently added and cells were placed in an incubator at 37 °C with 5% CO_2 for 24 hours.

After the contact time, the cell medium was removed by aspiration. Cells were washed with PBS 1x to remove all traces of FVS (Fetal Calf Serum) and 100µl of trypsin-EDTA 0.25% w/v were added in each well to detach the cells. Cells were then placed for 5 minutes at 37 °C 5% CO_2. The effect of trypsin was stopped adding 400µl of cell medium. After homogenization, 50 µl of cells were diluted with 350 µl of Trypan blue (0.05%) in a test tube and the obtained solution was homogenised. 100 µl were withdrawn and put in Malassez Chamber for counting with an inverted microscope. Cells were differentiated between living (transparent) and dead (blue). The results were reported in number of viable cells and the percentage was performed in relation to non-treated well, which was used as a control (100% viability).

The experiments were carried out in the Laboratory of INSERM UMR 756, collaborating with Dr. Vanessa Liévin-Le Moal, during my visiting period at the School of Pharmacy of the University Paris Sud from July to December 2011.

3.9 EX-VIVO TESTS

NLC formulations (empty and CLO containing; in liquid form and viscosized) were tested in *ex vivo* permeation and penetration studies, using porcine vaginal mucosa.

The experiments were performed in the Laboratory of UMR CNR 8612, collaborating with Prof. Kawthar Bouchemal, during my visiting period at the School of Pharmacy of the University of Paris Sud from July to December 2011.

3.9.1 *Preparation of phosphate buffer*

In order to simulate the systemic compartment, in which substances absorbed from mucosa are transported, we prepared a phosphate buffer with a pH of 7.4. 13.609 g of KH_2PO_4 were diluted in 900 ml of water contained in a beaker and stirred until complete dissolution. Then, the pH was adjusted to 7.4 with NaOH and the final volume of the solution adjusted to 1L. Before the use, the solution was filtered with Millipore Millex-GV® Syringe Driven Filter Unit (0.22 µm Hydrophilic PVDF).

3.9.2 *Animals*

Porcine vaginal mucosa was chosen because, among the larger experimental animals, the pig has the advantage of being remarkably similar to human in terms of anatomy, physiology, metabolism and histology. Furthermore, many research works have reported that excellent correlation was found between human and porcine vaginal tissues [143,144].

Experiments were carried out on female pigs (INRA Jouy en Josas, France) weighing between 60 and 63 kg in average. The animals were fasted for 24 h, but had free access to tap water. All experiments on animals adhered to the Communities Commission Directive (DE/86/609/CEE) and were performed in conformance with the French Ministry of Agriculture Permission No. 78-16.

Pigs were sacrificed by intravenous injection (20 mL) of overdosed sodium phenobarbital (Dolethal, Vetoquinol Laboratory, Lure, France), and the vaginal mucosa was taken over a 10

cm length. The mucosa was placed in SVF and stored at -20°C immediately after sacrifice of the animal and kept at this temperature until use. It has been shown that porcine mucosa can be frozen during storage without affecting the mucus layer [144]. Samples were cut in 1 cm square pieces by means of surgical scissors to obtain intact vaginal tissue and defrosted before experiments at ambient temperature in the presence of SVF.

3.9.3 *Permeation experiment*

To evaluate CLO permeation through the skin, samples of porcine mucosa were mounted on standard Franz diffusion cells (area = 1.0 ± 0.1 cm^2) and the receptor compartment (volume 11 ml) was filled with phosphate buffered saline (PBS, pH 7.4). After equilibration, 1 ml of each NLC formulation was added to the donor compartment. The receptor compartment was stirred at 250 rpm in a thermostatic water bath at a temperature of 37°C. Then, at fixed time intervals, 100 µl of the receptor phase were withdrawn and replaced with an equal amount of fresh PBS. The samples were filtered with Nalgene® Syringe Driven Filter Unit (0.20 µm Nylon).

The drug amount released was assayed by means of an HPLC apparatus (Waters®, USA) equipped with a binary pump (model 515), an autosampler (model 717 plus) and a tuneable absorbance detector (model 486) set at 233 nm wavelength. A C_{18} column (Waters®, XTerra RP-18 (5 µm) 3.9 x 150 mm) was the stationary phase. The mobile phase consisted of MeOH/Water (75:25 v/v). The flow rate was 0.5 ml/min and the injection volume was 50 µl.

3.9.4 *Penetration experiment*

In the case of penetration measurements, each sample (1 ml) was applied on a portion (1 cm^2) of the intact vaginal tissue isolated by means of surgical scissors and fixed between the donor and the report chamber of a Franz diffusion cell, using the same experimental protocol of the release measurements. The acceptor chamber was filled with PBS (pH 7.4) to maintain the mucosa hydrated and thermostated.

After 8 hours from the beginning of the experiment, Clotrimazole loaded samples were removed

from the mucosa which was rinsed twice with MilliQ water and stored at -4°C. Tissues were afterwards cut in vertical slices and collected in glass vials. Drug penetrated into slices was extracted with 2 ml of MeOH under overnight stirring with magnetic bars. The samples obtained were filtered with Nalgene® Syringe Driven Filter Unit (0.20 µm Nylon) and analysed with HPLC using the same protocol of permeation experiments.

3.10 IN VIVO TESTS

3.10.1 *Animals*

Male Sprague-Dawley rats were kept under regular lighting conditions (12 h light/dark cycle) and given food and water *ad libitum*. The experimental protocols used in the present study were approved by the Italian Ministry of Health (license n° 194/2008-B) and by the Ethical Committee of the University of Ferrara. Adequate measures were taken to minimize animal pain and discomfort and to limit the number of animals employed in the study.

3.10.2 *6-hydroxydopamine lesion*

Unilateral lesion of dopamine (DA) neurons was induced in isoflurane-anaesthetised male Sprague-Dawley rats (150 g; Harlan Italy; S. Pietro al Natisone, Italy) as previously described [145]. Eight micrograms of 6-OHDA, dissolved in 4 µl of saline containing 0.02 % ascorbic acid, were stereotaxically injected according to the following coordinates from bregma: antero-posterior -4.4 mm, medio-lateral -1.2 mm, dorso-ventral -7.8 mm below dura [146]. In order to select the rats, which had been successfully lesioned, the rotational model was employed. Two weeks after 6-OHDA injection, rats were tested for denervation with a dose of amphetamine (5 mg/kg i.p., dissolved in saline). Forty-nine rats showing a turning behavior >7 turns/min in a direction ipsilateral to the lesion side were enrolled in the study. Experiments were usually performed 6-8 weeks after lesion. Marked (>95%) reduction in striatal DA levels and tyrosine

hydroxylase positive DA terminals have been detected at this stage [147,148].

3.10.3 *Behavioural studies in hemi-parkinsonian rats*

The 6-OHDA hemilesioned rat is a well-established model of experimental parkinsonism, in which hypokinetic motor disturbance primarily affects the side of the body contralateral to the denervated hemisphere (i.e. the toxin injection side). Parkinsonian-like disabilities were investigated in rats by using two previously validated behavioural tests [146,148]. The “bar test” measures the ability of the rat to respond to an externally imposed static posture, and provides information on the time to initiate a movement (akinesia) [149]. The “drag test” measures the ability of the forepaws to adapt to an external dynamic stimulus (i.e. dragging backwards), and provides information on the time to initiate and execute (bradykinesia) a movement [145, 150].

In the bar test, the contralateral and ipsilateral forepaws of each rat were alternatively placed on blocks of increasing heights (3, 6 and 9 cm). The immobility time (in sec) of each paw on the blocks was recorded (cut-off time at each step of 20 sec) and summed. In the drag test, the animal was gently lifted from the tail, allowing the forepaws to rest on the table, and dragged backwards at a constant speed (20 cm/sec) for 100 cm. The adjusting steps made with the forepaws were counted by two distinct observers. Rats were trained on both motor tasks until their performance was reproducible. On the day of experiment, motor performance in the bar and drag test was evaluated before (control session) and at different time-points after drug administration (30, 90, 180, 300, 480 min). Drug effect has been expressed as a percent of pre-treatment values. BC preparations (free BC, BC-MAD and BC-NLC) were given intraperitoneally (i.p.) at a dose of 0.3 mg/Kg (9-13 animals each group). Free BC was administered in a saline solution (0.9 mg/ml in NaCl 0.9% w/v). The effect of vehicle (empty MAD and empty NLC) was also investigated (7-9 animals each group). The dose of the lipid given to each rat was calculated to be 70 mg/Kg and 67 mg/Kg for NLC and MAD respectively.

3.10.4 *Statistical analysis*

Statistical analysis was performed on percent data by one-way repeated measures (RM) analysis of variance (ANOVA). In case ANOVA yielded to a significant F score, post-hoc analysis was performed by contrast analysis to determine group differences. In case a significant time x treatment interaction was found, the sequentially rejective Bonferroni's test was used (implemented on excel spreadsheet) to determine specific differences (i.e. at the single time point level) between groups. P values <0.05 were considered to be statistically significant.

4. NLC AND MAD FOR THE DELIVERY OF BROMOCRIPTINE

4.1 INTRODUCTION

The use of lipid nanosystems for the therapy of brain diseases has been recently proposed [151,152]. Indeed, the pharmacological treatment of brain tumors, as well as neurological and psychiatric disorders is often hindered by the inability of potent drugs to pass the blood brain barrier (BBB) [153]. BBB significantly restricts water-soluble, charged and high molecular weight therapeutics to the vascular space, while allowing brain penetration of small and/or lipophilic molecules. Multiple strategies have been employed to circumvent BBB. An emerging approach is the use of colloidal carriers, which allow brain penetration of non-transportable drugs by masking their physico-chemical characteristics [154,155]. In fact, colloidal carriers represent a non-invasive mean of administration, which offers clinical advantages such as the reduction of drug dosage and side effects, the increase of drug viability, and the improvement of patient quality of life [156].

This follow-up study was aimed at investigating the use of NLC and MAD as formulations for controlled delivery of BC. An in-depth characterization of morphology, size, inner structure and drug distribution of nanosystems was made. In addition, the ability of both BC preparations to attenuate motor deficits in 6-hydroxydopamine (6-OHDA) hemilesioned rats, a model of PD, was determined in vivo and compared to that of free BC.

4.2 RESULTS AND DISCUSSION

4.2.1 Production and characterization of dispersions

Production of MAD was performed by the emulsification-hot homogenization method. The loss of disperse phase and the weight of dispersion were 0.1% ± 0.02 and 87% ± 0.2 with respect to W *MO/P407/H_20* before production, respectively. Thus the extent of water loss (calculated by difference) was about 13 ± 0.2%.

The weight of larger particles after desiccation was 10 ± 0.5% with respect to W *MO/P407* before production. It was found that the uptake of water by large particles was 3.3-fold their weight. All data were the mean of eight determinations on different batches of the same type of dispersions.

NLC were produced with a tristearin/tricaprin mixture by the use of homogenization/sonication method, obtaining stable and homogeneous dispersions. The highest loss of disperse phase was on the vessel (~0.8% with respect to the total weight of the lipid plus water phases before dispersion, 4.0 ± 0.3% with respect to the weight of the lipid phase before dispersion). The extent of water loss was 0.2 ± 0.03%. The final weight of dispersion was 99 ± 0.3% with respect to the lipid plus water phases before dispersion. All data were the mean of 8 determinations on different batches of the same type of dispersion.

BC recovery after the production process in the filtered dispersion was 70 ± 0.75% of the total amount used for the preparation in the case of MAD and 84 ± 0.58% in the case of NLC dispersions.

Table IX summarizes the results of PCS studies conducted to determine the dimensional distribution of MAD and NLC dispersions, in the absence and in the presence of BC.

Table IX. Mean diameters of MAD and NLC as determined by PCS

PARAMETER	MAD dispersion	MAD-BC dispersion*	NLC dispersion	NLC-BC dispersion*
ZAverage *mean diameter (nm)*	198.2±1.2	204.8±1.2	196.2±2.4	195.1±3.3
Analysis by number *mean diameter (nm)*	78±0.3 (Peak Area 99.7±0.1%)	84.3±0.4 (Peak Area 96.2±0.2%) 230.7±0.3 (Peak Area 3.8±0.1%)	125.7±0.2 (Peak Area 99.5±0.2 %)	104.3 ±0.2 (Peak Area 98.6±0.1%) 263.1±0.2 (Peak Area 1.4±0.2 %)
Polydispersity Index	0.18±0.02	0.19±0.01	0.18±0.02	0.19±0.03

**produced in the presence of Bromocriptine*
PCS data are means of 5 determinations on different batches of the same type of dispersion

Both MAD and NLC had mean intensity diameters of ~200 nm. Empty MAD had a mean diameter of 198.2 nm, expressed as Z Average. The analysis by volume revealed a mean diameter of 121.0 nm. BC incorporation slightly increased the mean diameter of nanostructures to 204.8 nm. In-depth analysis of the distribution by volume revealed a huge peak with a mean diameter of 109.1 nm (84.3 % of Peak Area) and a smaller one with a mean diameter of 286.3 nm (15.7 %). After filtration, the mean size of the larger particles measured by laser diffraction was 28 ± 2.7 nm (mean ± SD of three runs), ranging between 25 and 30 nm (data not shown).

NLC dispersions were not filtered since they did not display aggregates or large microparticles. Empty NLC showed a mean diameter of 196.2 nm, which was not affected by BC incorporation, even if the amount of larger nanoparticles increased, conferring the distribution a bimodal profile. Dimensional analysis by volume revealed a mean diameter of 131.4 nm for the more conspicuous population and a mean diameter of 392.4 nm for the other. On the other hand both populations displayed low polydispersity indexes (0.18 and 0.19), indicating a narrow dimensional distribution [157].

Size distribution was also determined by SdFFF. The fractograms obtained under the same separation conditions (to allow a direct comparison) were converted into PSD plots, i.e. the

amount of material per unit change of diameter, according to well-proven equations, by transforming the retention time in the diameter of the equivalent sphere (d), and the UV signal into a mass frequency function (dd) [158,159].

Figure 20 shows the PSD plots of a diluted amount of BC-MAD (panel A) and BC-NLC (panel B) dispersions. The conversion was performed by assuming an average density of 0.0133 g/ml for MAD and 0.0283 g/ml for NLC.

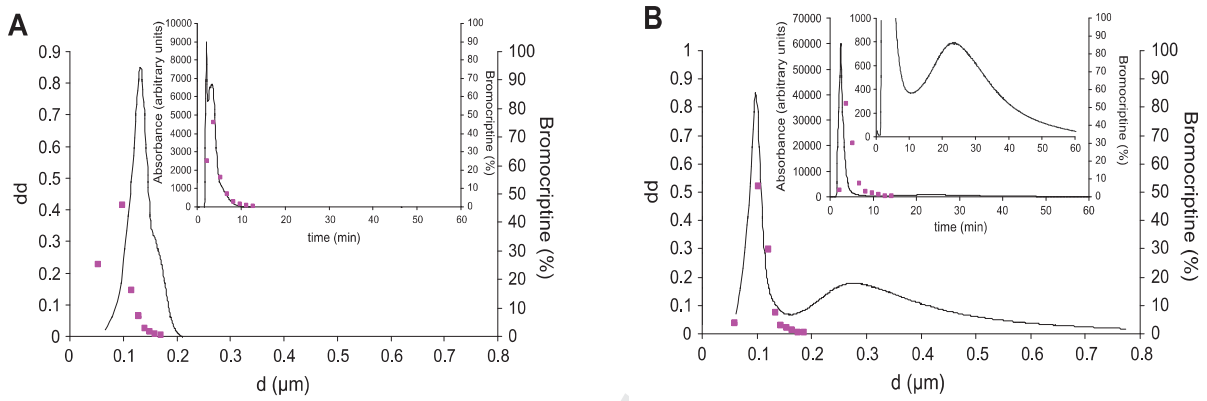

Figure 20. PSDs elaborated from the SdFFF fractograms. A) MAD particles were assumed to have a density of 0.9692 g/ml (d = diameter of nanoparticles; dd = dimensional distribution; the dots indicate BC content, as determined by HPLC). B) NLC particles: assumed density 0.9690 g/ml.

In panel A, the main peak had a maximum at ~ 130 nm and showed a small shoulder, possibly masking a minor population of particles of ~ 160 nm size, as also evidenced in the original fractogram reported in the inset of Panel A. These size distributions partly differed from PCS data reported in table IX. However, the cryo-TEM image reported below (Figure 21) confirms the presence of particles of different size, structure and possibly density, which generates particle masses difficult to be efficiently separated under these experimental conditions.

NLC particles had instead a quite regular and reproducible shape, independent of their size,

thus also their density might be considered constant, guaranteeing a better reliability to the SdFFF results presented in Panel B. The graph shows a thin peak centred at ~100 nm and another one, smaller and broader, with a maximum at ~275 nm. These data are in good agreement with the PCS analysis. The apparent discrepancy in the relative proportions between the two peaks is an artefact introduced by the conversion into PSD, as it can be verified by observing the original fractogram reported on the top of panel B, where the larger peak is scarcely visible from the baseline, unless to zoom in the graph.

Cryo-TEM analyses were conducted in order to investigate the internal structures of MAD and NLC. Figure 21 reports cryo-TEM images of a sample of non-filtered BC-MAD.

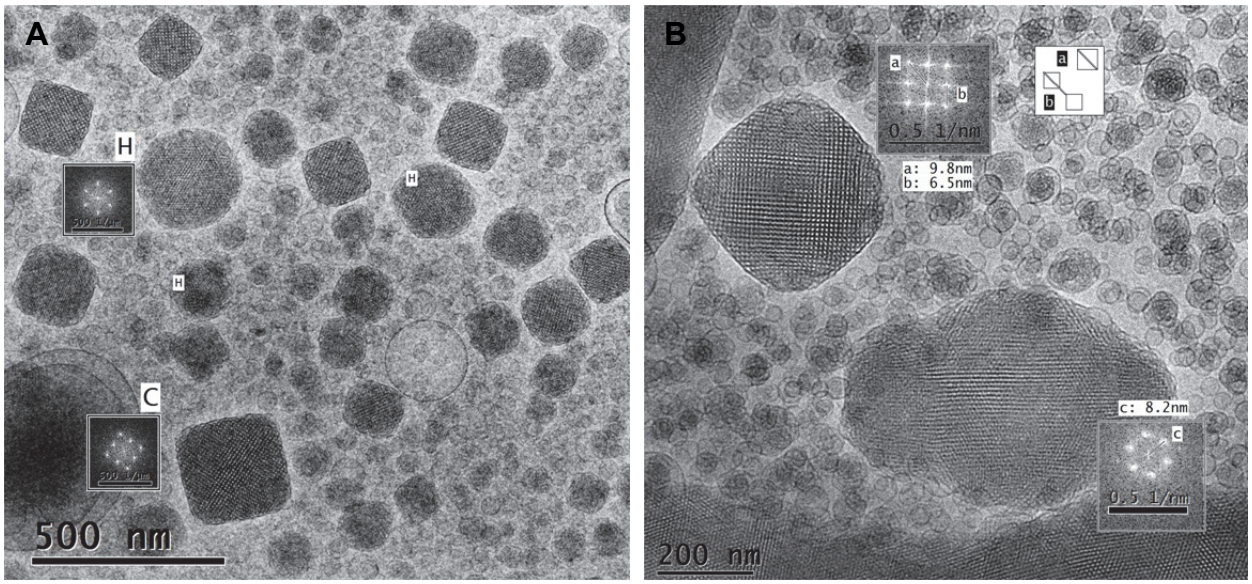

Figure 21. Cryo-transmission electron microscopy images (cryo-TEM) of BC-MAD. The insets show Fast Fourier transforms of some particles.

Well-shaped particles with a homogeneous, ordered inner structure can be observed. Upon closer inspection, images reveal two different internal patterns (labelled C and H), with a predominance of the C over the H structural motif (panel A). It should also be underlined that the H structural motif appears in some larger particles (panel B) with poly-"crystalline" nature,

whereas smaller particles show a single internal structure. Finally, particles with ordered inner structure and vesicular structures attached on their surface can be observed, as previously found by other authors in dispersions produced using monoolein and poloxamer 407 [160].

Fast Fourier transform (FFT) analysis was used to characterize the internal morphology of the particles, since FFT easily allows to obtain an optical diffractogram similar to an electron diffraction pattern. In this way, periodic or repeatable distances in the mesophase structure could be detected, together with the symmetry of the motif. According to the different internal morphologies shown in Figure 21, FFT evidenced two different patterns. The first, observed in the particles with the H structural motif, corresponds to a two dimensional (2D) hexagonal symmetry with 2D lattice parameters $v = w = 8.2$ nm (labelled *c* in panel B) and $\gamma = 120°$. The second, observed in the particles with the C structural motif, corresponds to a rectangular symmetry with 2D lattice parameters $v = 6.5$ nm (labelled a), $w = 9.8$ nm (labelled b) and $\gamma = 90°$. The presence of particles with two different inner structures was also indicated by X-ray diffraction results. However, because both structures are cubic, data definitely prove that MAD dispersions are cubosomes.

Figure 22 (top frames) shows the low angle X-ray diffraction profiles of empty and BC-MAD obtained as a function of temperature. At room temperature, diffraction profiles are characterized by two series of peaks, consistent with the presence of dispersed cubic phase particles of *Pn3m* and *Im3m* symmetry. In other words, in the presence and in the absence of BC, MAD dispersions can exhibit D-type or P-type structures.

Phase coexistence in the monoolein/poloxamer 407/water disperse system has already been observed [89], even if in the same conditions the presence of a pure *Im3m* phase was also reported [161]. As previously discussed [162], the different structural behaviours of MAD may be related to differences in composition (e.g. MO quality, buffer, ionic force of the aqueous solution) and production procedures (e.g. ultrasonication, homogenization, temperature and pressure parameters).

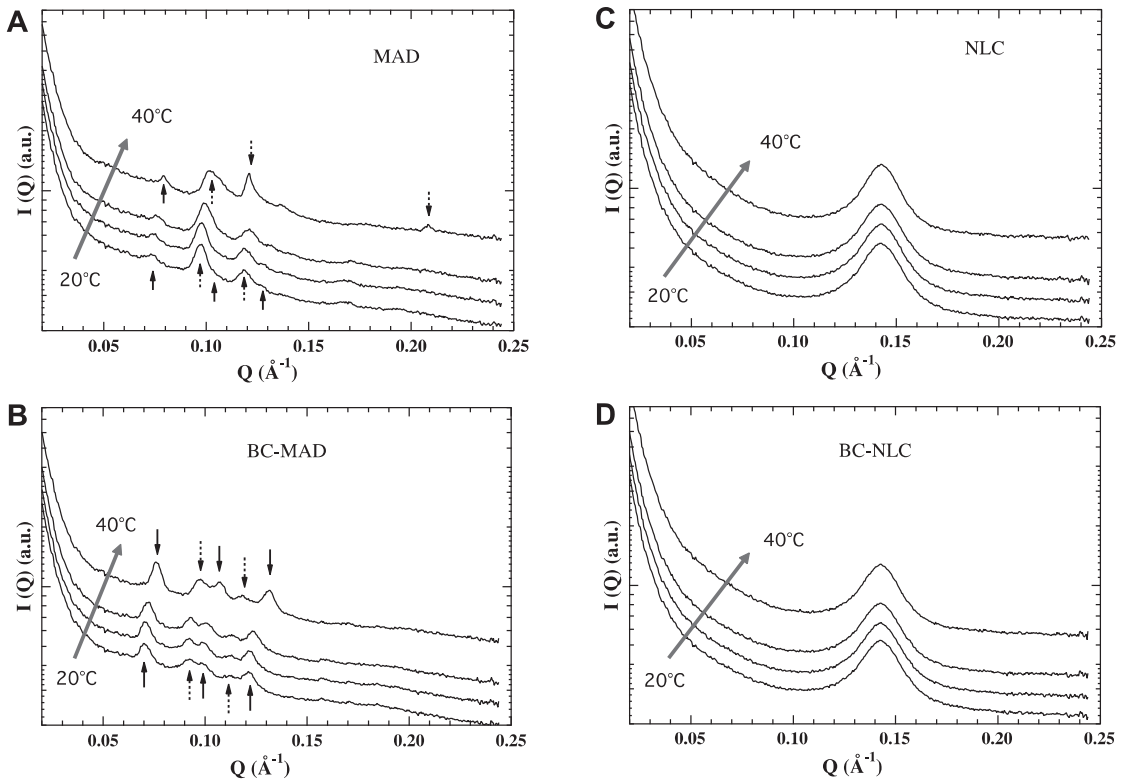

Figure 22. Low-angle X-ray diffraction profiles observed from MAD and NLC samples at different temperatures. Measurements have been performed at 20, 25, 30 and 40°C, scattering curves are stacked consistently, following the direction of the gray arrows. In panels A and B, small arrows indicate the peak indexing: upward, continuous arrow, *Im3m* phase (the indicated peak sequence is [110], [200], [211]); upward, dashed arrow, *Pn3m* phase ([110] and [111]); downward, pointed arrow, *H* phase ([10] and [21]).

However, the present results confirmed that at this poloxamer 407 concentration the cubic and not the vesicular structure is in the equilibrium state, even in the presence of BC. It should be noticed that both types of cubic structures detected in our preparation are bicontinuous, but the P-surface structure only occurs in the MO–water system when a third component is added [163]. Moreover, the lattice constants, which have been derived from peak positions (Table X), are very similar to those reported by Nakano et al. [89]. More interestingly, lattice constants are slightly sensitive to the presence of BC, probably due to an increased hydration of the lipid phases induced by BC.

Cryo-TEM and X-ray diffraction results are in perfect agreement. Indeed, the FFT patterns suggest that the H and C structural motifs correspond to planes normal to the crystallographic directions [111] and [110] of a cubic lattice, respectively (Figure 21). Concerning the H motif, it should be recalled that the projection of a 3D cubic array on 2D is hexagonal when visualized along the [111] direction, and that the corresponding 2D lattice parameters are related to the cubic unit cell dimension *a* by $v = w = a/\sqrt{2}$. This does neither allow to identify the space group of the particle internal structure, nor to differentiate between a hexagonal and a cubic structure. However, the comparison of 2D lattice values with the unit cell dimensions determined by X-ray diffraction (Table X) strongly suggests that the H particles are cubosomes with an inner cubic structure belonging to the *Im3m* space group. It is worthy of mention that only the *Pn3m* and *Im3m* space groups are allowed in cubosome dispersions because those are the only two space groups established in reversed bicontinuous cubic phases in excess water [91] or in reversed bicontinuous cubic phase dispersions [90]. Concerning the C-motif, the observed 2D lattice parameters are consistent with the ideal values for a cubic array ($v = w/\sqrt{2}$) and correspond to a cubic unit cell dimension of 9.8 nm. This value compares well with the unit cell of the *Pn3m* cubic phase determined in the same system by X-ray diffraction (Table X), indicating that C particles are cubosomes with an inner cubic structure belonging to the *Pn3m* space group. Overall, cryo-TEM images of BC-MAD dispersed particles gave strong and direct evidence for the coexistence of cubosomes with two different internal structures: one with a *Pn3m* space group and a lattice parameter of 9.8 nm, and another with *Im3m* space group and a lattice parameter of 11.6 nm.

Table X. Structure identifications and unit cell dimensions observed in the different samples at various temperatures

Sample	Temp. (°C)	Phase and unit cell (nm)									Hydrocarbon chain conformation
MAD	20	1	Im3m	12.11	**1.1**	**Pn3m**	9.16				α
	25	2	Im3m	12.01	**Pn3m**		9.11				α
	30	3	Im3m	11.77	**Pn3m**		8.99				α
	40	4	Im3m	11.25	**Pn3m**		8.71	5	H	6.01	α
MAD/BC	20	**6**	**Im3m**	12.69	6.1	Pn3m	9.66				α
	25	**7**	**Im3m**	12.64	Pn3m		9.65				α
	30	**8**	**Im3m**	12.41	Pn3m		9.58				α
	40	**9**	**Im3m**	11.72	Pn3m		9.14				α
NLC	20-40*	10	L	4.42							β
NLC/BC	20-40*	11	L	4.42							β

When samples show more than one structure the one characterized by the higher X-ray diffraction profile is shown in bold.
*Error in unit cells is ± 0.02 nm * from 20 to 40° C, i.e. 20, 25, 30 and 40 °C*

X-ray diffraction experiments also reveal the thermal stability of MAD. As shown in Figure 22, both D- and P-type cubosomes exist at all the investigated temperatures. However, in empty MAD samples, two other peaks, characteristic of a 2D hexagonal space group, appeared at 40°C. Since at this temperature the peaks of the *Pn3m* cubic structure broadened, it appears that temperature induces a D-type cubosome-to-hexasome phase transition [90,164]. Therefore, even if the inner structure of MAD can be highly dependent on manufacturing parameters and then be relevant for the properties of the dispersions, X-ray diffraction demonstrates that the presence of D-type cubosomes does not cause the complete loss of the cubic state of the particles at relatively high temperatures.

Empty and BC-NLC dispersions have been also characterized [157].

Figure 23 reports cryo-TEM images of NLC dispersions, prepared in the presence of BC. Both panels show deformed hexagonal, elongated and circular platelet-like particles, most likely

viewed on the top. In addition, “needle”-like structures and hemielliptical particles, characterized by inner striations, can be also observed.

If the firsts are probably due to the presence of tricaprin crystals, the second ones correspond to edge-on view of the NLC particles. In panel B, the inset evidences one side-viewed NLC particle, where the distance between the layers is about 5.0 nm.

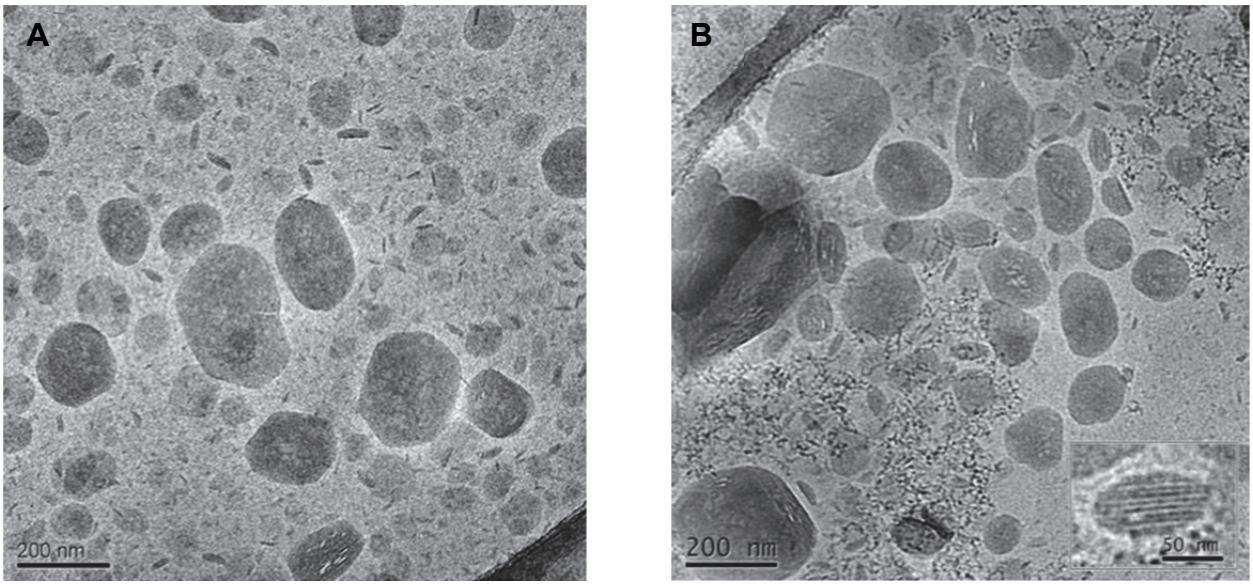

Figure 23. Cryo-transmission electron microscopy images (cryo-TEM) of BC-NLC dispersions.

Low-angle X-ray diffraction results obtained for NLC disperions as a function of temperature are reported in Figure 22, panels C-D. In agreement with previous observation [157], both in the absence and in the presence of BC, the diffraction profile is characterized by a large peak, whose position is unaffected by temperature and BC addition (Table X). The inner lamellar order and the strong structural stability of NLC, even in the presence of BC, appear also confirmed.

4.2.2 BC encapsulation

HPLC analyses revealed that BC recovery after the production process in the filtered dispersion was 70 ± 0.75 % (MAD) and 84 ± 0.58 % (NLC) of the total amount of drug used for the preparation. The values of drug loss were taken in consideration to determine BC encapsulation. SdFFF was employed to obtain information about the drug distribution in the dispersions. During the fractionation, some fractions were collected and analysed by HPLC to quantify the amount of drug contained in the different particle populations of the disperse phase. In figure 20, the concentration of BC determined by HPLC is reported. BC was found to be entirely associated with particles in both MAD and NLC dispersions.

The fraction corresponding to a mean diameter of about 54 nm contains 25% of the total drug, as shown in panel A. The highest amount of BC (46%) is contained in the most representative portion of nanoparticles/vesicles, having a diameter of 98 nm. The remaining 29% of BC is associated with the least representative population of particles, having larger diameters. In fact, cryo-TEM and PCS analyses showed that MAD are mainly characterized by vesicles and cubosomes with 90-100 nm mean diameter, and few structures with larger dimensions.

Also for NLC, whose PSD is reported in panel B, the highest amount of BC (52%) is contained in the most representative fraction, characterized by particles with a mean diameter of ~103 nm. The fraction corresponding to a mean diameter of ~59 nm contains only 3.5% of the total drug, the remaining 44.5% of BC being found into a less representative population of larger particles.

4.2.3 In vitro activity

The method employed for the determination of drug release kinetics from nanosystems is a crucial point; *in vitro* methods have been often criticized for different reasons including: the difficult application to lipophilic drugs and the scarce predictivity with respect to the *in vivo* bioavailability [84,165].

Indeed slow drug release from nanoparticles is often claimed, but a slow appearance of drug in

the release medium can be an artificial result of an inadequate experimental setup rather than a true property of the nanosystem [157]. Accordingly, we employed different *in vitro* systems and receiving phases to analyse their effect on BC release from NLC and MAD (Table XI).

Table XI. *In vitro* systems and receiving phases employed for NLC and MAD

Method	Formulations	Receiving phase			Agitation	Separation between donor and receiving phase	Sample processing after withdrawal	Glassware
		Composition	pH	Volume (ml)				
Dialysis	NLC/MAD	citrate buffer 50 mM/ethanol (50:50, %)	3.5	200.0	Horizontal shaker	Ultrafiltration membrane	none	beaker
Dialysis	NLC	citrate buffer 50 mM/methanol (80:20, %)	3.5	200.0	Horizontal shaker	Ultrafiltration membrane	dilution with ethanol	beaker
Dialysis	MAD	citrate buffer 50 mM/methanol (50:50, %)	7.0	200.0	Horizontal shaker	Ultrafiltration membrane	dilution with methanol	beaker
Reverse dialysis	MAD	citrate buffer 50 mM/methanol (50:50, %)	3.5	200.0	Horizontal shaker	Ultrafiltration membrane	none	beaker
Reverse dialysis	MAD	water/ethanol (50:50, %)	7.0	200.0	Horizontal shaker	Ultrafiltration membrane	none	beaker
USP XXII paddle	NLC	poloxamer 188 (0.1%, w/v) in phosphate buffer (100 mM)	7.4	200.0	Paddle	none	filtration (nylon, 100 nm pore)	flanged vessel
Franz cell	MAD	phosphate buffer (100 mM)	7.4	5.0	Magnetic stirring	nylon membrane	none	Franz cell

The use of a receiving phase based on aqueous buffers (often claimed to be physiological) usually leads to a negligible release of BC, because of its poor solubility in media with a pH > pKa (5.87) [157]. In reason of this fundamental constrain, the determination of BC release was conducted using a receiving phase characterized by a non-physiological pH and relatively high proportion of organic solvents in mixture with water.

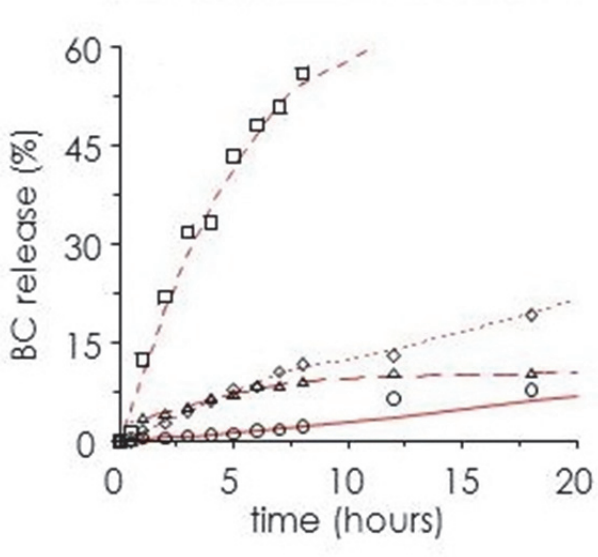

Figure 24. BC release kinetics from NLC determined by different dialysis method using different receiving phase.

For instance, figure 24 reports the BC release kinetics from NLC determined by dialysis method using different receiving phases (see Table XI). The use of citrate pH 3.5 buffer (circles) led to the slowest release (3% of BC released after 10 hours), the addition of an organic solvent, citrate/methanol (80/20 %, v/v) caused an increase of BC release up to 12% in the same period of time (diamonds); the faster release of BC was observed when the amount of organic solvent was further increased up to 50% (citrate/ethanol, 50:50 v/v), resulting in a 60% BC release in 10 hours.

As comparison, in figure 24 the release profile of BC is also reported from NLC determined by USP XXII paddle method, using as receiving buffer a poloxamer solution in phosphate buffer (triangles). This *in vitro* method resulted in a BC release of 11% after 10 hours.

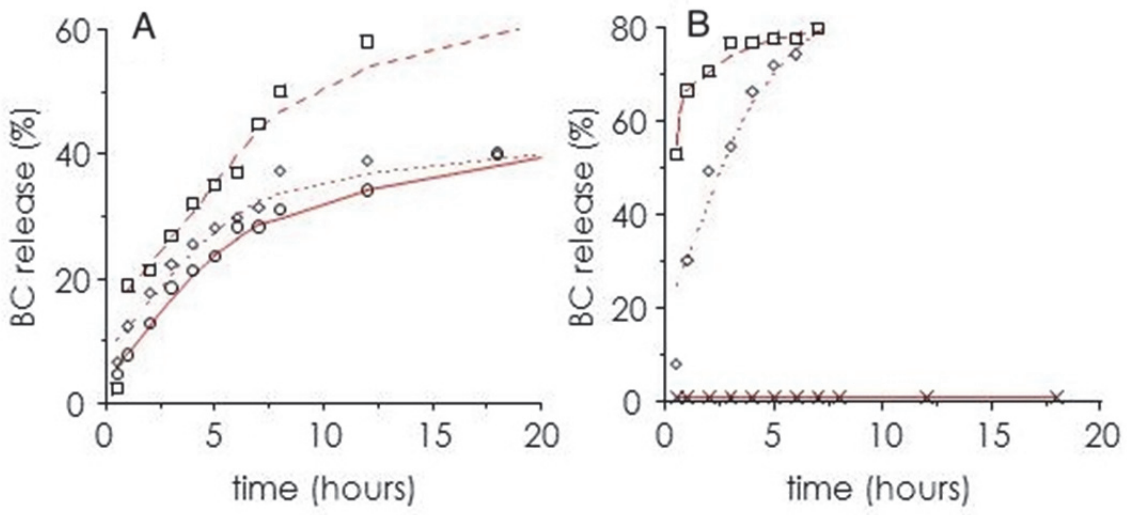

Figure 25. BC release kinetics from MAD determined by different dialysis method (A) or by reverse dialysis and Franz cell methods (B).

A further analysis of the effect of different release method was conducted on MAD (Fig. 25). For instance, figure 25A reports the effect of the receiving phase on the BC release profiles determined by dialysis method. Notably, in the case of MAD, plain citrate buffer (circles) or mixture water/methanol (50:50 v/v) (diamonds), resulted in similar profiles, characterized by BC release, after 12 h, comprised in the range of 30-35%. A remarkably higher BC release (58% after 12 h) was observed when, as receiving phase, a mixture of citrate/ethanol (50:50 v/v) was employed. These results reflect the influence of the organic phase on the solubility of BC.

Furthermore, figure 25B reports the BC release kinetics from MAD obtained by reverse dialysis and Franz cell methods. In the case of reverse dialysis, two receiving phases were tested, namely citrate/ethanol (50:50 v/v) (squares), or water/methanol (80:20 v/v) (diamonds) mixtures. In both cases BC was released from MAD more rapidly with respect to the other above reported experimental conditions, in fact 60% of release was reached within 4 h. The presence of ethanol promotes the release of BC because the solvent interacts with the MAD components [88], presumably resulting in a final disorganization of the cubic structure and drug leakage. Lastly we tested the Franz cell method using a dialysis membrane and 0.1 M phosphate buffer (pH

7.4) as receiving phase, that resulted in an almost negligible BC release within a period of 24 h (BC < 0.8%).

4.2.4 In vivo tests

In 6-OHDA hemilesioned rats, motor impairment mainly affects the side of the body contralateral to the denervated hemisphere (i.e. the toxin injection side). Consistently, the immobility time of the ipsilateral paw (35.7 ±1.9 sec; n=42) was lower compared to that of the contralateral (parkinsonian) one (47.4 ± 1.9, n=42). Moreover, the number of steps made by the ipsilateral paw was higher (11.1 ± 0.4; n=46) than that made by the contralateral one (1.9 ± 0.1; n=46).

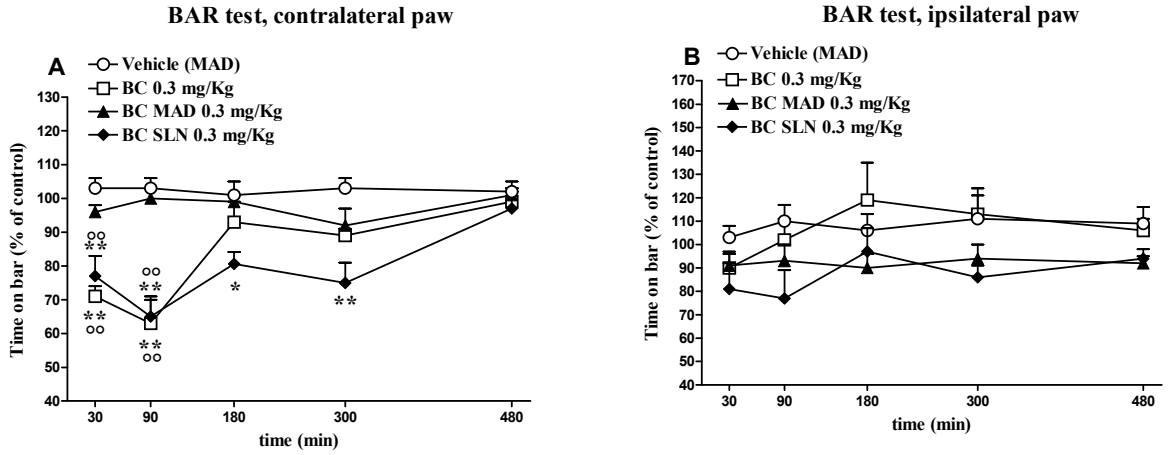

Figure 26. Systemic administration via i.p. of free bromocriptine (BC) and bromocriptine encapsulated in MAD (BC-MAD) or nanoparticles (BC-NLC) in hemiparkinsonian rats attenuated akinesia in the bar test. The administered dose of BC was always 0.3 mg/Kg. Rats injected with vehicles (empty MAD or NLC) are also shown. Immobility time was calculated at different time-points (30, 90, 180, 300 and 480 min from injection) both at the contralateral (panel A) and ipsilateral (panel B) forepaw (in sec), and expressed as percent of pre-treatment values. Data are means ± SEM of 7-11 animals per group.

**p<0.01 different from empty NLC.

°°p<0.01 different from empty MAD and NLC.

Repeated measure ANOVA on the immobility time at the contralateral paw in the bar test (Fig. 26A) revealed main effects of treatment ($F_{4,36}$=15.83, p<0.0001) and time ($F_{4,155}$=7.51, p<0.0001), and a time x treatment interaction ($F_{16,155}$=3.58, p<0.0001). Post-hoc analysis showed that both free BC and BC-NLC reduced the time spent on bar (i.e. attenuated akinesia) compared to vehicle-treated animals, although the action of BC-NLC was more prolonged (Fig. 26A). Indeed, both free BC and BC-NLC produced a significant reduction of akinesia 30 min after administration (~77 and ~71 % of control, respectively) and were maximally effective after 90 min (~63 and ~65 % of control, respectively). However, the effect of free BC was not significant after 3 hr (~93 %) whereas that of BC-NLC was still detectable up to 3 hr after administration (~80 %). No significant changes of the immobility time at the ipsilateral paw were induced by any BC formulations (Fig. 26B).

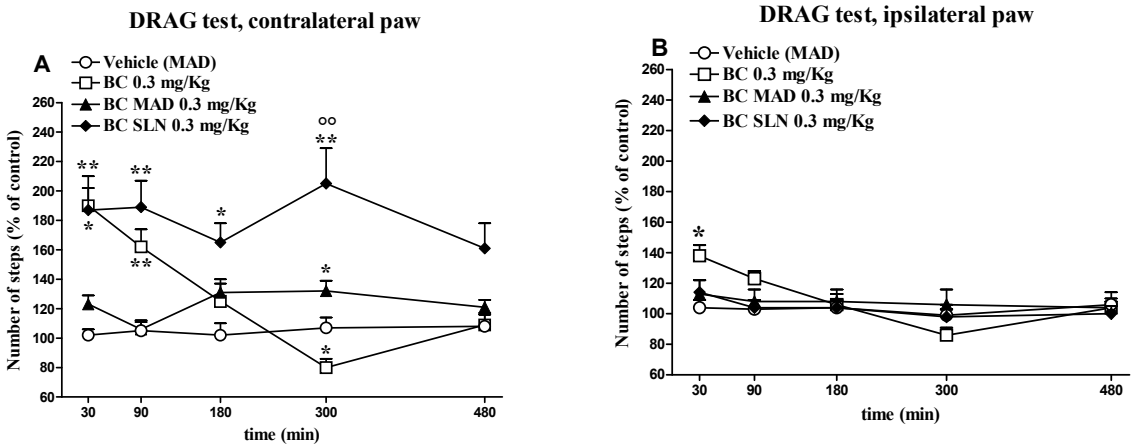

Figure 27. Systemic administration via i.p. of free bromocriptine (BC) and bromocriptine encapsulated in MAD (BC-MAD) or nanoparticles (BC-NLC) in hemiparkinsonian rats attenuated akinesia/bradykinesia in the drag test. The administered dose of BC was always 0.3 mg/Kg. Rats injected with vehicles (empty MAD or NLC) are also shown. The number of steps was calculated at different time-points (30, 90, 180, 300 and 480 min from injection) both at the contralateral (panel A) and ipsilateral (panel B) forepaw, and expressed as percent of pre-treatment values. Data are means ± SEM of 7-13 animals per group.

*p<0.05; **p<0.01 different from empty NLC.

°°p<0.01 different from empty MAD and NLC.

Repeated measure ANOVA on the number of steps at the contralateral paw in the drag test (Fig. 27A) revealed main effects of treatment ($F_{4,36}$=41.31, p<0.0001) and time ($F_{4,185}$=3.38, p=0.0106) and a significant time x treatment interaction ($F_{16,185}$=3.80, p<0.0001). Post hoc analysis revealed that the three BC preparations improved stepping activity at the contralateral paw although with different efficacies and time-courses. As shown in the bar test, both free BC and BC-NLC elevated stepping activity at 30 min after administration (both ~190 % of control). However, the effect of free BC vanished after 3 hr (~125 %) whereas that of BC-NLC was significant both at 3 hr (~165 %) and 5 hr (~205 %) after administration. At 8 hr after administration, rats treated with BC-NLC still showed an elevated stepping activity (~160 %), although this value did not reach the level of statistical significance. At variance with the bar test, BC-MAD was able to attenuate motor disability in the drag test, causing a mild elevation at 3 hr (~131 %) and 5 hr (~132 %) from administration.

Also stepping activity at the ipsilateral paw was affected by BC treatment (Fig. 27B). Repeated measure ANOVA on the number of steps at the ipsilateral paw did not reveal main effect of treatment ($F_{4,36}$=0.96, p=0.44) but a significant effect of time ($F_{4,185}$=9.82, p<0.0001) and a time x treatment interaction ($F_{16,185}$=3.43, p<0.0001). Post hoc analysis showed that among the different BC formulations, only free BC improved stepping activity at the ipsilateral paw, specifically at 30 min after administration (~139 %).

Among the various therapeutic applications of BC, we chose to focus on the antiparkinsonian activity since great therapeutic value has been attributed to formulations capable to provide continuous DA receptor stimulation [166,167]. Indeed, it has been demonstrated that long-term side effects of L-DOPA (mainly dyskinesia) arise from non-physiological “pulsatile” stimulation of DA receptors, which parallels plasmatic drug levels [168]. Thus, continuous delivery or sustained release formulations of L-DOPA have been proved to be less dyskinesiogenic than conventional formulations. Consistently, DA receptor agonists (the most effective alternative to L-DOPA) are less dyskinesiogenic than L-DOPA, probably due to the longer half-life. Achieving a stable and prolonged DA receptor stimulation may also be advantageous in the case of DA

agonists, as it allows for a reduction of the frequency of administration and occurrence of side effects at peak levels. In the present study we employed two different behavioural tests providing complementary information on motor function: the bar and the drag tests. The responses to BC and its NLC formulation were consistent in both tests. Thus, BC caused a reduction of immobility time (i.e. reduced akinesia) and improvement of stepping activity (i.e reduced akinesia/bradykinesia), which lasted for at least 90 min and disappeared after 3 h from administration. BC encapsulated in NLC essentially mimicked these effects providing a more prolonged attenuation of motor disability which lasted for at least 5 h and vanished within 8 hr. The obtained results extend our previous finding [157] and confirm the ability of BC-NLC to provide longer lasting therapeutic benefit compared to conventional BC formulations. The finding that free BC caused a rapid and transient (30 min) elevation of stepping also at the ipsilateral paw may reflect differences in drugs kinetics since it was not replicated by BC-NLC. In fact, in keeping with the view that conventional BC preparations result in higher peak levels, BC might also improve motility at the ipsilateral paw, which is controlled by the undenervated striatum.

Quite remarkably, BC-MAD was ineffective in the bar test and caused only a mild and delayed elevation of stepping activity in the drag test.

The different in vivo efficacies of BC-MAD and BC-NLC could be attributed to differences in nanoparticulate morphology. In fact, the former are characterized by the coexistence of cubosomes and vesicles while the latter are solid matrix systems.

It has been demonstrated that the intraperitoneal administration prolongs the blood circulation of colloidal drug carriers with respect to the intravenous administration, due to slow absorption of the carrier from the abdominal cavity [169]. On the other hand it is known that colloidal drug carriers are rapidly opsonised and cleared by the macrophages of the reticulo-endothelial system (RES). Thus, as a general rule, nanosystems are mostly taken up by the liver and the spleen within minutes after systemic administration [170]. In the case of BC-MAD, it can be hypothesized that cubosomes are mainly sequestered by the peritoneal and RES macrophages,

as shown for liposomes and nanoparticles [171,172]. Therefore, the mild and sustained effect of BC-MAD may be due to the smaller vesicular liquid-like component of MAD that is responsible for prolonging the half-life of the incorporated drug, having a long circulating time.

Conversely, the NLC structure allows to provide therapeutic BC concentrations to the brain for a long period of time [157]. This might be related to the ability of NLC to pass the BBB [151,155] and/or to a longer stability of NLC in the blood. In fact, previous studies [173] demonstrated that after intraperitoneal administration, nanoparticles show a biphasic absorption: an initial rapid distribution into blood, followed by a slow disposition from peritoneum, resulting in sustained drug release. Moreover NLC produced in the presence of poloxamer 188 in the aqueous phase, may behave as “stealth carriers”, thus being somewhat protected by opsonisation [156].

5. NLC AND SLN FOR THE DELIVERY OF L-DOPA DERIVATIVES

5.1 INTRODUCTION

Parkinson's disease (PD) is a neurodegenerative disorder associated primarily with loss of DA neurons in the nigrostriatal system [98]. Current therapy for PD is essentially symptomatic, and L-dopa (LD), the direct precursor of DA, is the treatment of choice for this neurodegenerative disease, despite the fact that several DA receptor agonists have been introduced for the treatment of PD [174]. LD is readily transported across the blood–brain barrier and is converted to DA by aromatic l-aminoacid decarboxylase (AADC).

After a good initial response, complications are associated with long-term therapy; these include motor fluctuations, dyskinesias, mental changes and loss of efficacy [175]. The main disadvantages of LD are low water solubility, its sensitivity to chemical and enzymatic oxidation and peripheral decarboxylation. With the aim to prolong the pharmacological activity, enhance absorption and provide a protection against metabolism, the group of Professor Di Stefano at the University of Chieti studied LD derivatives as potential prodrugs [117, 119, 176]. All the new compounds showed chemical stability at acidic pH and also at the physiological pH; a relatively slow release of LD in rat and human plasma was observed. However, all the compounds are characterized by a very low solubility in water, limiting their administration.

NLC and SLN have been used as drug carriers with the aim to enhance solubility, control the delivery, prolong the prodrug effect and reduce the toxicity.

5.2 RESULTS AND DISCUSSION

5.2.1 *Characterization of dispersions*

The NLC were obtained by dispersion of the lipidic phase in the aqueous phase. Four new synthetized LD derivatives, named Der-A, Der-B, Der-C and Der-D, were used as drug models as reported in chapters 2 and 3.

After production, nanoparticles were characterized in terms of morphology and dimensions.

Size and distribution of NLC were determined using the photon correlation spectroscopy (PCS). The analyses were made immediately after preparation and periodically at regular intervals for 2 months, in order to investigate the stability of nanoparticles by time.

In tables XII and XIII are reported the values of mean diameters and polydispersities obtained within two months.

Table XII. Mean diameters of NLC as determined by PCS

Day	Mean diameter (nm) ± s.d.				
	NLC	Der-A NLC	Der-B NLC	Der-C NLC	Der-D NLC
0	191.5 ± 3.7	197.0 ± 2.1	180.1 ± 1.0	188.5 ± 2.9	194.1 ± 2.1
10	193.8 ± 1.6	193.7 ± 2.1	n.d.	n.d.	196.6 ± 1.6
20	n.d.	198.7 ± 3.5	n.d.	n.d.	188.3 ± 0.6
30	192.1 ± 5.5	192.3 ± 0.8	186.9 ± 1.4	189.6 ± 1.3	n.d.
40	n.d.	187.9 ± 3.2	n.d.	n.d.	188.6 ± 0.5
50	n.d.	193.8 ± 0.3	n.d.	n.d.	186.9 ± 1.3
60	188.2 ± 0.9	186.6 ± 1.1	186.8 ± 5.2	182.8 ± 0.8	186.8 ± 3.5

s.d. = standard deviation calculated after 5 determinations on different batches of the same type of dispersion
n.d. = non determined

Table XIII. Polidispersity indexes of NLC as determined by PCS

Day	Polydispersity ± s.d.				
	NLC	**Der-A NLC**	**Der-B NLC**	**Der-C NLC**	**Der-D NLC**
0	0.11 ± 0.02	0.20 ± 0.04	0.36 ± 0.01	0.21 ± 0.01	0.21 ± 0.02
10	0.16 ± 0.01	0.22 ± 0.02	n.d.	n.d.	0.21 ± 0.01
20	n.d.	0.20 ± 0.02	n.d.	n.d.	0.21 ± 0.01
30	0.19 ± 0.07	0.25 ± 0.04	0.25 ± 0.01	0.27 ± 0.01	n.d.
40	n.d.	0.26 ± 0.05	n.d.	n.d.	0.25 ± 0.01
50	n.d.	0.24 ± 0.04	n.d.	n.d.	0.20 ± 0.03
60	0.24 ± 0.04	0.21 ± 0.02	0.25 ± 0.01	0.24 ± 0.01	0.20 ± 0.02

s.d. = standard deviation calculated after 5 determinations on different batches of the same type of dispersion
n.d. = non determined

Analysing the obtained values, it should be noted that in general a decrease of about 5-10 nm of the diameters occur by time. In addition, there are no difference in size between empty and drug containing NLC. Concerning the polydispersity indexes, empty NLC showed an increase of 0.1 units by time, while other formulations no variations were remarked, indicating that also in the case of derivatives containing, NLC are mono-disperse maintaining its size over time.

Cryo-transmission electron microscopy allowed an investigation of the inner structure of nanosized formulations, empty and derivatives containing. In figure 1, the cryo-TEM images of Der-A and Der-B containing NLC are reported as an example. No differences in term of morphology are evident for Der-C and Der-D NLC. As shown in figure 28, the structure of nanoparticles appears round and elliptical in shape due to the position of the nanoparticle with respect to the site of observation, i.e. round if the nanoparticle is placed at 180°, needle-like if disposed at 90°, elliptical in intermediate positions [159].

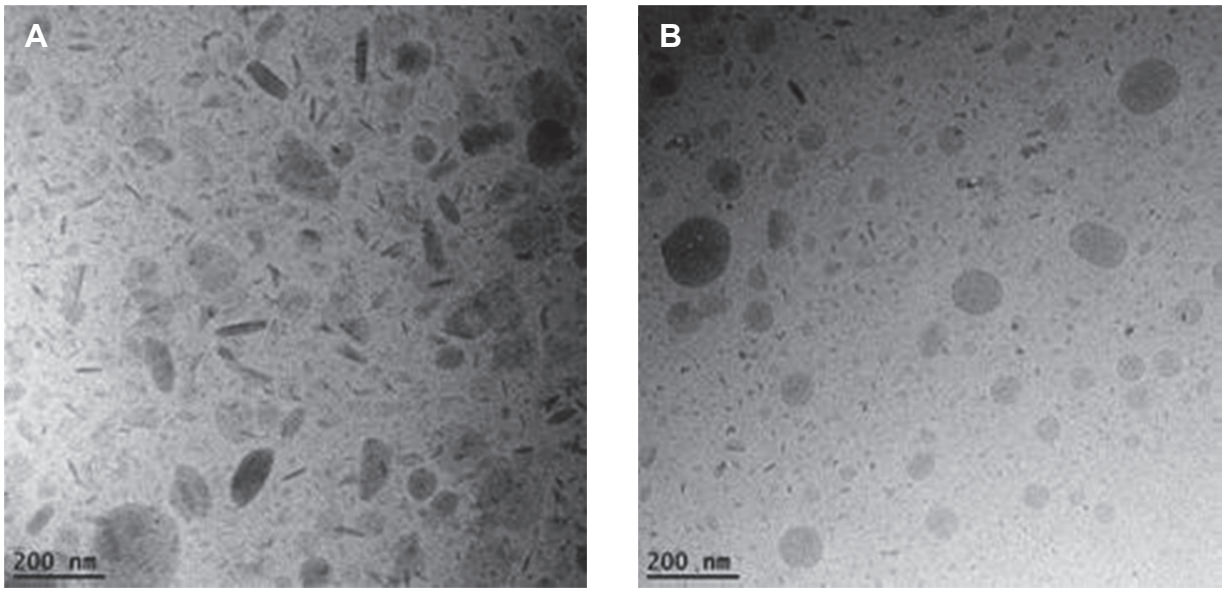

Figure 28. Cryo-transmission electron microscopy images (cryo-TEM) of Der-A NLC (Panel A) and Der-B NLC (Panel B). Data are the mean of 5 determinations on different dispersions.

5.2.2 *Prodrug recovery*

The amount of drug encapsulated in NLC was evaluated by high-performance liquid chromatography (HPLC) using a reversed-phase column as described in the experimental section. As reported in Table XIV, drug recovery after NLC production was almost quantitative of the total amount used for the preparation, except for Der-B. The recovery was 72.91% in the case of Der-A NLC, 75.31% in the case of Der-C and 81.87% in the case of Der-C NLC dispersions.

Der-B NLC showed a drug incorporation of 24.57% ± 5.89, probably due to the loss of the active substance during the preparation procedure, especially when the lipid phase is added to the poloxamer aqueous solution.

Table XIV. LD derivatives content in NLC

	% recovery	s.d.
Der-A NLC	72.91	15.45
Der-B NLC	24.75	5.89
Der-C NLC	75.31	10.68
Der-D NLC	81.87	18.67

The reported results represent the average of four independent experiments ± s.d.

5.2.3 *In vitro experiments*

The *in vitro* release from derivatives-containing NLC was studied by the dialysis method, mimicking the conditions of a release after *in vivo* intraperitoneal administration of the NPs dispersions.

The obtained results are summarized in Figure 29. It can be observed that all NLC formulations provide a controlled release of the drug.

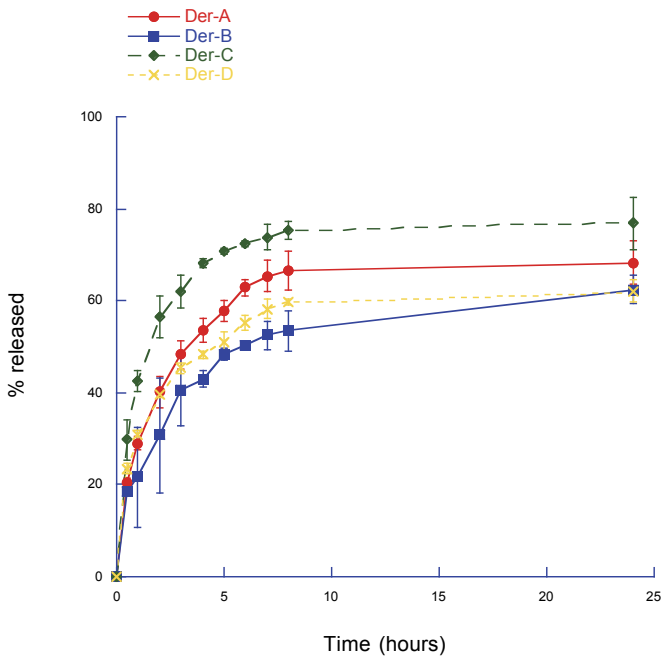

Figure 29. LD derivatives release kinetics from NLC determined by dialysis method

In particular, after the first hour Der-A and Der-B NLC released the 20% of total drug content, while Der-C and Der-D NLC released a higher amount being 25-30%. After 24 hours, the drug released reached almost 70% of total drug content as reported in table XV.

Table XV. Percentages of derivatives release after 24 hours.

	% release	**s.d.**
Der-A NLC	68.24	4.70
Der-B NLC	62.50	3.04
Der-C NLC	76.90	5.73
Der-D NLC	62.14	2.52

The reported results represent the average of three independent experiments ± s.d.

From the analyses of the obtained data, it is possible to notify that Der-C NLC showed the greater percentages of release if compared to other derivatives containing NLC.

However, analysing the drug recovery and *in vitro* results together, it is noteworthy that Der-A NLC are characterized by the best profile because they combine high percentages of drug recovery with great kinetics release in 24 hours. These results induced us to choose Der-A NLC dispersions for the subsequent *in vivo* tests.

5.2.4 In vivo tests

Firstly, the rats subjected to these experiments, were damaged with 6-OHDA (emiparkinsonians rats). The lesion with 6-OHDA was made unilaterally, presenting an important motor deficit in the contralateral body part at the site of injury.

After the lesion, rats were stabled and kept to rest for a period of two weeks, after which it was performed a behavioural test to evaluate the preliminary level of depletion (rotarod test). The

test allowed assessing the overall physical activity that consists in the evaluation of coordination, posture, balance and resistance. Evaluation of motor performance was done by the bar and drag tests.

The bar test obtained results, comparing the LD (used as positive control) with the derivatives-containing NLC, are showed in Table XVI.

Table XVI. Time of permanence on the lignum support.

	Control		30 min.		90 min.	
	IL	CL	IL	CL	IL	CL
LD (sec.)	36.0 ± 10.0	56.5 ± 5.1	20.8 ± 12.2	41.0 ± 5.1	19.3 ± 5.5	39.5 ± 5.7
Der-A NLC (sec.)	39.2 ± 12.8	55.0 ± 7.0	32.2 ± 10.4	45.6 ± 11.8	34.4 ± 13.2	49.2 ± 10.4

The reported results represent the average of 3 independent experiments ± s.d.
IL: Ipsilateral; CL: Controlateral

The obtained data showed that after 30 minutes from administration the time of permanence of the contralateral paw in animals treated with LD and Der-A NLC are almost superimposable being 41 and 45.6 sec. respectively. On the other hand, after 90 minutes the LD administration resulted in a greater reduction of the time spent on the step (i.e. akinesia) than Der-A NLC (39.5 sec. vs 49.2 sec.).

In addition, after 90 min from LD administration it can be noticed a substantial difference of the ipsilateral paw time of permanence (19.3 sec.) if compared to the contralateral paw (39.5). Conversely, in the case of Der-A NLC the ipsilateral paw permanence time on the step was not statistically different from the data concerning the contralateral side (Table XVI).

The drug test results, obtained counting the number of steps made by each paw, are reported in table XVII.

Table XVII. Number of steps made by each paw.

	Control		30 min.		90 min.	
	IL	CL	IL	CL	IL	CL
LD (sec.)	14.0 ± 1.3	1.3 ± 0.3	16.3 ± 1.1	4.0 ± 2.1	15.3 ± 0.9	2.7 ± 1.7
Der-A NLC (sec.)	11.8 ± 1.8	1.3 ± 0.5	13.2 ± 4.2	2.5 ± 1.4	12.2 ± 4.4	2.7 ± 1.8

The reported results represent the average of 3 independent experiments ± s.d.
IL: Ipsilateral; CL: Controlateral

On the other hand, the drag test data showed that LD and Der-A activity are superimposable. This result suggests the ability of NLC to successfully cross the blood-brain barrier by improving the pharmacological activity of the derivatives contained. In particular, the obtained data corroborate the results reported in literature about NLC capability to cross the intact blood-brain barrier via endocytosis and deliver the drug through diffusion.

5.2.5 *Der-A SLN characterization*

Considering the best characteristics shown in the previous tests and the possibility to increase the drug recovery, Der-A was chosen as model prodrug for SLN incorporation. The choice of formulating SLN for the delivery of Der-A was motivated by the necessity to increase the incorporation percentages obtained by the use of NLC. SLN, based on Tristearin, Labrasol and soybean phosphatidylcholine, were prepared, containing 0.125, 0.25 and 0.5 mg/ml of Der-A and named Der-A SLN (1x), Der-A SLN (2x) and Der-A SLN (4x), respectively.

The obtained SLN were firstly characterized in dimensions by PCS. The characterization was performed immediately after the production and up to two months. These analyses permitted to evaluate the stability of formulations.

In tables XVIII and XIX are reported the acquired results, related to mean diameters and polydispersity, respectively.

Table XVIII. Mean diameters of Der-A SLN as determined by PCS.

Day	Mean diameter (nm) ± s.d.		
	Der-A SLN (1x)	Der-A SLN (2x)	Der-A SLN (4x)
0	158.8 ± 2. 2	161.9 ± 0.8	149.9 ± 3.2
30	152.85 ± 0.9	164.5 ± 3.7	147.2 ± 2.8
120	151.7 ± 3.4	160.5 ± 2.4	146.1 ± 0.8

s.d. = standard deviation calculated after 5 determinations on different batches of the same type of dispersion
n.d. = non determined

Table XIX. Polydispersity of SLN as determined by PCS.

Day	Polydispersity ± s.d.		
	Der-A SLN (1x)	Der-A SLN (2x)	Der-A SLN (4x)
0	0.37 ± 0.02	0.36 ± 0.04	0.36 ± 0.01
30	0.40 ± 0.01	0.39 ± 0.02	0.43 ± 0.03
120	0.38 ± 0.04	0.40 ± 0.02	0.39 ± 0.02

s.d. = standard deviation calculated after 5 determinations on different batches of the same type of dispersion
n.d. = non determined

Comparing the obtained data, it can be observed that on the day of production Der-A SLN (4x) showed the smaller nanoparticle dimensions while Der-A SLN (2x) were characterized by the bigger mean diameters, even if the difference between the two formulations was of only 12 nanometres.

After four months, all the preparations didn't show a revealing change in dimensions and in particular, Der-A SLN (2x) resulted the most stable with a change in dimensions of only 1.5 nanometres.

In all cases, after 120 days the polydispersity resulted practically unchanged.

Cryo-transmission electron microscopy analyses were conducted in order to shed light on the

morphology of the dispersed particles in SLN dispersions. Figure 30 reports cryo-TEM images of SLN dispersions empty (panel A) and loaded with the prodrug (panel B).

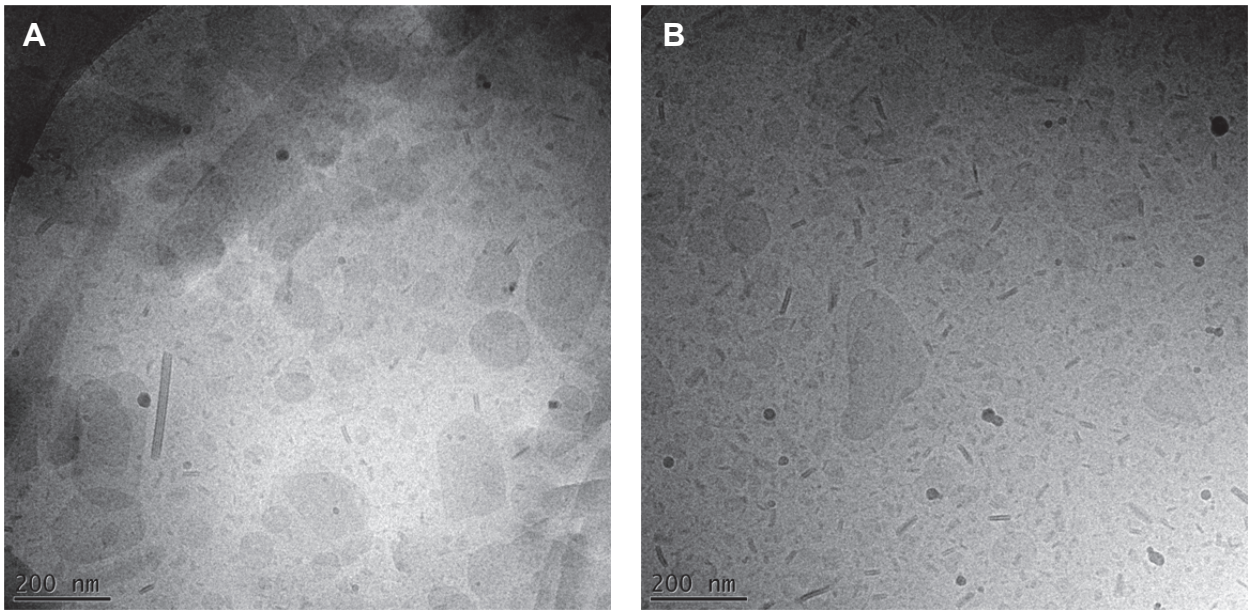

Figure 30. Cryo-transmission electron microscopy images (cryo-TEM) of empty SLN (Panel A) and Der-A SLN (2x) (Panel B). Data are the mean of 5 determinations on different dispersions.

In both cases, the SLN dispersions were characterized by weak circular and ellipsoidal structures representing thin platelets in top view. If the particles were viewed edge-on, they appeared as dark rods or “needles” since, in this position, the increased thickness of the structures leads to a darker appearance. The rod- or needle-like particles in the electron micrographs were typically of a thickness of about 10 nm and below. The presence of Der-A didn’t affect the structure of nanoparticles.

5.2.6 *Prodrug content of formulations*

The quantity of Der-A encapsulated in SLN was determined by HPLC. As shown in table XX, the highest quantity of prodrug was loaded to Der-A SLN (1x), but also in the case of Der-A SLN (2X) the encapsulation percentage was significant, being 71.21%.

On the contrary, in the case of Der-A SLN (4x) the quantity of loaded prodrug was only 43.36%. It is possible to hypothesize that, due to the high amount of Der-A to be incorporated to the SLN lipid phase, a great quantity of prodrug was lost during the preparation process. This evidences a limit especially thinking to a scaling-up development and for this reason, Der-A SLN (5x) were not considered in the following analyses.

Table XX. Der-A content in SLN

	% recovery	s.d.
Der-A SLN (1x)	83.01	9.38
Der-A SLN (2x)	71.21	7.76
Der-A NLC (4x)	43.36	6.63

The reported results represent the average of four independent experiments ± s.d.

5.2.7 *DSC characterization*

Calorimetric analysis on Der-A SLN (1x) and Der-A SLN (2x) were performed firstly by a heating scan from 5 to 65 °C (2 °C/min) and secondly by a cooling ramp from 65 to 5 °C (4 °C/min). The test were repeated for at least three times.

All SLN showed the first calorimetric curve different from the other curves.

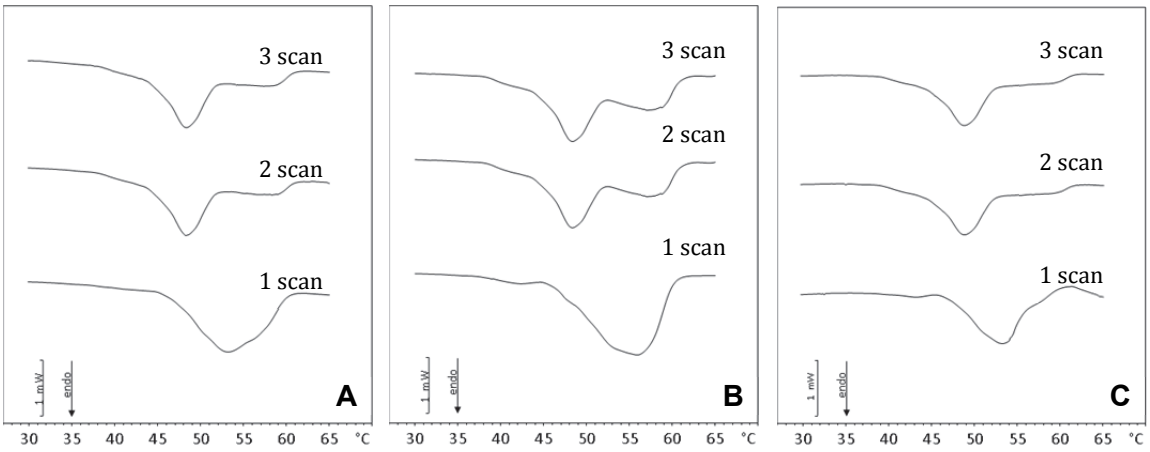

Figure 31. Calorimetric curves, in heating mode, of (A) empty SLN (B) Der-A SLN (1x) and (C) Der-A SLN (2x).

The first scan calorimetric curve of empty SLN (Fig. 31A), was characterized by a main peak at 56.4 °C and three shoulders at lower temperatures (about 43.0, 49.0 and 53.5 °C, respectively). In the second and third scans, we could observe: a shoulder at about 43.0 °C (overlapping that of the first scan), a well-defined peak at 48.4 °C (overlapping the second shoulder of the first scan), and a big, broad peak at about 57 °C (overlapping the third shoulder and the main peak of the first scan).

Der-A SLN (1x) showed (Fig. 31B) five calorimetric signals in the first scan: a small peak at about 43.0 °C, two shoulders at 46.0 and 50.0 °C, respectively, a main peak at 53.0 °C and a shoulder at about 57.0 °C. In the second and third scans three signals were visible: a shoulder at about 43.0 °C (that in the first scan was a peak), a main peak at 48.3 °C and a large shoulder at higher temperature.

The first calorimetric scan of Der-A SLN (2x) (Fig. 31C) showed the same signals of the first scan of Der-A SLN (1x) with the only exception represented by the loss of the shoulder at higher temperature. The second and third scans are similar to those of SLN containing 1X of prodrug. This behaviour could be due to a rearrangement of the molecules of the SLN on the first heating that remains unaltered in the subsequent scans.

The comparison of the first calorimetric scans of unloaded and prodrug loaded SLN gave important information (Fig. 32A and 32B).

The first scans showed interesting differences with the exception of the small peak at about 43.0 °C which was present in all SLN. With respect to empty SLN, the main peak of Der-A SLN moved towards lower temperature. In Der-A SLN (1x) two shoulders were present at about 50.5 °C and 57.0 °C, respectively. In Der-A SLN (2x) only the shoulder at about 50.5 °C was visible. In addition the peak intensity decreased on going from empty to Der-A SLN (2x). With regard to the second scan, the most evident difference concerned the broad peak at about 58.0 °C whose intensity decreased as the amount of prodrug in the SLN increased.

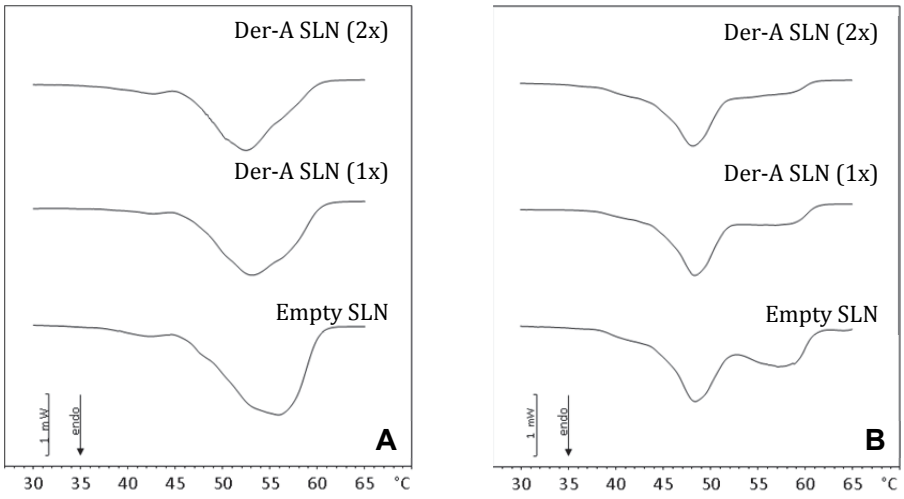

Figure 32. Calorimetric curves, in heating mode, of (A) first scan of empty and Der-A SLN and (B) second scan of empty and Der-A SLN.

These results clearly indicate that the prodrug affects the thermotropic behaviour of SLN and that the effect is related to the amount of prodrug loaded. This evidence was strengthened by the enthalpy change values (of the second scans) reported in figure 33 as a function of prodrug in the SLN. The enthalpy change decreases with the increase of prodrug amount in the SLN. These data suggest that the Der-A arranged inside the SLN and caused a decrease of the lipid molecules cooperativity.

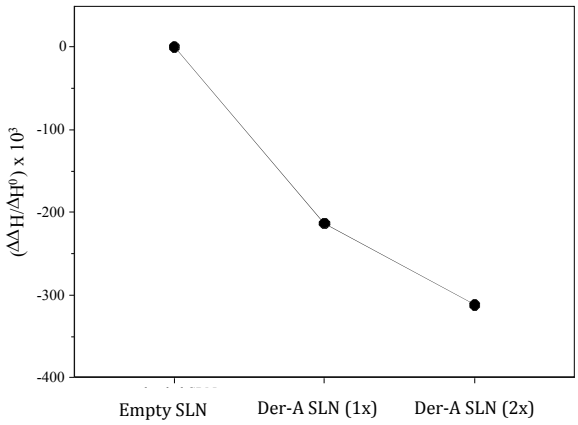

Figure 33. Enthalpy change, as $\Delta\Delta H/\Delta H^0$, of empty and Der-A SLN.
$\Delta\Delta H=\Delta H-\Delta H^0$; ΔH=enthalpy change on Der-A SLN and ΔH^0 is the enthalpy change of empty SLN.

5.2.8 *In vitro activity*

Der-A SLN (2x) were analysed in *in vitro* tests and compared to a Der-A Labrasol solution (5% w/v). This choice was suggested to ameliorate the Der-A solubility in water (LogP 2.29 ± 0.11) []. Labrasol was added to the aqueous solution in the lowest quantity that allowed the complete dissolution of the prodrug and permit to have a similar condition to Der-A SLN (2x).

Therefore, the *in vitro* release studies was conducted with the aim to determine the capability of SLN to control the release of Der-A. A dialysis method, having as receiving phase a solution of Methanol/Water 50:50 v/v was used.

The obtained results are shown in figure 34.

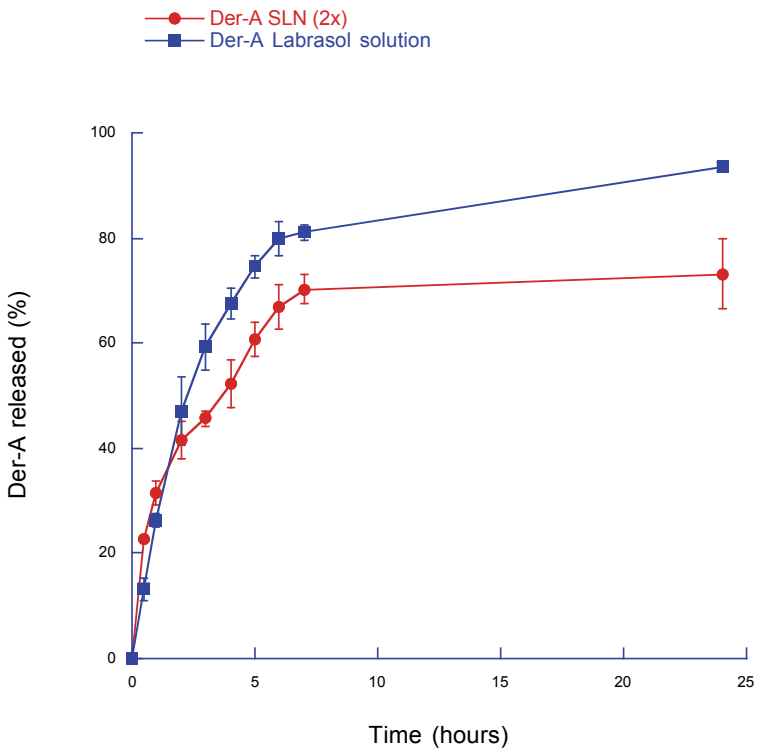

Figure 34. Der-A release kinetics from SLN and Labrasol aqueous solution (5% w/v) determined by dialysis method

As it can be observed, SLN showed a progressive release of Der-A within the first 8 hours. Subsequently, the release percentage remained constant up to 24 hours. The kinetics is typical of controlled release. Comparing these data with the curve obtained by Der-A dissolved in Labrasol solution, it is noteworthy that in the latter case the kinetics is typical of burst release.

It is therefore possible to conclude that the inclusion of Der-A in SLN assures a perpetuated release over time and, at the same time, facilitates the dissolution in aqueous media.

5.2.9 *Esterase degradation*

A prodrug is a compound (drug) administered in an inactive (or significantly less active) form that once administered is metabolised in vivo into an active metabolite. Der-A is a prodrug of LD and, for this reason, the aim of this test was the evaluation of the quantity of prodrug degraded

that is an index of the quantity of the LD released.

The Der-A degradation by FCS esterases was monitored by time within 24 hours and the obtained results were plotted in figure 35. The attention was focused on Der-A SLN (2x) and Der-A Labrasol aqueous solution (5% w/v).

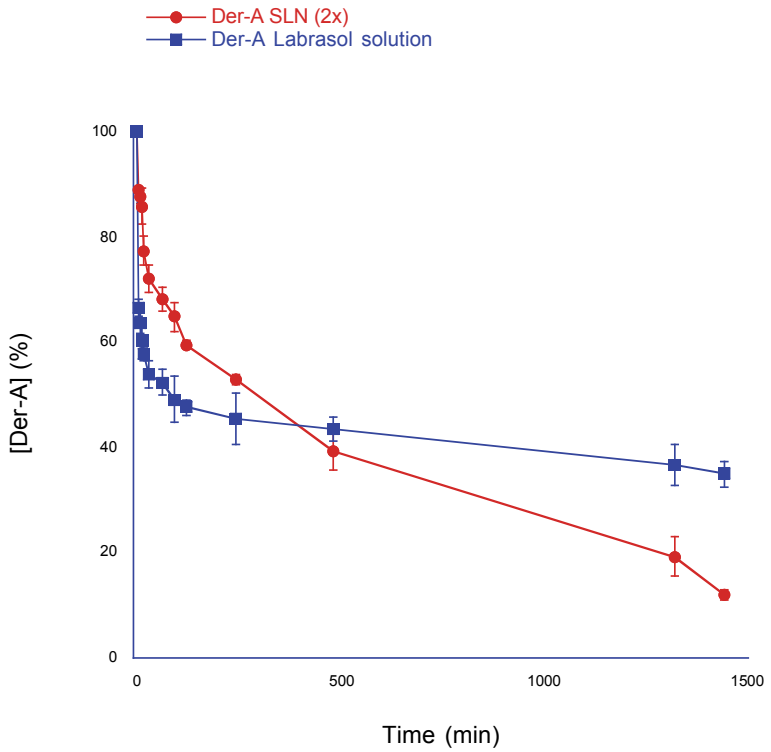

Figure 35. Der-A release kinetics from SLN and Labrasol aqueous solution (5% w/v) determined by dialysis method

Table XXI. Der-A half-time degradation in SLN (2x) and Labrasol solution.

	T ½ (min.)	**s.d.**
Der-A SLN (2x)	296	3
Der-A Labrasol solution	87	2

The reported results represent the average of three independent experiments ± s.d.

The values of half-time degradation were extrapolated by the graph and reported in table XXI. It is noteworthy that the half-lives are very different in the two samples examinated. Der-A SLN (2x) showed a 50% Der-A degradation correspondent to a time 3.5 fold higher than the aqueous solution of Labrasol, being the T ½ 86 min. for the Der-A Labrasol solution and 296 min. for the Der-A SLN (2x).

In addition, after 24 hours (1440 min.) the quantities of non-degraded Der-A were 34.9% for Labrasol solution and 12.3% for SLN (2x).

Therefore, it can be highlighted that SLN are not only able to delay the half-life of Der-A but also to promote an almost complete degradation of the prodrug in 24 hours.

6. NLC AND MAD FOR THE DELIVERY OF CLOTRIMAZOLE

6.1 INTRODUCTION

Oral and vaginal mucosae are characterized by a complex bacterial flora, susceptible to infections [177].

Candida albicans (*C. albicans*) is an ubiquitous fungus normally found on the skin, in the stomach, colon, vagina, rectum, mouth and throat [178-180]. When this organism proliferates, it may produce symptomatic infections ranging from relatively trivial conditions, such as oral and genital thrush, to crucial, systemic superinfections in immuno-depressed and chemotherapy patients [181,182].

For this reason, in recent years, interest in Candida infections, and in *C. albicans* in particular, has become huge since fatal infections have increased in number and new Candida-based pathologies have been recognized [183].

Clotrimazole (CLO), an imidazole derivative, is a synthetic antifungal agent widely used for the treatment of this type of infections [184]. Unfortunately, the oral administration of this active is not convenient, due to his severe side effects and his short half-life (3-6 hours) that requires frequent dosing. For these reasons, a topical administration is suitable and recommended.

However, since CLO exhibits a very low water solubility, it needs to be incorporated into a proper vehicle to have right levels of topical absorption and now it is available in the pharmaceutical market as a 1% topical cream. In spite of this, it has been reported that users usually prefer gel than cream, because of its better characteristics in easiness of use, absence of odour and absence of colour [185].

In addition, another problem about vaginal products, that influences their use by women, is the necessity to administer the formulation several times during the day.

In order to overcome these problems, some authors proposed the design of solid lipid nanoparticles (SLN) and nanoparticle lipid carrier (NLC) as delivery system for CLO, afterwards

they studied SLN containing CLO incorporated in an hydrophilic cream [186-187].

Aim of the present investigation is the design of viscous nanosystems based on NLC or monoolein aqueous dispersion (MAD) as devices able to exert anticandidal activity. In particular this study described the production, characterization and comparison of NLC and MAD suitable for CLO mucosal administration.

Since the nanosystem dispersion should have a viscosity enabling permanence on the mucosa surface, in the present investigation different gelified systems have been specifically designed for NLC and MAD, respectively based on carbomer and poloxamer.

After the production, dimensional distribution and morphology of NLC and MAD have been investigated by Photon Correlation Spectroscopy (PCS), SdFFF (Sedimentation Field Flow Fractionation) and Cryo-Transmission Electron Microscopy (Cryo-TEM). CLO recovery has been investigated by time up to three months from production. The rheological and calorimetric properties of CLO containing NLC and MAD viscous forms have been studied.

At last the anticandidal and cytotoxicity activity of CLO containing NLC and MAD has assayed against *C. albicans* and HeLa cells, respectively.

6.2 RESULTS AND DISCUSSION

6.2.1 *Characterization of dispersions*

Cryo-transmission electron microscopy allowed an investigation of the inner structure of nanosized formulations, empty and CLO containing (Fig. 36). In particular, the attention was focused on CLO containing nanoparticles. As shown in figure 36A, NLC sample is characterized by the presence of ovoidal and circular platelet like particles together with needle like structures edge on viewed. In figure 36B can be observed that in MAD sample there is a coexistence of vesicles and almost spherical particles with a homogeneous ordered inner structure, typical of cubosomes.

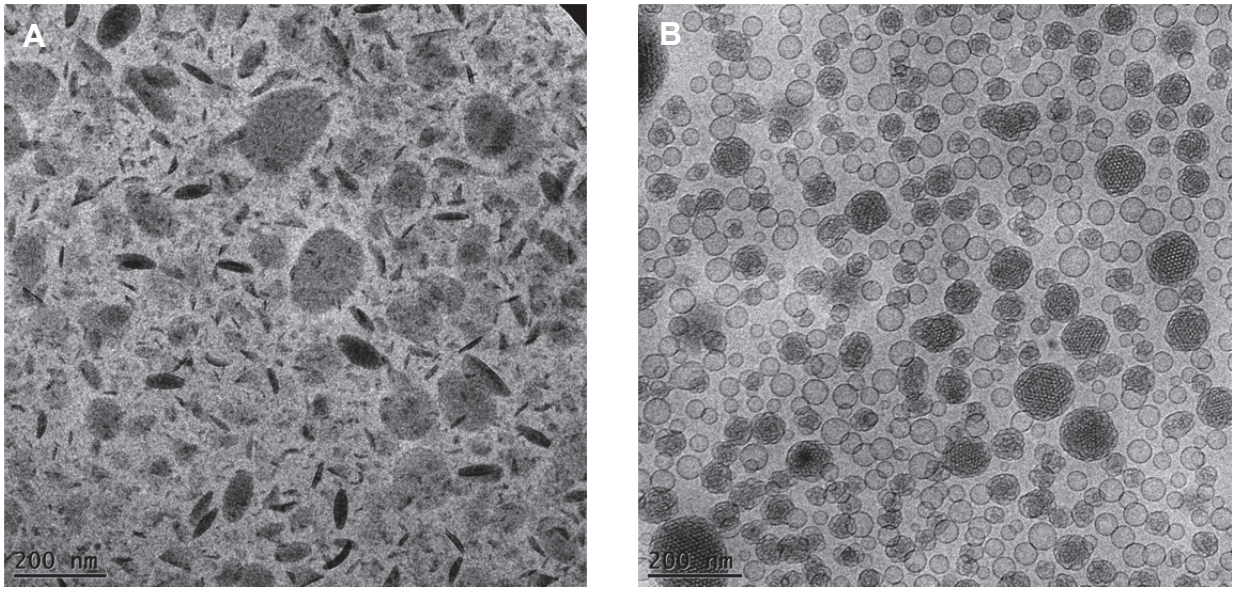

Figure 36. Cryo-transmission electron microscopy images (cryo-TEM) of CLO-NLC (Panel A) and CLO-MAD (Panel B). Data are the mean of 5 determinations on different dispersions.

In table XXII are reported the PCS measurements conducted to determine the dimensional distribution of the produced NLC and MAD dispersions. It was observed that both NLC and MAD have mean intensity diameters around 200 nm, the drug presence slightly increased polydispersity indexes.

Empty NLC showed a mean diameter of 196.2 nm, which slightly increased by CLO incorporation, passing to 201.6 nm. Dimensional analysis by number revealed for empty NLC a mean diameter of 125.7 nm and a monomodal distribution, while in the presence of CLO the distribution profile was bimodal, with one main peak of 120 nm and another less representative peak of 297 nm.

Empty MAD had a mean diameter of 198.2 nm, expressed as Z Average. The analysis by number revealed a mean diameter of 78.0 nm. CLO incorporation didn't affect the nanostructures' dimensions, having a mean diameter of 195.5 nm. In-depth analysis of the distribution by number revealed two peaks: the main one with a mean diameter of 156.2 nm and a second less representative peak with a mean diameter of 250.2 nm.

Table XXII. Mean diameters of NLC and MAD as determined by PCS

Parameter	**NLC dispersion**	**NLC-CLO dispersion**	**MAD dispersion**	**MAD-CLO dispersion**
ZAverage *mean diameter (nm)*	196.2±2.4	201.6±2	198.2±1.2	195.5±3
Analysis by number *mean diameter (nm)*	125.7±0.2 (Peak Area 99.5±0.2%)	120.0±6.5 (Peak Area 82.2±2.6%) 297.0±4.4 (Peak Area 17.8±3.2%)	78±0.3 (Peak Area 99.7±0.1%)	156.2±4.0 (Peak Area 82%±0.5%) 250.2±3.0 (Peak Area 18%±0.8%)
Polydispersity Index	0.18±0.02	0.24±0.03	0.18±0.02	0.31±0.05

Size distribution was also determined by SdFFF, an elution technique that sorts particles depending on their specific mass. The graphical results of the separations, the fractograms, are converted into PSD plots, i.e. the amount of material per unit change of diameter, by transforming the retention time in the diameter of the equivalent sphere (d), and the UV signal into a mass frequency function (dd), according to well-proven equations by assuming the

density is known [129,159]. To allow a direct comparison, the fractograms were obtained under the same separation conditions.

Figure 37 shows the derived PSD plots of a diluted amount of CLO-NLC (panel A) and CLO-MAD (panel B) dispersions. The conversion was performed assuming an average density of 0.0283 g/ml for NLC and 0.0133 g/ml for MAD.

In figure 37A, the CLO-NLC plot shows a broad peak due to the overlapping of two particle populations, the first peaking at ~ 140 nm and the second at ~ 200 nm. The broad and composite signal evidences the presence of a heterogeneous population of particles with different mean diameters.

In panel B one can observe a main peak with maximum at ~ 160 nm and a small secondary peak, corresponding to a minor population of particles of ~ 247 nm size. These size distribution is in agreement with PCS data reported in table XXII.

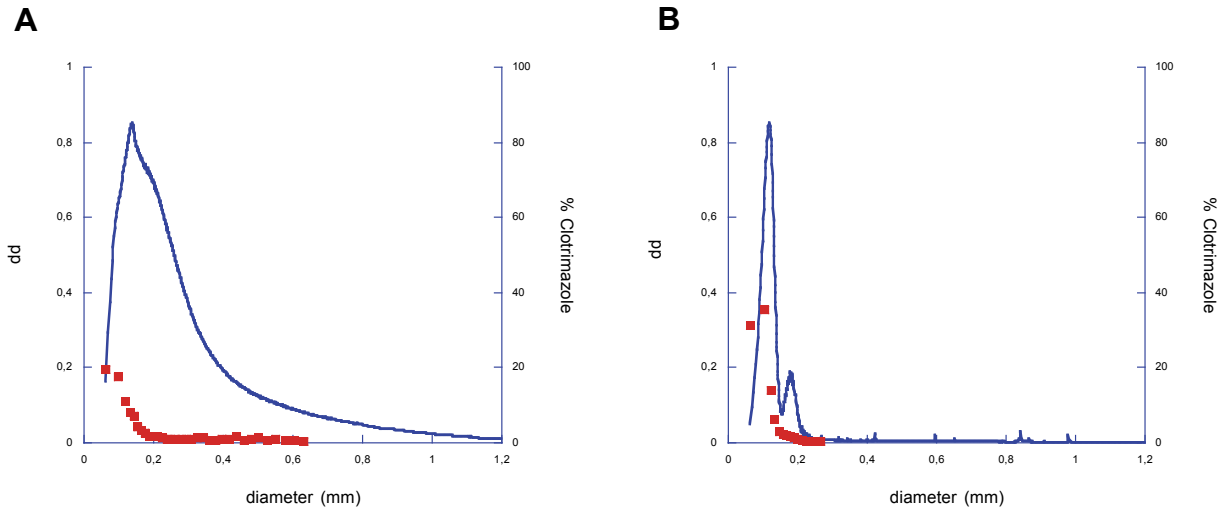

Figure 37. PSDs elaborated from the SdFFF fractograms. **A**) NLC particles were assumed to have a density of 0.0283 g/ml **B**) MAD particles; assumed density of MAD particles 0.0133 g/ml (dd = dimensional distribution; the dots indicate CLO content, as determined by HPLC)

6.2.2 *Drug recovery and distribution*

As reported in Table XXIII, CLO recovery after the nanosystems production was almost quantitative, being 97.21% of the total amount used for the preparation in the case of NLC and 90.62% in the case of MAD dispersions.

Table XXIII. CLO content in NLC and MAD as a function of time

CLO recovery (%)[a]

Time (days)	in NLC	in MAD
0	97.21±0.2	90.62±0.4
15	96.05±0.1	89.71±0.2
30	95.02±0.3	85.14±0.6
60	94.40±0.2	74.02±0.8
90	93.21±0.5	59.03±0.2

Shelf life values

K	0.00018	0.00484
t_{90} (days)[b]	241.93	21.87

a: as a function of initial CLO content.

b: Time at which the drug concentration has lost 10%.

The reported results represent the average of four independent experiments ± s.d.

SdFFF was employed to obtain information about the drug distribution within the produced dispersions. During the fractionation, some fractions were collected and analysed by HPLC to quantify the amount of drug contained in the different particle populations of the disperse phase. In Figure 37, the CLO concentration determined by HPLC is graphed as the secondary y-axis in the PSD plots. CLO was found to be entirely associated with particles in both NLC and MAD dispersions, even if in both plots, the first CLO concentration value is out of the dd profile. This is a consequence of the fractogram-PSD conversion procedure, which excludes the data not

resolved from the void peak, where the lightest (smallest) particles are eluted [158].

In the case of NLC, whose PSD is reported in panel A, 19.45% of CLO is contained in a fraction characterized by particles with a mean diameter of ~60 nm, the fraction corresponding to a mean diameter of ~95 nm contains 17.7% of the total drug, 26.5 % of CLO is contained in fractions ranging between 115 and 140 nm and the remaining 36.35% of CLO is associated to a less representative population of larger particles.

In the case of MAD, CLO distribution is narrower than in MAD. In fact, the fraction corresponding to a mean diameter of about 84 nm contains 31.1% of the total drug, as shown in panel A. The highest amount of CLO (35.2%) is contained in the most representative portion of nanoparticles/vesicles, having a mean diameter of 140 nm. The fraction corresponding to a mean diameter of 179 nm contains only 6.3% of the total drug, the remaining 27.4% of CLO is associated with the less representative population of particles, having diameters comprised between 200 and 300 nm.

6.2.3 *Stability studies*

Table XXIII reports CLO content in the different formulations as a function of time, expressed as percentage of the total amount used for the preparation.

Shelf life stability was calculated plotting Log (CLO residual content, % with respect to drug content at time 0) against time, obtaining first order kinetics. From the slopes (*m*), obtained by linear regression, shelf life values (t_{90}), i.e. the time at which the drug concentration has lost 10%, were calculated and reported in Table XXIII.

t_{90} calculated for CLO-NLC was longer than 8 months (241.93 days), whilst in the case of CLO-MAD it resulted only in 21 days. These data could be due to the differences in the nanostructure of NLC and MAD, the former characterized by solid matrixes, the latter by a mixture of vesicles and cubosomes. For this reason it is hypothesized that NLC could better control the stability of the incorporated drug.

The macroscopic aspect of NLC dispersions didn’t change by time; in fact, dispersions

maintained their white colour and the absence of aggregates also after six months from production. On the other hand, in the case of MAD, some aggregates were found after 2 weeks from production, with a slow progressive increase by time.

6.2.4 *Production of viscous forms*

In order to adequately adjust the viscosity of NLC and MAD, different gels based on poloxamer 407 and carbomer were designed and produced.

In the case of NLC, thermo-reversible gels were developed. NLC dispersions were adequately viscosized to obtain a thermo-reversible bioadhesive organogel, characterized by a low viscosity at room temperature, in order to enable an easy application onto mucosa. After application, the contact with the body allows the gel to increase its viscosity, controlling CLO diffusion.

In the first case, NLC were viscosized by mean of poloxamer following a dilution procedure. Precisely, an adequate volume of NLC suspension (alternatively empty and CLO containing) was added at 0°C to a 30% w/w poloxamer 407 gel until a final polymer concentration of 24% w/w. The final solution (NLC-D) was stored at 4°C overnight and resulted homogeneous without aggregates.

In the second case, NLC suspensions were viscosized following a one step process based on the dispersion at low temperature of solid poloxamer 407 within the aqueous phase of NLC (NLC-S). Also in this case, a final concentration of polymer of 24% w/w was obtainedIt has to be underlined that it was not possible to viscosize MAD in the same way, due to precipitation of MAD at low temperature.

Thus, MAD viscosization was obtained by addition of a carbomer gel (1.2% w/w) previously prepared, resulting in the formation of a homogeneous whitish formulation, with an adequate viscosity for the mucosal administration. Differently from NLC containing gels, MAD containing gel was not thermo-reversible.

6.2.5 *Rheological characterization of hydrogels*

Rheological analyses were performed both on NLC-D and NLC-S, empty and CLO-containing. Rheological characterizations were preformed both on the gels as such and after the addition of SVF in physiological quantities to each formulation. Particularly, variations in sol-gel transition temperatures were analysed.

Usually, the gelling temperatures of vaginal hydrogels are considered to be suitable for vaginal administration when they are lower than human vaginal temperature (37.2 °C). If gelling temperature is higher than 37.2 °C, hydrogels will lose their gelling properties resulting in a leakage of the formulations from the vagina.

Initially, the thermosensitive properties of hydrogels were evaluated considering their sol/gel transition temperature. The curves of G' and G'' obtained from preparations are presented in figures 38 and 39. Particularly, formulations before and after dilution with SVF respectively were considered. The obtained curves are typical for poloxamer systems since the elastic modulus, (G') very low at solution stage, increased drastically when gelling temperature was reached. In fact, since a high elastic modulus is an inherent characteristic of solid materials, a phase change process from liquid to semisolid can be described by an increment of elastic modulus [188].

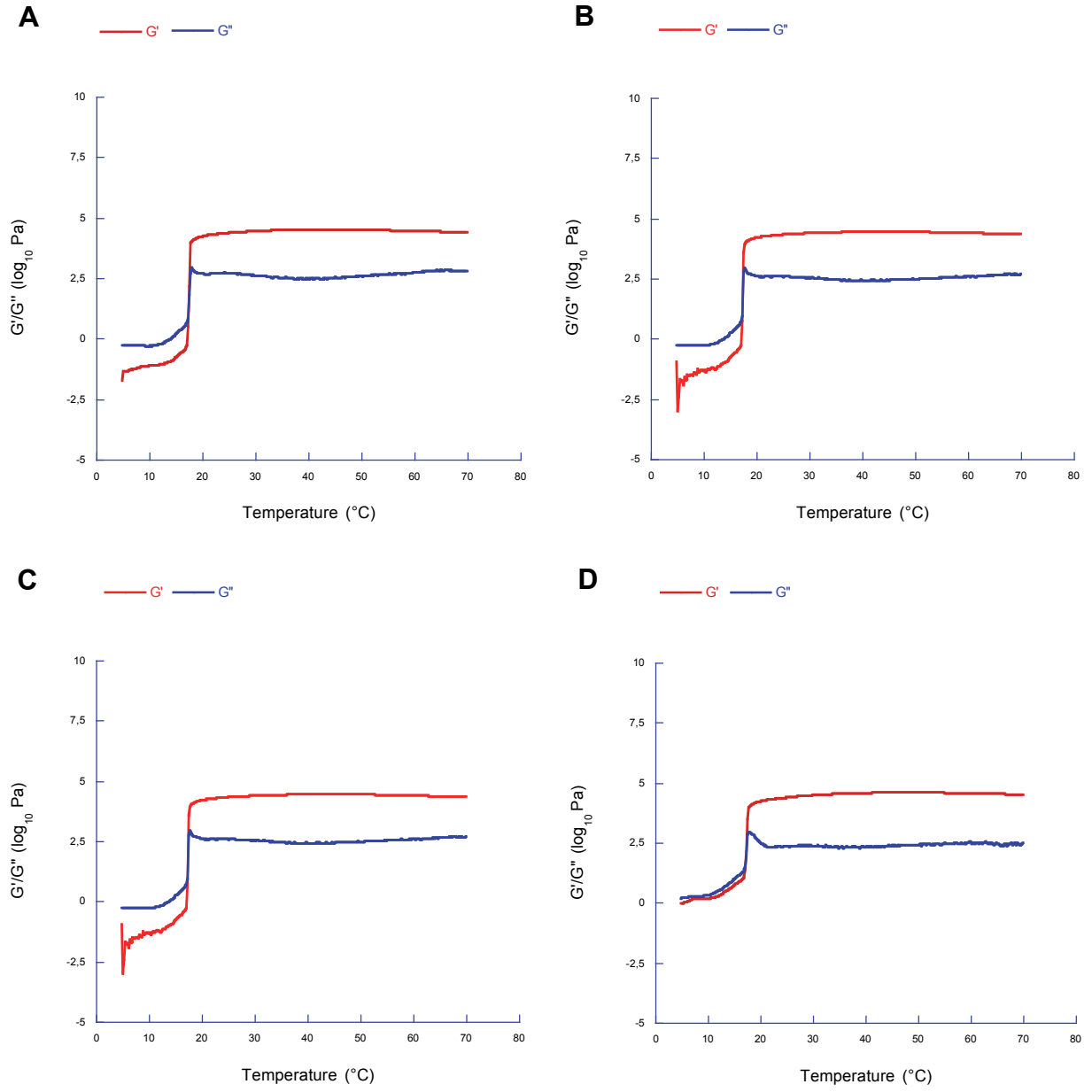

	T_{gel} (°C)	G' (10^3 Pa)	G'' (10^3 Pa)	δ (°)
A) NLC-D gel	17.6 ± 0.8	2.1535 ± 0.2	1.8132 ± 0.1	0.5630
B) CLO-NLC-D gel	17.5 ± 0.6	2.1558 ± 0.1	1.8409 ± 0.2	0.5683
C) NLC-S gel	16.8 ± 1.2	1.6027 ± 0.1	1.5120 ± 0.1	0.2238
D) CLO-NLC-S gel	17.4 ± 1.0	2.0899 ± 0.3	1.8537 ± 0.2	0.3141

T_{gel} = sol-gel transition temperature **G'** = elastic (storage) modulus **G''** = viscous (loss) modulus **δ** = phase angle at 37.2°C

Figure 38. Rheological characterization of NLC-D and NLC-S gels, empty and CLO-containing.

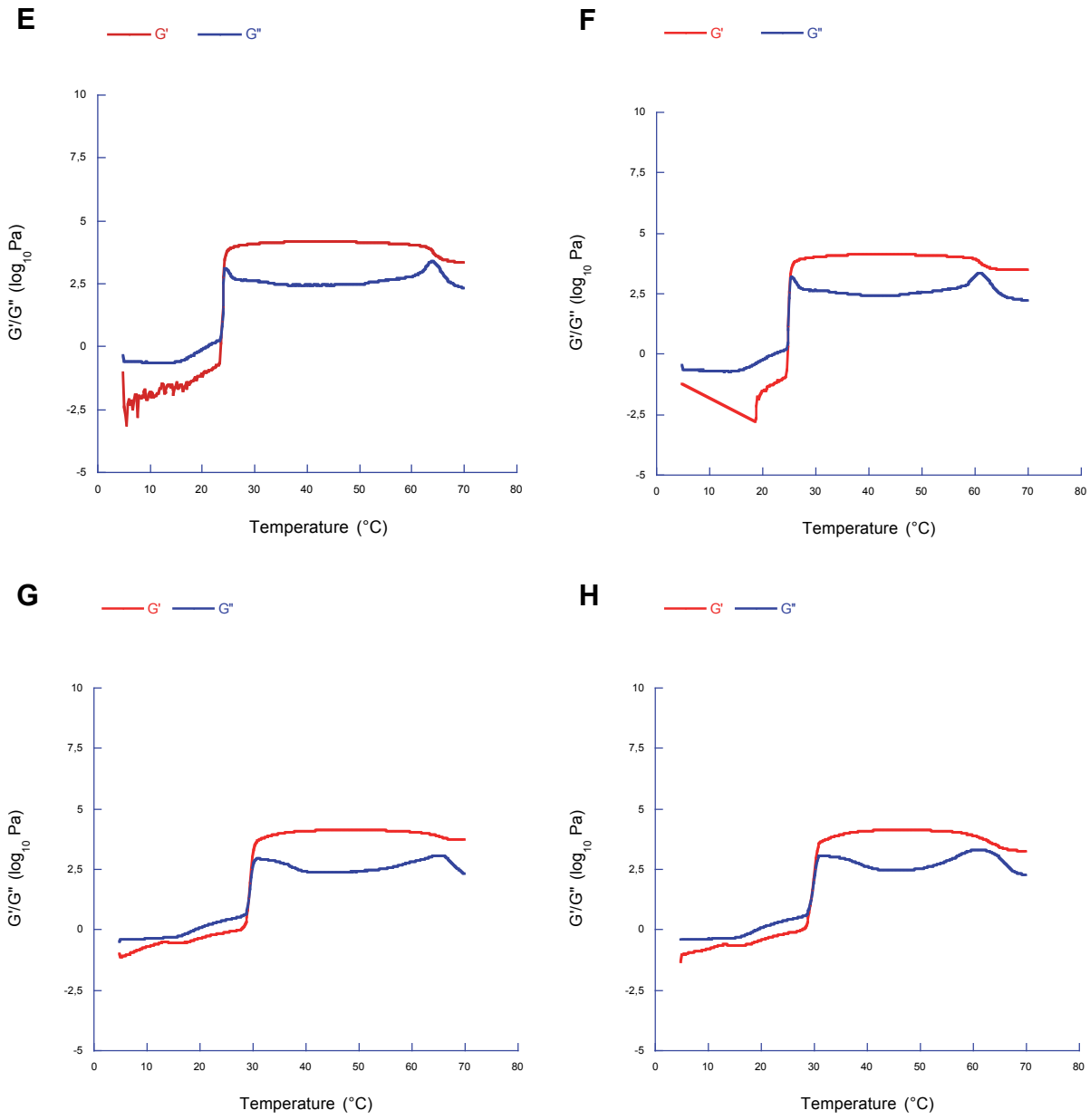

	T_{gel} (°C)	G' (10^3 Pa)	G'' (10^3 Pa)	δ (°)
E) NLC-D gel + SVF	23.7 ± 1.0	0.5704 ± 0.1	0.5752 ± 0.1	1.091
F) CLO-NLC-D gel + SVF	24.9 ± 0.8	0.7187 ± 0.3	0.7146 ± 0.1	1.352
G) NLC-S gel + SVF	29.3 ± 0.4	1.0447 ± 0.2	1.0862 ± 0.3	2.220
H) CLO-NLC-S gel + SVF	29.6 ± 0.2	1.2749 ± 0.1	1.2420 ± 0.2	3.873

T_{gel} = sol-gel transition temperature **G'** = elastic (storage) modulus **G''** = viscous (loss) modulus **δ** = phase angle at 37.2°C

Figure 39. Rheological characterization of NLC-D and NLC-S gels, empty and CLO-containing, after the addition of SVF.

As can be seen from the results reported in the table linked to figure 38, gelling temperatures were in all cases lower than body temperature and didn't show significant variation neither considering the two different methods of gelification, nor evaluating the absence or the presence of CLO.

As shown in figure 39, even after addition of SVF all poloxamer systems maintained a typical thermoreversible behaviour, with a rapid increase of G' values at sol-gel temperature. It is important to highlight that the addition of 0.75 mL of SVF resulted in a decrease of poloxamer concentration from 24% to 17.45% and consequently, in a dramatic increase of gelling temperature, remarkable in the table linked to figure 39.

For NLC-S, the final gelling temperatures were around 30 °C, while in the case of NLC-D the values were about 24-25 °C. More than 10 °C of difference were observed before and after the addition of 2 mL of viscosized gels with 0.75 mL of SVF, about 5°C of difference were found in diluted samples. CLO presence didn't cause further variations of temperature.

The addition of SVF leads to a decrease in the elasticity of the hydrogels. As we can see from the table linked to figure 39, when hydrogels were diluted with SVF elastic modulus (G') was always decreased. It is noteworthy that the variation of gelling temperature is not only due to the decrease in copolymer concentration after the dilution of the formulations, but also caused by a modification of the physicochemical properties of the hydrogels. In fact, the obtained results can be also explained by the presence of co-solutes, e.g., ions, proteins, electrolytes in the SVF medium, which could interact with poloxamer [189]. As demonstrated by Scherlund [190], in the case of poloxamers, gelation and micellization processes are strongly connected.

Considering the loss modulus (G''), NLC-S maintained higher values of viscosity after dilution with SVF than diluted hydrogels. For this reason, it is expected that these superior viscosity modulus will result in an increase in the spreading of the viscosized hydrogel over the vaginal mucosa after its *in vivo* administration.

The properties of CLO-MAD carbomer gel were tested and compared to a correspondent carbomer gel in terms of polymer concentration.

After a macroscopic analysis, carbomer hydrogels appeared to be stable formulations that could incorporate MAD without changing their original texture properties. One possible explanation can be that MAD accommodate themselves in the empty spaces inside the gel's three-dimensional structure.

Concerning the rheological evaluation, as shown in figure 40, both empty and CLO-MAD carbomer gel evidenced a non-Newtonian behaviour with pseudoplastic characteristics. The relationship between shear stress and shear rate was not constant and the viscosity changed as the shear rate was varied. In particular, in both samples a decreasing viscosity with an increasing shear rate was displayed.

In addition, it can be observed that CLO-MAD carbomer gel shows a higher value of viscosity at low shear stress if compared to the empty formulation. This increase in viscosity could be attributed to the complete incorporation of MAD in carbomer gel.

In vaginal environment, where the temperature is higher than room temperature and vaginal fluids cause a dilution of formulations, the cross-linked bounds inside the gel can get weak and can partially become degraded. For these reasons, an increase in viscosity values, when the shear stress is low, is a suitable characteristic for CLO-MAD Carbomer gel, because it preserves the formulation from an immediate degradation and permits a deposition on the site of action for a prolonged period of time.

After the physiological dissolution of gel, when strong bounds become weaker, MAD and vesicles can come out and explain their activity directly on the vaginal mucosa, releasing CLO in a controlled manner.

Taken together these considerations, a double action could be ascribed to CLO-MAD Carbomer gel: initially, high viscosity guarantees a localization of gel in the site of action and secondly, a controlled release of CLO from MAD permits a prolonged activity in the vaginal site.

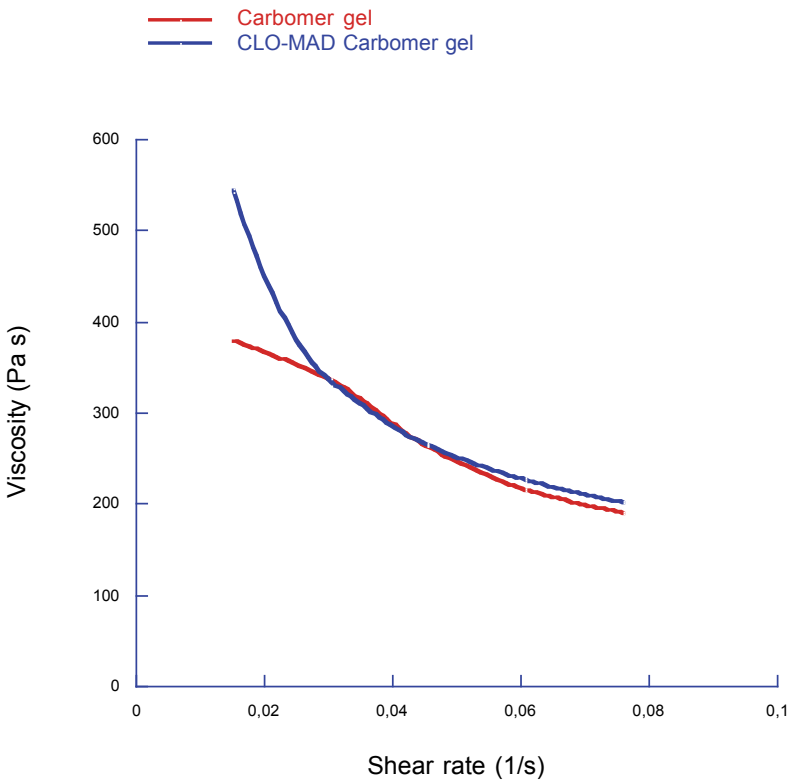

Figure 40. Viscosity of Carbomer gel (red line) and CLO-MAD Carbomer gel (blue line) as a function of the shear rate

6.2.6 *Micro-DSC*

NLC-D, CLO-NLC-D, NLC-S and CLO-NLC-S were subjected to micro-DSC as described in the material and method section. As control, a plain solution of Poloxamer 407 (24% w/w) dispersed in water was examined under the same conditions (Fig. 41).

From the analyses of heating and cooling ramp reported in figure 41, it could be observed that the two curves, namely endothermic peak (red) and exothermic peak (blue) are perfectly symmetric exhibiting the thermal equilibrium of micelle formation in this condition. In fact, the obtained two peaks correspond to the progressive formation and fusion of the micelles in the solution with increasing and decreasing temperatures.

In calorimetric assays, it is possible to extrapolate from the micro-DSC traces the temperatures T_{onset}, T_{peak} and T_{endset} of micelle's formation and fusion from the Micro-DSC traces. Particularly,

they are the temperatures of the incipient polymer association (T_{onset}), the temperature of the maximum of the heat flow (T_{peak}) and the temperature of the end of micellization process (T_{endset}). In this study, the critical micellization temperature (CMT) was defined as the T_{onset} that is the temperature resulting from the intersection of the tangent of the first inflection point of the peak with the baseline [191].

The obtained results of the thermal analysis conducted on NLC-D and NLC-S, empty and CLO-containing, are shown in figures from 42 to 45.

The evident variation in shape of cooling curve with respect to heating one can be attributed to a partial disorganization of lipids during the stationary phase when the gels NLC-D or NLC-S are maintained at 37° C for 6 hours. Nanoparticles, having trycaprin as component, whose melting point is 33° C, are subjected to a structural modification that allows a gradual release of CLO and its specific action in the application site. During the cooling phase, the gel, consisting in an organized structure of polymeric micelles and NLC, is characterized by a disorganized mixture of free lipids and polymer, due to the partial melting of trycaprin. As result, in the case of NLC-D or NLC-S (Fig. 42 and 44), when micelles form themselves again, the hydrophobic tails of the polymer can interact not only with each other, but also with the lipids freely present in solution or in aggregated to form NLC. This phenomenon is evidenced by an increase of the time required to form micelles of mixed nature and consequently, in a reduction of CMT.

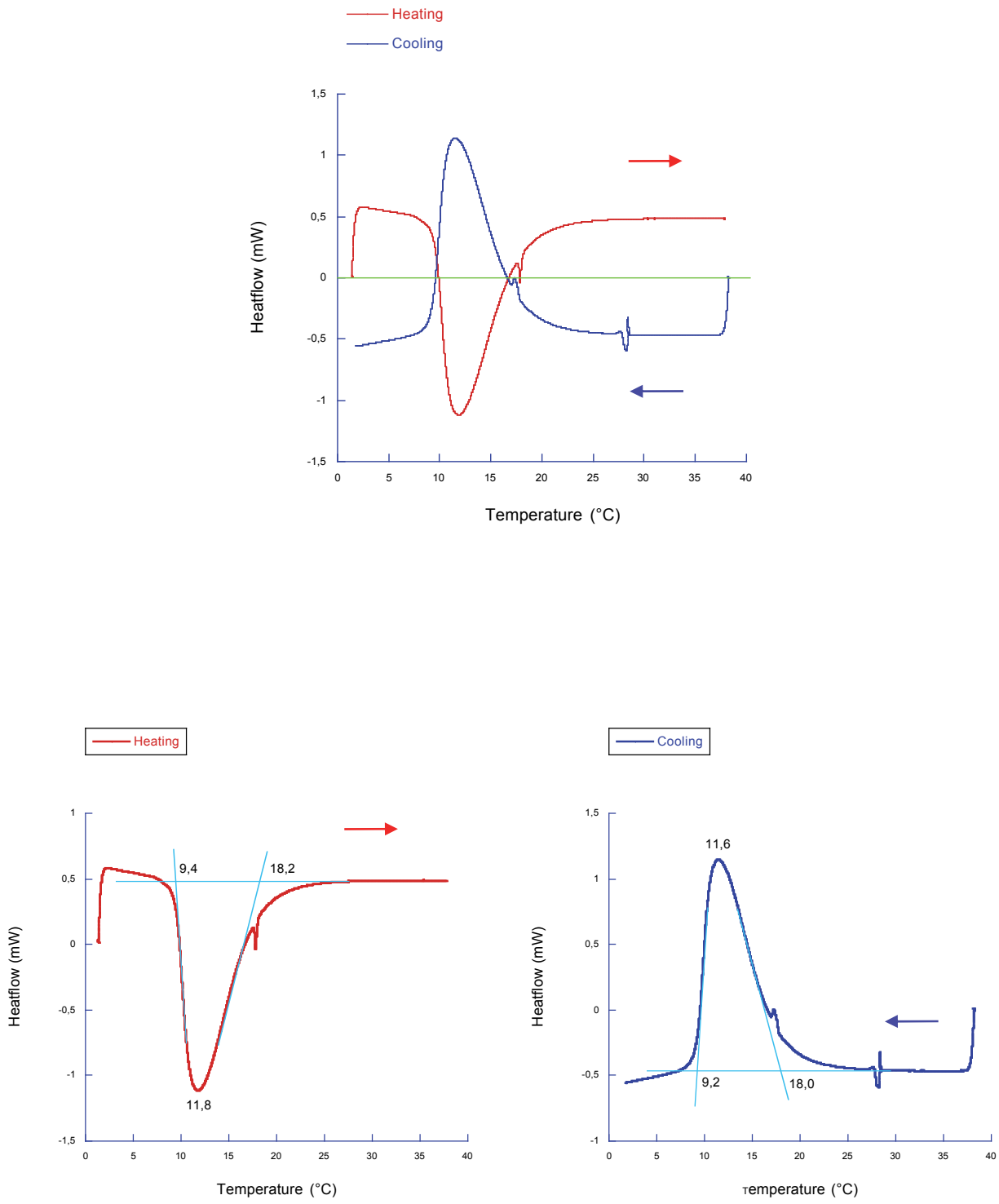

Fig. 41: Heat flows versus temperature for a water solution of poloxamer F127 gel (24% w/w) during heating and cooling ramps.

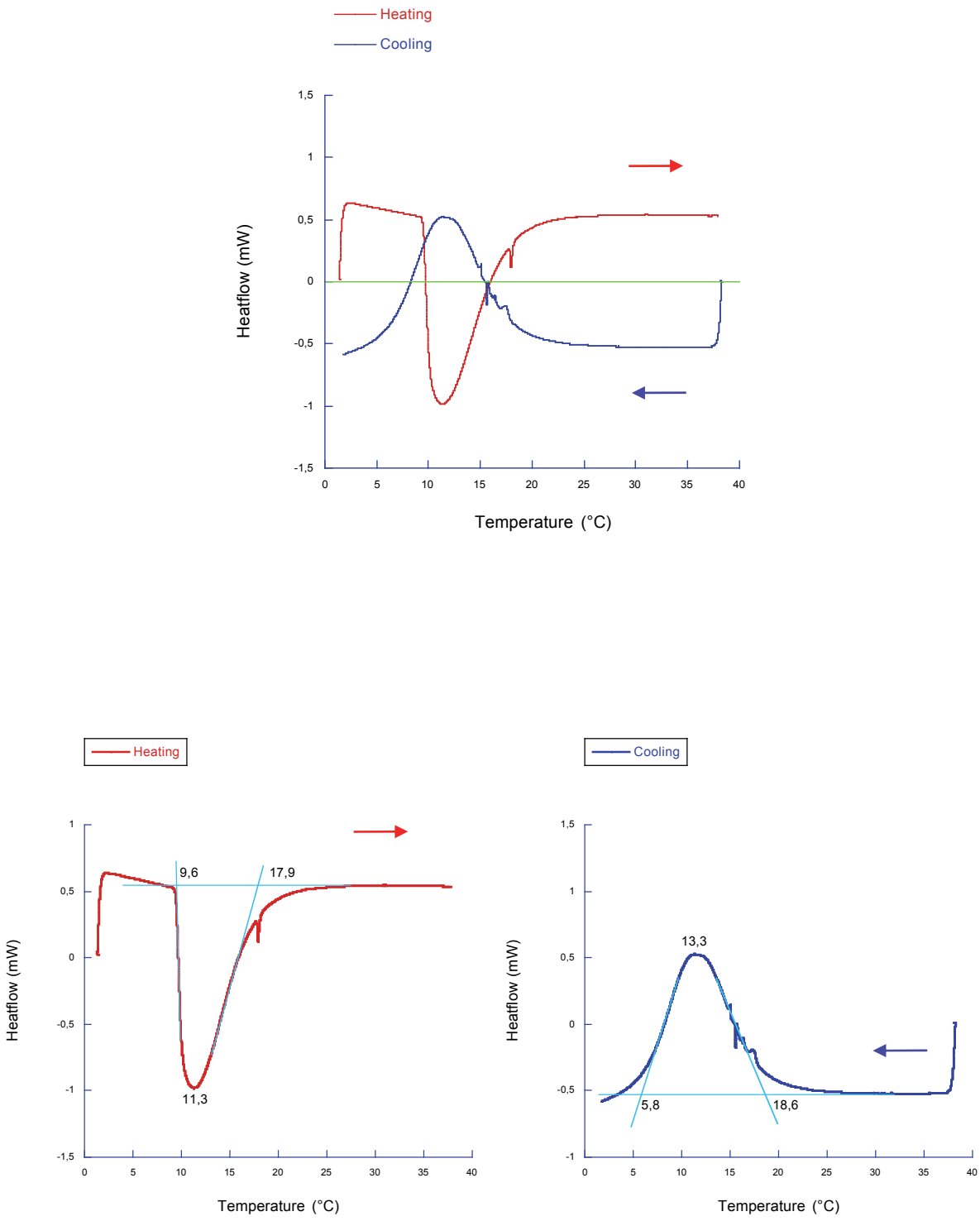

Fig. 42: Heat flows versus temperature for a solution of NLC-D gel during heating and cooling ramps.

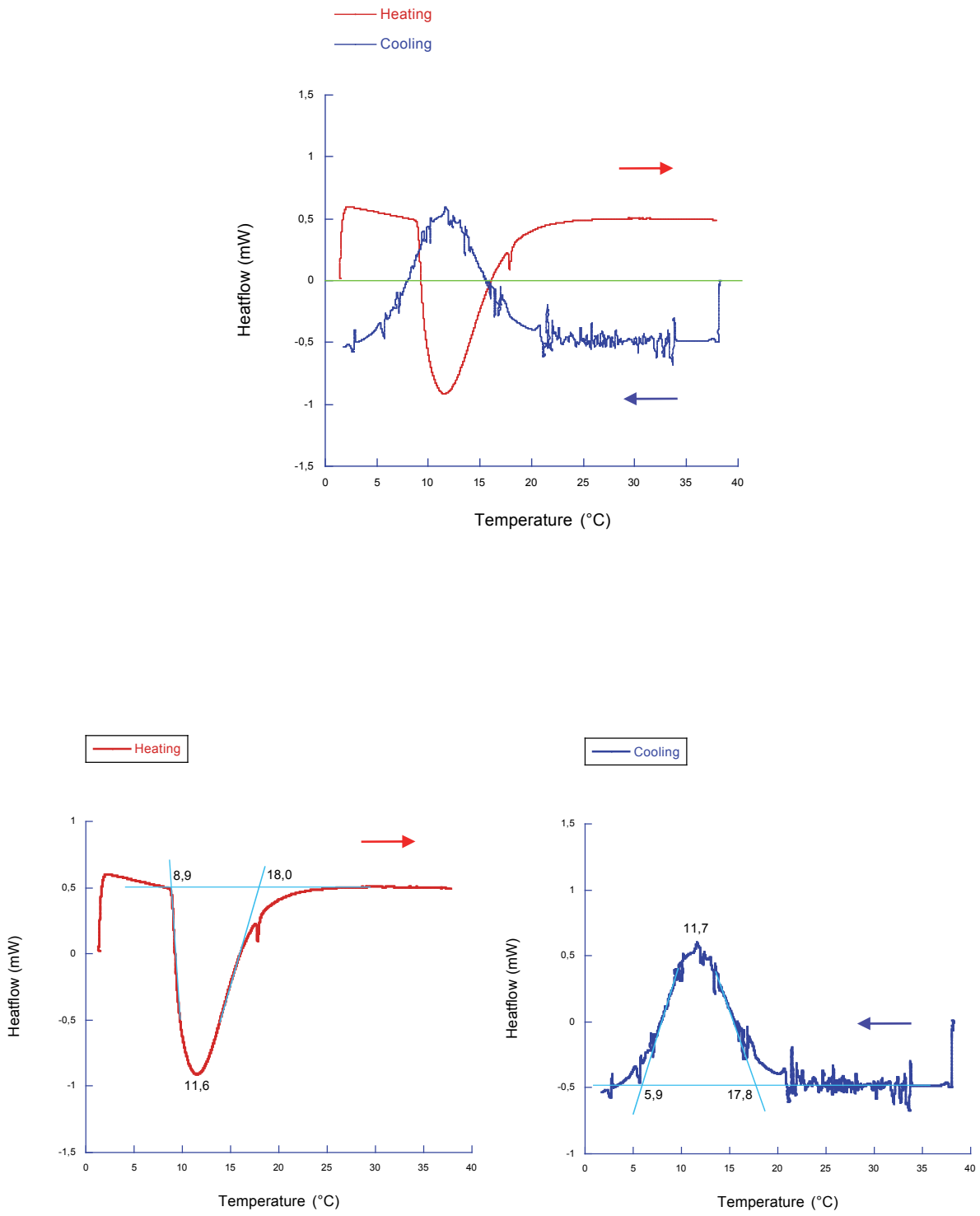

Fig. 43: Heat flows versus temperature for a solution of CLO-NLC-D gel during heating and cooling ramps.

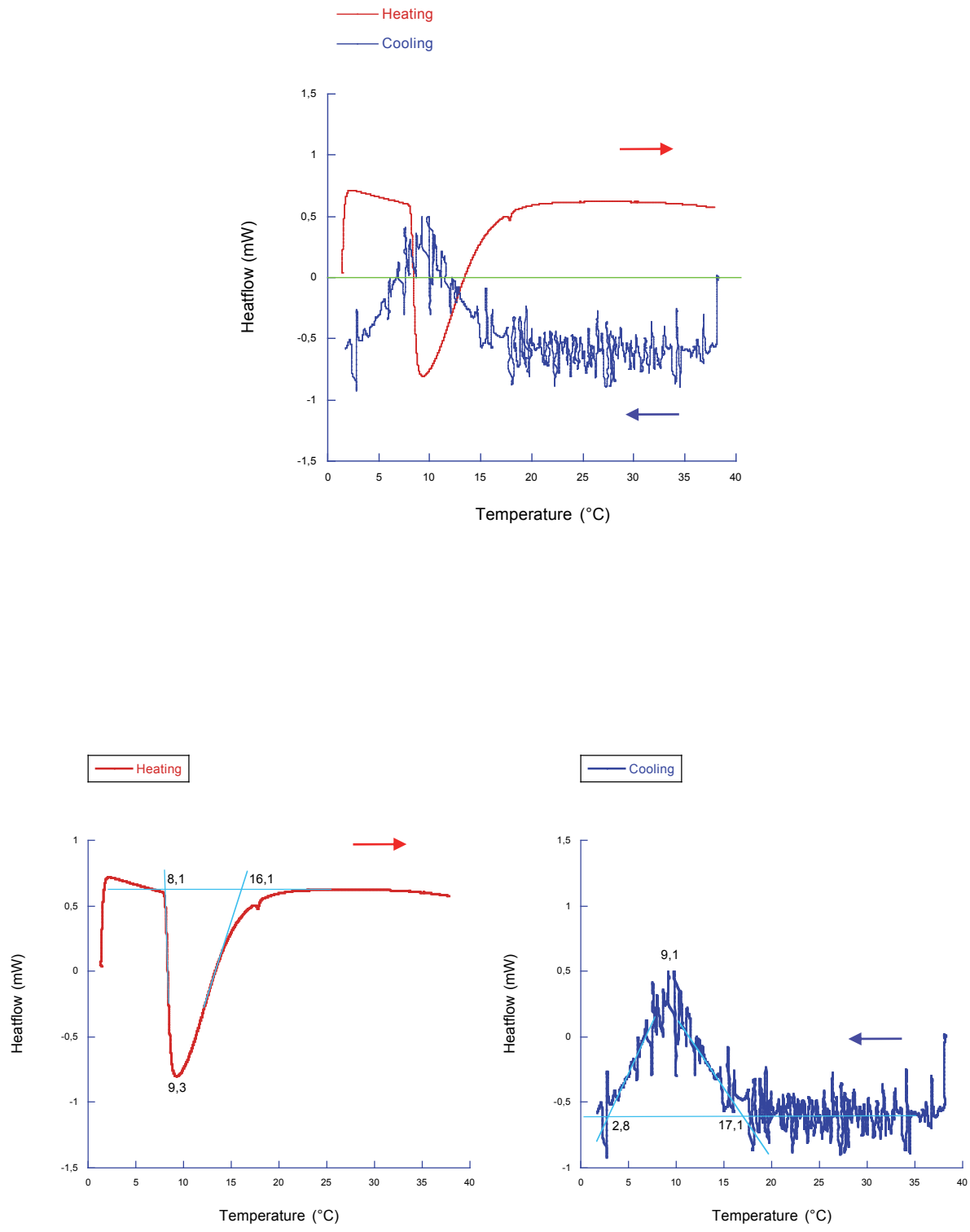

Fig. 44: Heat flows versus temperature for a solution of NLC-S gel during heating and cooling ramps.

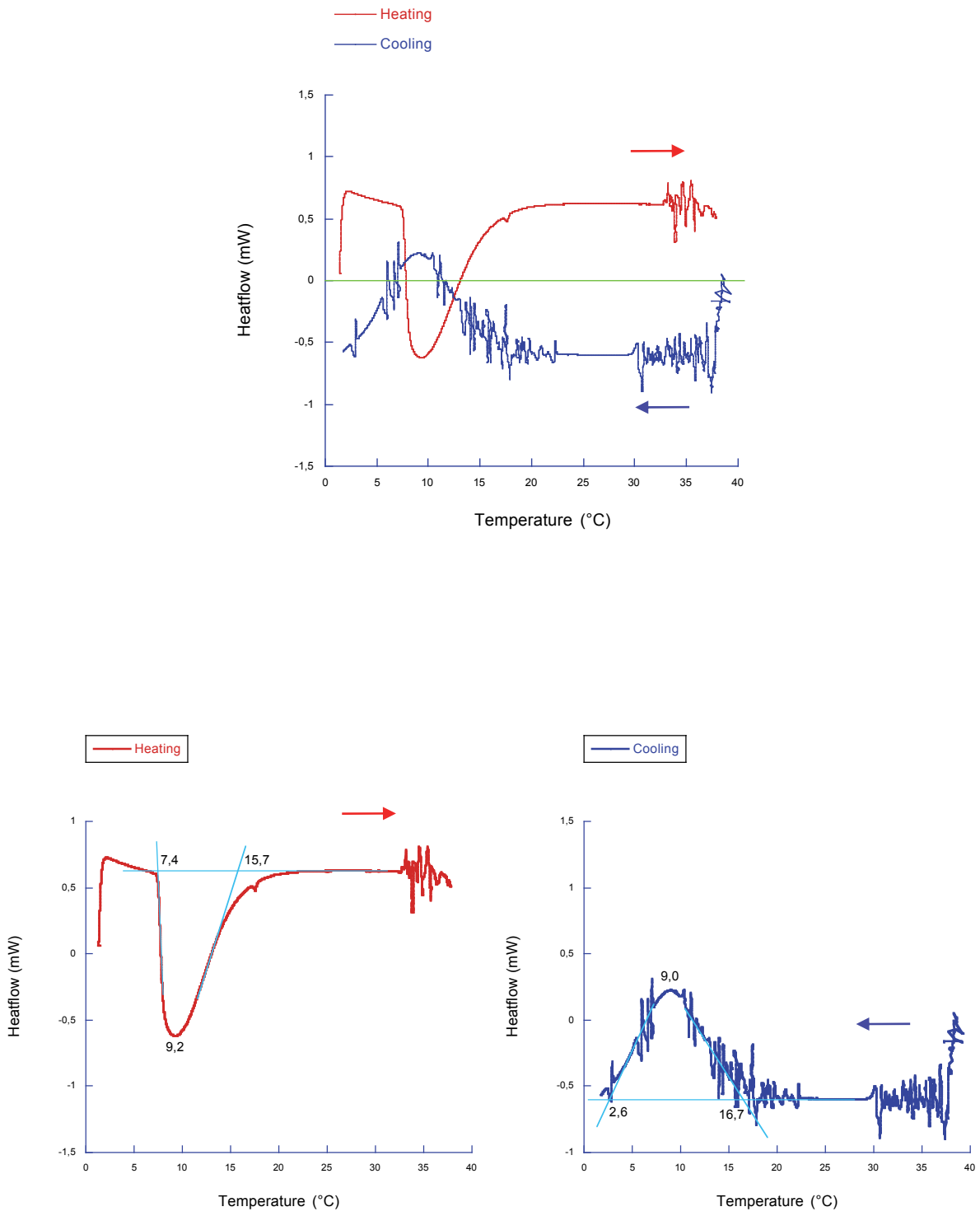

Fig. 45: Heat flows versus temperature for a solution of CLO-NLC-S gel during heating and cooling ramps.

The greater the disorganization of the system, the more evident the effect one can hypothesize that the gel network of NLC-D formed incorporates NLC without structural interactions, otherwise, in the case of NLC-S gel, interactions occur between the polymer in solid form and the NLC during the gelification, due to the dissolution of poloxamer directly in the aqueous phase of the formulation. This behaviour could permit an initial interaction between hydrophobic tails of polymer and the NLC. In this latter case, after the stationary phase at 37° C, the system is more destabilized and this involves greater difficulties in the formation of micelles. The greater disorganization of the NLC-S gels could be also highlighted with the background noise that appeared in fusion enthalphograms (Fig. 44 and 45).

CMT values were extrapolated and reported in Table XXIV. While in the plain solution of Poloxamer gel the CMTs related to the phase of formation and fusion of micelles are slightly superimposable, when NLC are present there is a considerable difference between the CMT data obtained in the phase of formation and fusion. NLC-D gels were characterized by a reduction of 40% of CMT during the fusion phase, while NLC-S showed a reduction of 65%.

Table III. CMTs obtained by enthalphograms related to formation and fusion of micelles, obtained by micro-DCS

Sample	CMT Formation (°C)	CMT Fusion (°C)
Poloxamer gel 24% w/w	9.4 ± 0.2	9.2 ± 0.1
NLC-D gel	9.6 ± 0.1	5.8 ± 0.2
CLO-NLC-D gel	8.9 ± 0.1	5.9 ± 0.1
NLC-S gel	8.1 ± 0.2	2.8 ± 0.2
CLO-NLC-S gel	7.4 ± 0.1	2.6 ± 0.1

This trend confirms the hypothesis indicated above and suggests that despite NLC-S lose their thermo-reversibility after the phase at 37° C, there is an advantage in their administration. In fact, at body temperature, NLC-S gels disorganized themselves more efficiently ensuring a

improved therapeutic efficacy due to the combined action of gel and nanoparticles.

The presence of CLO didn't change the performance of the system. It is possible to evidence the presence of the active linked to the lipidic phase in background noise that can be detected especially in the fusion phase.

Furthermore, in all samples a second weak peak appears at the end of micellization corresponding to the temperature where the micelles arrange in a crystalline structure. The crystallization small peak in micro-DSC could be superimposed to the sol-gel transition temperature in rheology. For this reason, it has been evaluated whether there was a correspondence between the micro-DSC and rheology data.

Table XXV shows the crystallization temperature compared to the sol-gel temperature obtained by rheology analyses.

Table XXV. Temperatures of crystallization peaks and sol-gel transition, obtained by micro-DCS and rheology analyses

Sample	Crystallization peak (°C)	Sol-gel transition temperature (°C)
NLC-D gel	17.89 ± 0.2	17.6 ± 0.8
CLO-NLC-D gel	17.78 ± 0.4	17.5 ± 0.6
NLC-S gel	17.78 ± 0.3	16.8 ± 1.2
CLO-NLC-S gel	17.56 ± 0.6	17.4 ± 1.0

We could observe that values are nearly superimposable both in the comparison between micro-DSC and rheology data, both evaluating the different gelification method used. Also in this case, the presence or the absence of CLO didn't cause variation of crystallization temperature. These values confirmed that all formulated gels are able to change their structure, with a rapid passage from liquid to solid (crystalline) form, at a temperature lower than vaginal temperature, allowing a selective action in the site of application.

Considering the better performances obtained by empty and CLO containing NLC-S gels in calorimetric assays, these formulations were chosen for *in vitro* and *ex vivo* experiments as representative samples for viscous forms of NLC.

6.2.7 *Diffusion experiments*

To compare diffusion of CLO from the different formulations, Franz-cell diffusion method was used. CLO diffusion kinetics from liquid and viscosized NLC and MAD and from the commercial cream Canesten® have been analysed. In particular, the following forms have been tested: CLO-NLC, CLO-MAD, CLO-NLC-S gel, CLO-MAD carbomer gel, CLO-poloxamer gel, CLO-carbomer gel and Canesten®.

Experiments were performed at 37°C, in order to mimic the mucosal temperature. Table XXVI reports diffusion rates (obtained from the slope of the diffusion line), correlation coefficients and amount of released drug after 7 hours.

From the obtained results, it can be observed that CLO diffusion rates from NLC and MAD are comparable, while the corresponding viscous forms display slower diffusion rates, as expected. CLO diffusion rate from Canesten® is similar to those displayed by the drug in NLC and MAD. The slowest rate was obtained by CLO-MAD carbomer gel (0.69), while plain CLO-poloxamer gel exhibited the fastest one (3.1). It is interesting to note that CLO diffuses more slowly from NLC than from poloxamer gel, due to the semi-solid structure of nanoparticles, whilst CLO diffusion from MAD, being characterized by the presence of soft amphiphilic structures such as vesicles and cubosomes, is faster than from the corresponding plain carbomer gel.

At last it can be observed that on one hand the presence of MAD in carbomer gel causes a 1.2-fold reduction in CLO diffusion, on the other NLC-S gel decreases CLO diffusion with respect to the plain poloxamer gel (1.7-fold lower). In this respect it can be concluded that the diffusion of the drug is controlled both by the NLC matrix and by the network of the poloxamer gel, in agreement with the indications obtained by the rheological study.

Table XXVI. CLO diffusion data from the indicated formulations obtained by Franz cell.

Formulation	Diffusion rate (slope of the lines)	Correlation coefficient	Released drug during 7 h (μg/cm^2)
CLO-NLC	2.319	0.997	49.375
CLO-NLC-S gel	1.812	0.998	38.560
CLO-MAD	2.141	0.999	44.865
CLO-MAD carbomer gel	0.695	0.999	14.183
CLO -poloxamer gel	3.101	0.999	63.320
CLO-carbomer gel	0.839	0.998	16.655
Canesten®	2.469	0.999	50.325

CLO-NLC: CLO containing NLC; ***CLO-NLC poloxamer gel***: CLO-NLC directly viscosized by poloxamer gel, ***CLO-MAD***: CLO containing MAD; ***CLO-MAD carbomer gel***: CLO-MAD diluted with carbomer gel; ***CLO-poloxamer gel***: CLO containing gel based on poloxamer 407 (24% w/w); ***CLO-carbomer gel***: CLO containing gel based on carbomer (0.7%, w/w); ***Canesten®***: CLO-commercial formulation.

6.2.8 *Ex vivo study*

Ex vivo experiments were performed only on NLC formulations, considering their better stability by time in terms of drug loading and structure, evaluated by previous tests.

The aim of this further characterization was the investigation of possible systemic side effects of CLO. Even if this drug is also administrated by oral forms, it is noteworthy the liver toxicity of CLO, its use as anticancer drug and the possibility of resistance especially in patients with a compromised immune system [192,193].

After HPLC analyses of fractions related to permeation experiment, no CLO was found in all

samples withdrawn from 0 to 8 hours in the receptor compartment. Neither CLO-NLC dispersion nor CLO-NLC-S gel determined a passage of the active through the vaginal mucosa.

Table XXVII shows the obtained results after penetration measurements.

Table XVII. CLO diffusion data from the indicated formulations obtained by Franz cell.

Sample	Clotrimazole penetrated (%)
CLO-NLC	0.33
CLO-NLC-S gel	0.03

The percentages of CLO penetrated related to the total amount of active calculated after drug recovery characterization are very low and are in accord with permeation data.

It could be observed that CLO-NLC dispersion and CLO-NLC viscosized gel didn't reach the systemic circulation and for this reason, a systemic toxicity could be avoided.

6.2.9 *Anticandidal activity*

NLC and MAD (0.169 mg/ml) dispersions, empty and CLO containing, have been assayed against *C. albicans* (Fig. 46). DMSO has been employed as negative control. Empty MAD and NLC, tested as aqueous dispersions, evidenced a significant CFU reduction capacity of 17.8% and 24.7% with reference to negative control respectively, due to intrinsic cytotoxicity of nano-supports [194,195]. The difference in bioactivity between MAD and NLC was instead not significant (8.4%), evidencing their comparable efficacy against the yeast strain.

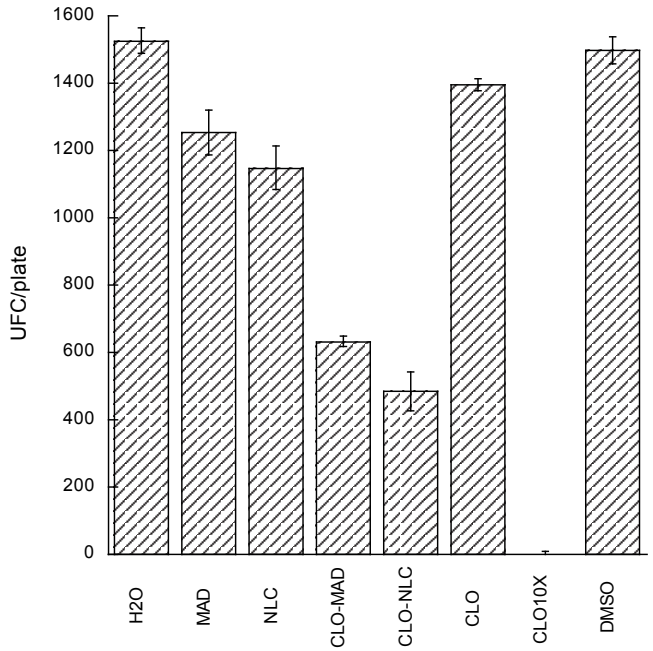

Fig 46. Clotrimazole bioactivity against *C. albicans* ATCC 48274 strain expressed as colony forming units (CFU) per plate ± standard deviation after 5 days of cell incubation with the drug free or encapsulated in different nanoparticulate systems

H_2O: Negative Control as sterile water; MAD: empty monoolein aqueous dispersion; NLC: empty nanostructured lipid carrier dispersion; CLO-MAD: Clotrimazole (0.169 mg/ml) containing MAD; CLO-NLC: Clotrimazole (0.169 mg/ml) containing NLC; CLO: Clotrimazole (0.169 mg/ml) in dimethyl sulfoxide (DMSO); CLO10X: Clotrimazole solution in DMSO (1.69 mg/ml); DMSO: Negative Control as DMSO.

As expected, CLO-NLC and CLO-MAD showed an important decrease of *C. albicans* CFU, with an efficacy of 54.6% and 65.3% respectively if compared to the CLO-DMSO system. In fact, pure CLO (0.169 mg/ml) in DMSO evidenced only a 6.8% CFU reduction capacity with respect to the negative control (DMSO), while significant bioactivity has been instead expressed only at a concentration ten fold higher (1.69 mg/ml).

Since the DMSO negative control evidenced a number of CFU comparable to that displayed by the negative control with sterile H_2O (gap 1.9%), the differences between the CLO-nanosystems

and the pure CLO could be ascribed both to intrinsic cytotoxicity of the nano-matrixes and to the presence of incorporated CLO. It could be tentatively suppose that nanoparticles are able to enhance CLO penetration through fungal cell walls to inhibit ergosterol synthesis [196].

6.2.10 *Cytotoxicity assay*

In figure 47 the results of the toxicity study after 24 hours of exposure of the HeLa cells are illustrated for empty samples in comparison to CLO-containing (1 mg/ml) ones.

The empty solution of ethanol caused less toxicity than the relative CLO-containing solution. In this case CLO is completely dissolved in the organic solvent so we might think of a combined toxic action of solvent and solute in the same time.

Empty NLC induced a cell vitality of 90.2%, otherwise CLO-NLC caused extended cell mortality and only the 27% of cells were living at the end of the experiment.

On the contrary, CLO containing NLC-S showed a toxicity profile only slightly higher than empty NLC-S, resulting in a cell vitality of 74.9% for CLO NLC-S and 77.2% for NLC-S.

A similar result was obtained in the case of a poloxamer aqueous solution (24% w/w) used as control. Empty poloxamer gel caused a cell vitality of 82.5% while CLO containing poloxamer gel 74.3%.

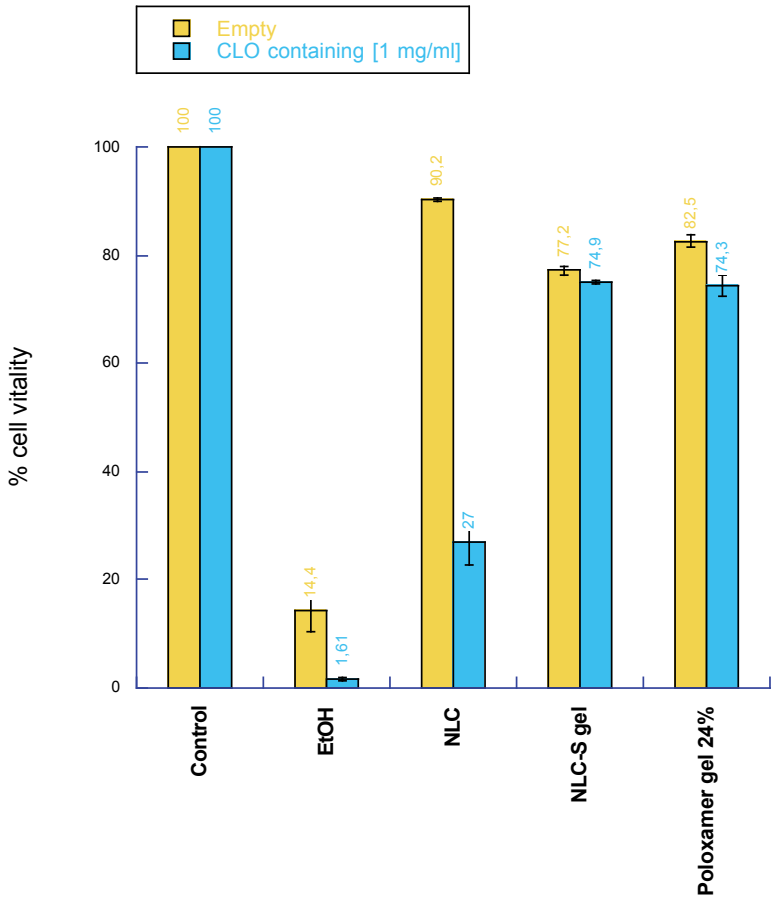

Fig 47. Results of the toxicity study (% of survival referred to the control) after 24 hours contact of HeLa cells with ethanol and a CLO solution in ethanol, NLC and CLO-NLC dispersions, NLC and CLO-NLC-S gels, an aqueous solution of Poloxamer 24% w/w empty and CLO-containing.

7. CONCLUSIONS

In recent years, the use of nanometric devices as delivery systems has been widely studied especially because of their novel engineered properties that provide medical and pharmaceutical benefits. Nanotechnology plays an important role in development of proper formulations that address the drug delivery issues related to NMEs or well-known actives with poor biopharmaceutical properties. Thus, nanoparticulate drug delivery systems are being used to alter the drug's biopharmaceutics and pharmacokinetics such as drug absorption, distribution, metabolism and elimination.

The present work focuses on the development and characterization of Nanostructured Lipid Carriers (NLC) and Monoolein Aqueous Dispersions (MAD) as drug delivery systems for chronic and recurring diseases. The obtained results permitted to better understand structure and behaviours of these complex carrier systems.

7.1 NLC AND MAD FOR THE DELIVERY OF BROMOCRIPTINE

The investigation reported in chapter 4 describes a formulative study for the development of innovative drug delivery systems for an old antiparkinsonian drug.

The first interest in this molecule arose from its wide therapeutic potential. BC is a dopamine receptor agonist used for the treatment of pituitary tumours, PD, hyperprolactinaemia, neuroleptic malignant syndrome and recently approved for the treatment of type 2 diabetes [197].

NLC and MAD based on different lipidic components were produced and characterized, and their morphology and dimensional distribution investigated. BC was perfectly solubilized by the tristearin/tricaprin NLC mixture and encapsulated with high entrapment efficiency. X-ray diffraction analyses demonstrated that the presence of BC did not affect the scattering profile, indicating maintenance of the order inside the hydrocarbon chains.

Like NLC, MAD represents an interesting alternative to liposomes, being characterized by a

higher viscous resistance to rupture and a consequent prolonged stability.

X-ray diffraction studies revealed the presence of dispersed cubic phase particles of *Pn3m* and *Im3m* symmetry, in full agreement with cryo-TEM observations. In addition, these studies evidenced in MAD the typical liquid-like conformation of lipid molecules and the complete dissolution of the drug in the nanoparticles.

Concerning the *in vitro* analyses, the use of different experimental approaches to determine the release kinetic from disperse systems can give distinct results in term of drug availability. This point is particularly crucial, especially if we consider that information contained in the release curve are generally used for the determination of the therapeutic dose (bioavailable drug) and for quality control to ensure batch to batch uniformity.

Our data indicate that the *in vitro* release of poorly water soluble drugs (as BC used in our study) is more affected by the composition of the receiving phase (i.e. in term of presence of water miscible polar organic solvents) rather than by the experimental modality adopted for the *in vitro* determinations.

In vivo studies showed that only BC-NLC were able to markedly attenuate motor deficit in 6-OHDA hemilesioned rats, suggesting that NLC represent a more effective carrier to prolong the half-life of BC in vivo.

7.2 NLC AND SLN FOR THE DELIVERY OF L-DOPA DERIVATIVES

In chapter 5 is reported a study aimed at improve the biopharmaceutical properties of new synthetized LD derivatives, named Der-A, Der-B, Der-C and Der-D, by the use of NLC or SLN.

It was possible to produce NLC for controlled release of molecules with potential activity against neurodegenerative diseases. All the produced formulations resulted homogeneous in terms of size and remain stable until two months from the preparation. Morphological characterization highlighted that no substantial difference characterized empty and derivatives containing NLC.

All the derivatives used, only with the exception of Der-B, showed great yields of incorporation compared to the total amount of medication used for preparation. *In vitro* kinetics release

performed by equilibrium dialysis highlighted that NLC were able to release the contained derivatives in a controlled manner and permit to select Der-A for *in vivo* tests and further inclusion tests in SLN. *In vivo* tests demonstrated that the Der-A possess antiparkinson activity, despite the best therapy in Parkinson's disease remains the LD.

The inclusion of Der-A in SLN was performed using three different concentrations of prodrug. All the obtained SLN resulted dimensionally and morphologically stable within four months. The determination of Der-A content allowed to highlight that only two concentrations gave good yields of incorporation: Der-A SLN (1x) and Der-A SLN (2x). These preparations were chosen for calorimetric test that showed an effective interaction between lipid phase and the prodrug. *In vitro* studies performed by dialysis method and enzymatic degradation showed that the Der-A SLN were able to ensure a controlled release, also thanks to the extension of the half-life of the prodrug. Further tests should be conducted in order to evaluate the *in vivo* activity of Der-A SLN (2x) that showed the best characteristics in these characterization studies.

7.3 NLC AND MAD FOR THE DELIVERY OF CLOTRIMAZOLE

In chapter 6, Clotrimazole, an imidazole derivative, was chosen for the inclusion in NLC or MAD, with the aim to improve its bioavailability and obtain a suitable mucosal formulation, after gelification of nanosystems.

This study demonstrated that CLO can be incorporated both in MAD and in NLC with high recovery. Shelf life stability evidenced that the solid matrix of NLC enabled to control drug degradation better than MAD. *In vitro* experiments on candida cells demonstrated that CLO-MAD and CLO-NLC exhibit a higher activity than the free drug.

In addition rheological and diffusion studies indicated that both the matrix and the gel network of CLO-NLC poloxamer gel can control CLO diffusion. The gel enables to solubilize lipophilic drugs in an aqueous structured vehicle and to control their release.

Micro calorimetric assays permitted to better characterize the viscosized preparations and confirmed that all formulated gels are able to change their structure, with a rapid passage from

liquid to solid (crystalline) form at a temperature lower than vaginal temperature, allowing a selective action in the site of application.

Finally it is noteworthy that the production of CLO-NLC poloxamer gel is simple and suitable for industry scaling up.

BIBLIOGRAPHY

[1] J. Kreuter. *Nanoparticles - a historical perspective.* International Journal of Pharmaceutics 331 (2007) 1-10

[2] A.S. Hoffman. *The origins and evolution of "controlled" drug delivery systems.* Journal of Controlled Release 132 (2008) 153-163

[3] W. Mehnert and K. Mäder. *Solid lipid nanoparticles: production, characterization and applications.* Advanced Drug Delivery Reviews. 47 (2001) 165-196.

[4] G.M. Barratt. *Therapeutic applications of colloidal drug carriers.* Pharmaceutical Science and Technology Today. 3 (2000) 163-169.

[5] P. Couvreur, C. Dubernet, and F. Puisieux. *Controlled drug delivery with nanoparticles: current possibilities and future trends.* European Journal of Pharmaceutics and Biopharmaceutics. 41 (1995) 2-13.

[6] G.L. Amidon, H. Lennernas, V. P. Shah, J.R. Crison. *A theoretical basis for a biopharmaceutic drug classification: the correlation of in vitro drug product dissolution and in vivo bioavailablility.* Pharmaceutical Research. 12 (1995) 413-420.

[7] R. Löbenberg and G.L. Amidon. *Modern bioavailability, bioequivalence and biopharmaceutics classification system. New scientific approaches to international regulatory standards.* European Journal of Pharmaceutics and Biopharmaceutics. 50 (2000) 3-12.

[8] J. B. Dressman and C. Reppas. *In vitro-in vivo correlations for lipophilic, poorly water-soluble drugs.* European Journal of Pharmaceutics and Biopharmaceutics. 11 (2000) S73-S80.

[9] R.L. Juliano. *Drug delivery systems: a brief review.* Canadian Journal of Physiology and Pharmacology. 56 (1978) 683-690.

[10] S. Parveen, S.K. Sahoo. *Nanomedicine: clinical applications of polyethylene glycol conjugated proteins and drugs.* Clinical Pharmacokinetics. 45 (2006) 965-988.

[11] H.J. Lee. *Protein drug oral delivery: the recent progress.* Archives of Pharmacal Research. 25 (2002) 572-584.

[12] O. Kayser, A. Lemke, N. Hernandez-Trejo. *The impact of nanobiotechnology on the development of new drug delivery systems.* Current Pharmaceutical Biotechnology.6 (2005) 3-5.

[13] C. W. Burke, Y. H. J. Hsiang, E. Alexander, A. L. Kilbanov and R. J. Price. *Covalently linking Poly(lactic-co-glycolic acid) nanoparticles to microbubbles before intravenous injection improves their Ultrasound-Targeted delivery to skeletal muscle.* Small. 7 (2011) 1227–1235.

[14] M. Schafer-Korting, W. Mehnert, H.-C. Korting. *Lipid nanoparticles for improved topical application of drugs for skin disease.* Advanced Drug Delivery Reviews. 59 (6) (2007) 427-443.

[15] R. H. Mu□ller, M. Radtke, and S. A. Wissing. *Solid lipid nanoparticles (SLN) and nanostructured lipid carriers (NLC) in cosmetic and dermatological preparations.* Advanced Drug Delivery Reviews. 54 (2002) S131-S155.

[16] A. Lippacher, R.H. Muller, K. Mader. *Preparation of semisolid drug carriers for topical application based on solid lipid nanoparticles.* International Journal of Pharmaceutics. 214 (1-2) (2001) 9-12.

[17] T. Jung, W. Kamm, A. Breitenbach, E. Kaiserling, J.X. Xiao, T. Kissel. *Biodegradable nanoparticles for oral delivery of peptides: is there a role for polymers to affect mucosal uptake?* European Journal of Pharmaceutics and Biopharmaceutics. 50 (1) (2000) 147-160.

[18] A. des Rieux, V. Fievez, M. Garinot, Y.-J. Schneider, V. Preat. *Nanoparticles as potential oral delivery systems of proteins and vaccines: a mechanistic approach.* Journal of Controlled Release. 116 (1) (2006) 1-27.

[19] R. Cavalli, M.R. Gasco, P. Chetoni, S. Burgalassi, M.F. Saettone. *Solid lipid nanoparticles (SLN) as ocular delivery system for tobramycin.* International Journal of Pharmaceutics. 238 (1-2) (2002) 241-245.

[20] Mark M. Bailey, Cory J. Berkland. *Nanoparticle formulations in pulmonary drug delivery.* Medicinal Research Review. 29 (1) (2009) 196–212.

[21] H. Maeda, J. Wu, T. Sawa, Y. Matsumura, K. Hori. *Tumor vascular permeability and the EPR effect in macromolecular therapeutics: a review.* Journal of Controlled Release. 65 (2000) 271-284.

[22] Y. Matsumura, H. Maeda. *A new concept for macromolecular therapeutics in cancer chemotherapy: mechanism of tumoritropic accumulation of proteins and the antitumor agent smancs.* Cancer Research. 46 (1986) 6387-6392.

[23] S.K. Sahoo, V. Labhasetwar. *Enhanced Antiproliferative Activity of Transferrin-Conjugated Paclitaxel-Loaded Nanoparticles Is Mediated via Sustained Intracellular Drug Retention.* Molecular Pharmacology. 2 (5) (2005) 373–383

[24] P.E. Thorpe. *Vascular targeting agents as cancer therapeutics.* Clinical Cancer Research.10 (2004) 415-427.

[25] G. Molema, D.K. Meijer, L.F. de Leij. *Tumor vasculature targeted therapies: getting the players organized.* Biochemical Pharmacology. 55 (1998) 1939-1945.

[26] J.M. Koziara, P.R. Lockman, D.D. Allen, R.J. Mumper. *Paclitaxel nanoparticles for the potential treatment of brain tumors.* Jornal of Controlled Release. 99 (2) (2004) 259-269.

[27] S.K. Sahoo, V. Labhasetwar. *Nanotech approaches to drug delivery and imaging*. Drug Discovery Today. 8 (2003) 1112-1120.

[28] S. Parveen, S.K. Sahoo. *Polymeric nanoparticles for cancer therapy.* Journal of Drug Targeting. 16 (2008) 108-23.

[29] S. Parveen, R. Misra, S.K. Sahoo. *Nanoparticles: a boon to drug delivery, therapeutics, diagnostics and imaging.* Nanomedicine: Nanotechnology, Biology, and Medicine. 8 (2012) 147-166

[30] T.C. Yih, M. Al-Fandi. *Engineered nanoparticles as precise drug delivery systems.* Journal of Cellular Biochemistry. 97 (2006) 1184-90.

[31] M. C. Venier-Julienne and J. P. Benoît. *Preparation, purification and morphology of polymeric nanoparticles as drug carriers.* Pharmaceutica Acta Helvetiae. 71 (1996) 121-128.

[32] J. Kreuter. *Nanoparticles.* In: J. Kreuter (ed), Colloidal drug delivery systems, Vol. 6, Drugs and the pharmaceutical sciences, Marcel Dekker Inc., New York, Basel and Hong Kong. (1994) 219-342.

[33] R. Gurny, N.A. Peppas, D.D. Harrington, and G.S. Banker. *Development of biodegradable and injectable latices for controlled release of potent drugs.* Drug Development and Industrial Pharmacy. 7 (1981) 1-25.

[34] R. Bodmeier and H. Chen. *Indomethacin polymeric nanosuspensions prepared by microfluidization.* Journal of Controlled Release. 12 (1990) 223-233.

[35] E. Allémann, R. Gurny, and E. Doelker. *Drug-loaded nanoparticles – preparation methods and drug targeting issues.* European Journal of Pharmaceutics and Biopharmaceutics. 39 (1993) 173-191.

[36] J. Panyam, V. Labhasetwar. *Biodegradable nanoparticles for drug and gene delivery to cells and tissue.* Advanced Drug Delivery Reviews. 55 (2003) 329-347.

[37] J. Panyam, S.K. Sahoo, S. Prabha, T. Bargar, V. Labhasetwar. *Fluorescence and electron microscopy probes for cellular and tissue uptake of poly(D,L-lactide-co-glycolide) nanoparticles.* International Journal of Pharmaceutics. 262 (2003) 1-11.

[38] J. Panyam, W.Z. Zhou, S. Prabha, S.K. Sahoo, V. Labhasetwar. *Rapid endo-lysosomal escape of poly(DL-lactide-co-glycolide) nanoparticles: implications for drug and gene delivery.* The Faseb Journal. 16 (2002) 1217-1226.

[39] I. Brigger, C. Dubernet, P. Couvreur. *Nanoparticles in cancer therapy and diagnosis.* Advanced Drug Delivery Reviews. 54 (2002) 631-651.

[40] C. Vauthier, C. Dubernet, C. Chauvierre, I. Brigger, P. Couvreur. *Drug delivery to resistant tumors: the potential of poly(alkyl cyanoacrylate)nanoparticles.* Journal of Controlled Release. 93 (2003) 151-160.

[41] J. Wang, X. Tao, Y. Zhang, D. Wei, Y. Ren. *Reversion of multidrug resistance by tumor targeted delivery of antisense oligodeoxynucleotides in hydroxypropyl-chitosan nanoparticles.* Biomaterials 31 (2010) 4426-33.

[42] R.S. Fisher, J. Ho. *Potential new methods for antiepileptic drug delivery.* CNS Drugs. 16 (2002) 579-593.

[43] P.R. Lockman, R.J. Mumper, M.A. Khan, D.D. Allen. *Nanoparticle technology for drug delivery across the blood-brain barrier.* Drug Development and Industrial Pharmacy. 28 (2002) 1-13.

[44] H. Sun, H. Dai, N. Shaik, W.F. Elmquist. *Drug efflux transporters in the CNS.* Advanced Drug Delivery Reviews. 55 (2003) 83-105.

[45] Y. Zhang, F. Calon, C. Zhu, R.J. Boado, W.M. Pardridge. *Intravenous nonviral gene therapy causes normalization of striatal tyrosine hydroxylase and reversal of motor impairment in experimental parkinsonism.* Human Gene Therapy. 14 (2003) 1-12.

[46] Z.H. Wang, Z.Y. Wang, C.S. Sun, C.Y. Wang, T.Y. Jiang, S.L. Wang. *Trimethylated chitosan-conjugated PLGA nanoparticles for the delivery of drugs to the brain.* Biomaterials 31 (2010) 908-915.

[47] T.K. Jain, I. Roy, T.K. De, A.N. Maitra. *Nanometer silica particles encapsulating active compounds: a novel ceramic drug carrier.* Journal of the American Chemical Society. 120 (1998) 11092-11095.

[48] R. Gref, Y. Minamitake, M.T. Peracchia, V. Trubetskoy, V. Torchilin, R. Langer *Biodegradable long-circulating polymeric nanospheres.* Science. 263 (1994) 1600-1603.

[49] I.□I. Slowing, B.□G. Trewyn, S. Giri, V.□S.-Y. Lin. *Mesoporous Silica Nanoparticles for Drug Delivery and Biosensing Applications.* Advanced Functional Materials. 17 (8) (2007) 1225-1236.

[50] M. Vallet-Regí, F. Balas, D. Arcos. *Mesoporous Materials for Drug Delivery.* Angewandte Chemie International Edition. 46 (40) (2007) 7548-7558.

[51] J. Dobson. *Magnetic micro- and nano-particle-based targeting for drug and gene delivery.* Nanomedicine (London, England) 1 (2006) 31-37.

[52] J. Tian, K.K. Wong, C.M. Ho, C.N. Lok, W.Y. Yu, C.M. Che, J.F. Chiu, P.K. Tam. *Topical delivery of silver nanoparticles promotes wound healing.* ChemMedChem. 2 (2007) 129-136.

[53] Y.Y. Song, F. Schmidt-Stein, S. Bauer, P. Schmuki. *Amphiphilic TiO_2 nanotube arrays: an actively controllable drug delivery system.* Journal of the American Chemical Society. 131 (2009) 4230-4232.

[54] V.P. Torchilin. *Targeted polymeric micelles for delivery of poorly soluble drugs.* Cellular and Molecular Life Science. 61 (2004) 2549-2559.

[55] W.B. Turnbull, J.F. Stoddart. *Design and synthesis of glycodendrimers.* Journal of Biotechnology. 90 (2002) 231-255.

[56] Y. Li, Y.D. Tseng, S.Y. Kwon, L. D'Espaux, J.S. Bunch, P.L. McEuen, et al. *Controlled assembly of dendrimer-like DNA.* Nature Materials. 3 (2004) 38-42.

[57] R.H. Muller, D. Ruhl, S. Runge, K. Schulze-Forster, W. Mehnert. *Cytotoxicity of solid lipid nanoparticles as a function of the lipid matrix and the surfactant.* Pharmaceutical Research. 14 (1997) 458-462.

[58] A.A. Attama, S. Reichl, C.C. Muller-Goymann. *Diclofenac sodium delivery to the eye: In vitro evaluation of novel solid lipid nanoparticle formulation using human cornea construct.* International Journal of Pharmaceutics. 335 (1-2) (2008) 307-313.

[59] S.C. Yang, L.F. Lu, Y. Cai, J.B. Zhu, B.W. Liang, C.Z. Yang. *Body distribution in mice of intravenously injected camptothecin solid lipid nanoparticles and targeting effect on brain.* Journal of Controlled Release. 59 (1999) 299-307.

[60] S.A. Wissing, O. Kayser, R.H. Muller. *Solid lipid nanoparticles for parenteral drug delivery.* Advanced Drug Delivery Reviews. 56 (2004) 1257-1272.

[61] A. Fundaro, R. Cavalli, A. Bargoni, D. Vighetto, G.P. Zara, M.R. Gasco. *Non-stealth and stealth solid lipid nanoparticles (SLN) carrying doxorubicin: pharmacokinetics and tissue distribution after i.v. administration to rats.* Pharmacological Research. 42 (2000) 337-343.

[62] C.S. Maia, W. Mehnert, M. Schafer-Korting. *Solid lipid nanoparticles as drug carriers for topical glucocorticoids.* International Journal of Pharmaceutics. 196 (2000)165-167.

[63] M. Uner, S.A. Wissing, G. Yener, R.H. Muller. *Influence of surfactants on the physical stability of solid lipid nanoparticle (SLN) formulations.* Pharmazie. 59 (2004) 331-332.

[64] G.P. Zara, R. Cavalli, A. Bargoni, A. Fundaro, D. Vighetto, M.R. Gasco. *Intravenous administration to rabbits of non-stealth and stealth doxorubicin-loaded solid lipid nanoparticles at increasing concentrations of stealth agent: pharmacokinetics and distribution of doxorubicin in brain and other tissues.* Journal of Drug Targeting. 10 (2002) 327-335.

[65] G. Livesey. *The absorption of stearic acid from triacylglycerols: an inquiry and analysis.* Nutrition Research Reviews. 13 (2000) 185-214.

[66] U. Bracco. *Effect of triglyceride structure on fat absorption.* The American Journal of Clinical Nutrition. 66 (1994) 1002S-1009S.

[67] L.P. Klemann, J.W. Finley, G.A. Leveille. *Estimation of the absorption coefficient of stearic acid in SALATRIM fats.* Journal of Agricultural and Food Chemistry. 42 (1994) 484-488.

[68] J.W. Finley, L.P. Klemann, G.A. Leveille, M.S. Otterburn, C.G. Walchak. Caloric availability of SALATRIM in rats and humans. Journal of Agricultural and Food Chemistry. 42 (1994) 495-499.

[69] L. Hernqvist, *Crystal structures of fats and fatty acids.* In: N. Garti, K. Sato, (Eds.), Crystallization and Polymorphism of Fats and Fatty Acids, Marcel Dekker, New York, Basel, (1988) 97–138.

[70] K. Westesen, H. Bunjes, M.H.J. Koch. *Physiochemical characterization of lipid nanoparticles and evaluation of their drug loading capacity and sustained release potential.* Journal of Controlled release. 48 (1997) 223-236.

[71] R.H. Muller, M. Radtke, S.A. Wissing. *Nanostructured lipid matrices for improved microencapsulation of drugs.* International Journal of Pharmaceutics. 242 (2002) 121-128.

[72] H. Qiu, M. Caffrey. *The phase diagram of the monoolein/water system: metastability and equilibrium aspects.* Biomaterials. 21 (2002) 223-234.

[73] P.T. Spicer. Cubosomes: Bicontinuous Cubic Liquid Crystalline Nanostructured Particles. Encyclopedia of Nanoscience ad Nanotechnology. (2004) 1-11.

[74] S.T. Hyde, S. Andersson, B. Ericsson, K. Larsson. *A cubic structure consisting of a lipid bilayer forming an infinite periodic minimal surface of the gyroid type in the glycerol monooleate water system.* Zeitschrift für Kristallographie. 168 (1984) 213-219.

[75] P. Mariani, V. Luzzati, H. Delacroix. *Cubic phases of lipid containing systems. Structure analysis and biological implications.* Journal of Molecular Biology. 204 (1988) 165-189.

[76] V. Luzzati, R. Vargas, P. Mariani, A. Gulik, H. Delacroix. *Cubic phases of lipid-containing systems. Elements of a theory and biological connotations.* Journal of Molecular Biology. 229 (1993) 540-551.

[77] H. Chung, M. Caffrey. *The neutral area surface of the cubic mesophases: location and properties.* Biophysical Journal. 66 (1994) 377-381.

[78] K. Larsson. *Aqueous dispersion of cubic lipid-water phases.* Current Opinion in Colloid Interface Science. 5 (2000) 64-69.

[79] T. Landh, K. Larsson. *Particles, method of preparing said particles and uses thereof.* US patent no. 5531925 (1996).

[80] J.S. Patton, M.C. Carey. *Watching fat digestion*. Science. 204 (1979) 145-148.

[81] K. Larsson. *Cubic lipid-water phases: Structures and biomembrane aspects.* The Journal of Physical Chemistry. 93 (1989) 7304-7314.

[82] H.W. Meyer, W. Richter, J. Gumpter. *Periodically curved bilayer structures observed in hyphal cells or stable L-form cells of a Streptomyces strain, and in liposomes formed by the extracted lipids.* Biochimica et Biophysica Acta. 1026 (1990) 171-178.

[83] H. Ljusberg-Wharen, L. Nyberg, K. Larsson. Dispersion of the cubic liquid crystalline phase: Structure, preparation and functionality aspects. Chimica oggi. 14 (6) (1996) 40-43.

[84] B.J. Boyd. *Characterisation of drug release from cubosomes using the pressure ultrafiltration method.* International Journal of Pharmaceutics. 260 (2003) 239-247.

[85] J. Borne, T. Nylander, A. Khan. Effect of lipase on monoolein-based cubic phase dispersion (cubosomes) and vesicles. The Journal of Physical Chemistry B. 106 (40) (2002) 10492-10500.

[86] H.Bunjes, J. Kuntsche. *Lipid Nanoparticles Based on Liquid Crystalline Phases.* In: V. Torchlin, M.M. Amiji. Handbook of Materials for nanomedicine. Pan Stanford Publishing (2010) 445-494.

[87] E. Esposito, N. Eblovi, S. Rasi, M. Drechsler, G.M. Di Gregorio, E. Menegatti, R. Cortesi. *Lipid based supramolecular systems for topical application: a preformulatory study*. AAPS AAPS Pharm.Sci.Tech. 5 (2003) 4 (article 30).

[88] P.T. Spicer, K.L. Hayden. *Novel process for producing cubic liquid crystalline nanoparticles (cubosomes).* Langmuir 17 (2001) 5748–5756.

[89] M. Nakano, A. Sugita, H. Matsuoka, T. Handa. *Small angle X-ray scattering and 13C NMR investigation on the internal structure of cubosome*. Langmuir. 17 (2001) 3917–3922.

[90] L. Sagalowicz, R. Mezzenga, M.E. Leser. *Investigating reversed liquid crystalline mesophases.* Current Opinion in Colloid Interface Science. 11 (2006) 224–229.

[91] J. Lai, J. Chen, Y. Lu, J. Sun, F. Hu, Z. Yin,W.Wu. *Glyceryl monooleate/Poloxamer 407 cubic nanoparticles as oral drug delivery systems: I. In vitro evaluation and enhanced oral bioavailability of the poorly water-soluble drug simvastatin,* AAPS Pharm.Sci.Tech. 10 (2009) 960-966.

[92] H. P. Fiedler. *Lexikon der Hilfsstoffe fu□r Pharmazie, Kosmetik und angrenzende Gebiete*, Editio Cantor Verlag, Aulendorf (1996).

[93] Hem, S.L., Feldkamp, J.R., White, J.L.. *Basic chemical principles related to emulsions and suspension dosage forms*, in *The theory and practice of industrial pharmacy*, Lachman, L., Lieberman, H.A., Kanig, J.L., Editors., Lea & Febiger: Philadelphia. (1986) 100-22.

[94] P. Alexandridis and T. A. Hatton. *Poly(ethylene oxide)-poly(propylene oxide)-poly(ethylene oxide) block copolymer surfactants in aqueous solutions and at interfaces: thermodynamics, structure, dynamics, and modeling.* Colloids and Surfaces B. 96 (1995) 1-46.

[95] BASF. *Technical information for Lutrol F 68TM*, Ludwigshafen, Germany, 1997.

[96] G. Dumortier, J. L. Grossiord, F. Agnely, J. Cl. Chaumeil. *A Review of Poloxamer 407 Pharmaceutical and Pharmacological Characteristics.* Pharmaceutical Research. 23 (12) (2006) 2709-2728

[97] K. W. Wirtz. *Phospholipid transfer proteins*. Annual Review of Biochemistry. 60 (13) (1991) 73–99

[98] P. A. Serra, G. Esposito, P. Enrico, M. A. Mura, R. Migheli, M. R. Delogu, M. Miele, M. S. Desole, G. Grella, E. Miele. *Manganese increases L-DOPA auto-oxidation in the striatum of the freely moving rat: potential implications to l-DOPA long-term therapy of Parkinson's disease.* British Journal of Pharmacology. 130 (2000) 937-945.

[99] T. S. Smith, P W. Jr. Darker, J. P. Jr. Bennet. *L-Dopa increases nigral production of hydroxyl radicals in vivo: potential L-Dopa toxicity?* Neuroreport. 5 (1994) 1009-1011.

[100] B. Pardo, M. A. Mena, M. J. Casarejos, C. L. Paino, J. G. De Yebenes. *Toxic effects of L-Dopa on mesencephalic cell cultures: protection with antioxidants.* Brain Research. 682 (1-2) (1995) 133-143.

[101] S. Przedborski, V. Jackson-Lewis, U. Muthane, H. Jiang, M. Ferreira, A. B. Naini, S. Fahn. *Chronic levodopa administration alters cerebral mitochondrial respiratory chain activity.* Annals of Neurology. 34 (5) (1993) 715-723.

[102] J. W. Miller, J. Selhub, J. A. Joseph. *Oxidative damage caused by free radicals produced during catecholamine autoxidation: protective effects of O-methylation and melatonin.* Free Radical Biology and Medicine. 21 (2) (1996) 241-249.

[103] W. S. Enoch, T. Sarna, L. Zecca, P. A. Riley, H. M. Swartz. *The roles of neuromelanin, binding of metal ions, and the oxidative cytotoxicity in the pathogenesis of Parkinson's disease: a hypothesis.* Journal of Neural Transmission. 7 (1994) 83-100.

[104] J. D. Adams, I. N. Odunze. *Oxygen free radicals and Parkinson's disease.* Free Radical Biology and Medicine. 10 (2) (1991) 161-169.

[105] M. Roghani, G. Behzadi. *Neuroprotective effect of vitamin E on the early model of Parkinson's disease in rat: behavioral and histochemical evidence.* Brain Research. 892 (1) (2001) 211-217.

[106] J. A. Stamford, D. Isaac, C. A. Hicks, M. A. Ward, D. J. Osborne, M. J. O¢Neill. *Ascorbic acid is neuroprotective against global ischaemia in striatum but not hippocampus: histological and voltammetric data.* Brain Research. 835 (2) (1999) 229-240.

[107] C. Hershko, D. J. Weatherall. *Iron-chelating therapy.* Critical Reviews in Clinical Laboratory Sciences. 26 (1988) 303-345.

[108] C. C. Chiueh. *Iron overload, oxidative stress and axonal dystrophy in brain disorders.* Pediatric Neurology. 25 (2001) 138-147.

[109] M. Rosini, V. Andrisano, M. Bartolini, M. L. Bolognesi, P. Hrelia, A. Minarini, A. Tarozzi, C. Melchiorre. *Rational Approach to discover multipotent anti-Alzheimer drugs.* Journal of Medicinal Chemistry. 48 (2005) 360-363.

[110] J. A. M. Christiaans, H. Timmerman. *Cardiovascular hybrid drugs: combination of more than one pharmacological property in one single molecule.* European Journal of Pharmaceutical Sciences. 4 (1996) 1-22.

[111] N. M.Mahfouz, T. Aboul-Fadl, A. K. Diab. *Ester Twin Drugs of Metronidazole: synthesis, physiochemical properties, kinetics studies and antigardial activity.* European Journal of Medicinal Chemistry. 33 (1998) 675-683.

[112] L. I. Giannola, G. Giammona, R. Alotta. *Pro-drugs of isoniazid: synthesis and diffusion characteristics of acyl derivatives.* Pharmazie. 47 (6) (1992) 423-425.

[113] M. Langlois, D. Quintard, C. Abalain. *Synthesis of symmetrical pseudopeptides as potential inhibitors of the human immunodeficiency virus-1 protease.* European Journal of Medicinal Chemistry. 29 (1994) 639-647.

[114] N. Bodor, K. B. Sloan, T. Higuchi, K. Sasahara. *Improved elivery through biological membranes. Prodrugs of L-DOPA.* Journal of Medicinal Chemistry. 20 (11) (1977) 1435–1445.

[115] S.H. Park, S.H. Kang, S.H. Lim, H.S. Oh, K.H. Lee. *Design and synthesis of small chemical inhibitors containing different scaffolds for Ick SH2 domain.* Bioorganic and Medicinal Chemistry Letters. 13 (20) (2003) 3455–3459.

[116] C. Chavis, F. Grodenic, J.L. Imbach. *Ribosides et dérivés de la L-méthyl dopa et de la L-dopa.* European Journal of Medicinal Chemistry.- Chim. Ther. 16 (1981) 219-227.

[117] P. Sozio, A. Iannitelli, L.S. Cerasa, I. Cacciatore, C. Cornacchia, G. Giorgioni, M. Ricciutelli, C. Nasuti, F. Cantalamessa, A. Di Stefano. *New L-Dopa Codrugs as Potential Antiparkinson Agents.* Archiv der Pharmazie - Chemistry in Life Sciences. 341 (2008) 412-417.

[118] S. Bharath, B.C. Cochran, M. Hsu, B. N. Ames, J. K. Andersen. *Pretreatment with R-Lipoic acid alleviates the effects of GSH depletion in PC12 cells: implications for Parkinson's disease therapy.* Neurotoxicology. 23 (2002) 479-486.

[119] A. Di Stefano, B. Mosciatti, G.M. Cingolani, G. Giorgioni, M. Ricciutelli, I. Cacciatore, P. Sozio, F. Claudi. *Dimeric L-Dopa Derivatives as Potential Prodrugs* Bioorganic & Medicinal Chemistry Letters. 11 (2001) 1085–1088

[120] Marieb & Hoehn. *Human Anatomy and Physiology.* Toronto: Pearson. (2010) 643.

[121] http://www.rxmed.com

[122] FDA. *Clotrimazole Official FDA information, side effects and uses.* Retrieved 28 December 2011.

[123] *Clotrimazole.* Fungal Guide. Vancouver. BC. Canada. Retrieved 15 February 2011.

[124] R.H. Müller, R. Schuhmann. *Teilchengrößenmessung in der Laborpraxis*. Stuttgart: Wissenschaftliche Verlagsgesellschaft mbH. (1996) 191.

[125] R.H. Müller. *Colloidal carriers for controlled drug delivery and targeting. Modification, characterization, and In vivo distribution,* Stuttgart, Boston: Wissenschaftliche Verlagsgesellschaft GmbH, CRC Press (1991).

[126] M. Kaszuba, D. McKnight, M.T. Connah, F.K. McNeil-Watson, U. Nobbmann. *Measuring sub nanometre sizes using dynamic light scattering*. Journal of Nanoparticle Research. 10(5) (2007) 823-829.

[127] K. Thode, R.H. Müller, M. Kresse. *Two-time window and multiangle photon correlation spectroscopy size and zeta potential analysis - Highly sensitive rapid assay for dispersion stability*. Journal of Pharmaceutical Sciences. 89(10) (2000) 1317-1324.

[128] R. Pecora. *Dynamic Light Scattering measurement of nanometer particles in liquids*. Journal of Nanoparticle Research. 2 (2000) 123-131.

[129] C. Contado, G. Blo, F. Fagioli, F. Dondi, R. Beckett. *Characterisation of River Po particles by sedimentation field-flow fractionation coupled to GFAAS and ICP-MS.* Colloids and Surfaces, A: Physicochemical and Engineering Aspects. 120 (1997) 47-59.

[130] E. Esposito, E. Menegatti, R. Cortesi, M. Drechsler. *Lipid-based dispersions for drug delivery.* Handbook of Particulate Drug Delivery. 1 (2008) 235-243.

[131] B. Ericsson, K. Larsson, K. Fontell. *A cubic protein-monoolein-water phase*. Biochimica et Biophysica Acta – Biomembranes (BBA). 729 (1) (1983) 23-27.

[132] P. Andreozzi, S.S. Funari, C. La Mesa, P. Mariani, M. G. Ortore, R. Sinibaldi, F. Spinozzi. *Multi- to unilamellar transitions in catanionic vesicles*. The Journal of Physical Chemistry B. 114 (2010) 8056-8060.

[133] F. Spinozzi, L. Paccamiccio, P. Mariani, L.Q. Amaral. *Melting regime of the anionic phospholipid DMPG: new lamellar phase and porous bilayer model,* Langmuir, 26 (2010) 6484-6493.

[134] J.L. Ford, P. Timmins, E. Horwood. *Pharmaceutical thermal analysis - techniques and applications*. Ed. Horwood, E. West Sussex, England: Ellis Horwood Limited (1989).

[135] C. Freitas, R.H. Müller. *Correlation between long-term stability of solid lipid nanoparticles (SLN) and crystallinity of the lipid phase*. European Journal of Pharmaceutics and Biopharmaceutics. 47(2) (1999) 125-132.

[136] H. Bunjes, T. Unruh. *Characterization of lipid nanoparticles by differential scanning calorimetry, X-ray and neutron scattering*. Advanced Drug Delivery Reviews. 59(6) (2007) 379-402.

[137] T. Unruh, H. Bunjes, K. Westesen, M.H.J. Koch. *Observation of Size-Dependent Melting in Lipid Nanoparticles*. The Journal of Physical Chemistry B. 103(47) (1999) 10373-10377.

[138] T. Unruh, H. Bunjes, K. Westesen, M.H.J. Koch. *Investigations on the melting behaviour of triglyceride nanoparticles*. Colloid and Polymer Science. 279(4) (2001) 398-403.

[139] L.C. Pham Trong, M. Djabourov, A. Ponton. *Mechanisms of micellization and rheology of PEO–PPO–PEO triblock copolymers with various architectures.* Journal of Colloid and Interface Science. 328 (2008) 278–287.

[140] J.I. Wells. Pharmaceutical Preformulation: *The Physicochemical Properties of Drug Substances*. Ellis Hortwood, Chichester, England (1988).

[141] D.H. Owen, D.F. Katz. *A vaginal fluid stimulant*. Contraception 59 (1999) 91–95.

[142] F.P. Bonina, L. Montenegro, N. Scrofani, E. Esposito, R. Cortesi, E. Menegatti, C. Nastruzzi. *Effect of phospholipid based formulations on in vitro and in vivo percutaneous absorption of methyl nicotinate.* Journal of Controlled Release. 34 (1995) 53–63.

[143] A. van Eyk, P. van der Bijl. *Porcine vaginal mucosa as an in vitro permeability model for human vaginal mucosa.* International Journal of Pharmaceutics. 305 (2005) 105–111.

[144] C.A. Squier, M.J. Mantz, P.M. Schlievert, C.C. Davis. *Porcine vagina ex vivo as a model for studying permeability and pathogenesis in mucosa.* Journal of Pharmaceutical Sciences. 97 (2008) 9–21.

[145] M. Marti, F. Mela, M. Fantin, S. Zucchini, J.M Brown, J. Witta, M. Di Benedetto, B. Buzas, R.K. Reinscheid, S. Salvadori, R. Guerrini, P. Romualdi, S. Candeletti, M. Simonato, B.M. Cox, M. Morari**.** *Blockade of nociceptin/orphanin FQ transmission attenuates symptoms and neurodegeneration associated with Parkinson's disease*. The Journal of Neuroscience. 95 (2005) 9591-9601.

[146] G. Paxinos, C. Watson. *The rat brain in stereotaxic coordinates*. Ed. Academic, Sydney (1982).

[147] M. Marti, C. Trapella, R. Viaro, M. Morari**.** *The nociceptin/orphanin FQ receptor antagonist J-113397 and L-DOPA additively attenuate experimental parkinsonism through overinhibition of the nigrothalamic pathway*. The Journal of Neuroscience. 27 (2007) 1297-1307.

[148] M. Marti, F. Mela, C. Bianchi, L. Beani, M. Morari. *Striatal dopamine-NMDA receptor interactions in the modulation of glutamate release in the substantia nigra pars reticulata in vivo. Opposite role for D_1 and D_2 receptors.* Journal of Neurochemistry. 83 (2002) 635-644.

[149] P.R. Sanberg, M.D. Bunsey, M. Giordano, A.B. Norman. *The catalepsy test: its ups and downs*. Behavioral Neuroscience. 102 (1988) 748-759.

[150] T. Schallert, M. De Rick, I.Q. Whishaw, V.D. Ramirez, P. Teitelbaum. *Excessive bracing reactions and their control by atropine and L-DOPA in an animal analog of parkinsonism*. Experimental Neurology. 64 (1979) 33-43.

[151] E. Barbu, E. Molnàr, J. Tsibouklis, D.C. Gorecki. *The potential for nanoparticle-based drug delivery to the brain: overcoming the blood–brain barrier*. Expert Opinion on Drug Delivery. 6 (2009) 553-565.

[152] S. Pasha, K. Gupta. *Various drug delivery approaches to the central nervous system*. Expert Opinion on Drug Delivery. 7 (2010) 113-135.

[153] V. Kabanov, E.V. Batrakova. *New technologies for drug delivery across the blood brain barrier*. Current Pharmaceutical Design. 10 (2004) 1355-1363.

[154] K. Andrieux, P. Couvreur. *Polyalkylcyanoacrylate nanoparticles for delivery of drugs across the blood–brain barrier.* Nanomedicine and Nanobiotechnology. 1 (2009) 463-474.

[155] I.P. Kaur, R. Bhandari, S. Bhandari, V. Kakkar*, Potential of solid lipid nanoparticles in brain targeting*. Journal of Controlled Release. 127 (2008) 97-109.

[156] M.D. Joshi, R. H. Müller. *Lipid nanoparticles for parenteral delivery of actives.* European Journal of Pharmaceutics and Biopharmaceutics. 71 (2009) 161-172.

[157] E. Esposito, M. Fantin, M. Marti, M. Drechsler, L. Paccamiccio, P. Mariani, E. Sivieri, F. Lain, E. Menegatti, M. Morari, R. Cortesi. *Solid lipid nanoparticles as delivery systems for Bromocriptine*. Pharmaceutical Research. 25 (2008) 1521-1530.

[158] C. Contado, A. Dalpiaz, E. Leo, M. Zborowski, P. S.Williams. *Complementary use of flow and sedimentation field-flow fractionation techniques for size characterizing biodegradable poly(lactic acid) nanospheres.* Journal of Chromatography A. 1157 (2007) 321–335.

[159] K. Jores, W. Mehnert, M. Drechsler, H. Bunjes, C. Johann, K. Maeder. *Investigations on the structure of solid lipid nanoparticles (SLN) and oil-loaded solid lipid nanoparticles by photon correlation spectroscopy, field-flow fractionation and transmission electron microscopy*. Journal of Controlled Release. 95 (2004) 217-227.

[160] L. de campo, A. Yaghmur, L. Sagalowicz, M.E. Leser, H. Watzke, O. Gattler. *Reversible phase transitions in emulsified nanostructured lipid systems.* Langmuir. 20 (2004) 5254-5261.

[161] J. Gustafsson, H. Ljusberg-Wharen, M. Almgrem, K. Larsson. *Submicron particles of reversed lipid phases in water stabilized by a nonionic amphiphilic polymer*. Langmuir. 13 (1997) 6964-6971.

[162] G. Worle, M. Drechsler , M.H.J. Koch, B. Siekmann, K. Westesen, H. Bunjes. *Influence of composition and preparation parameters on the properties of aqueous monoolein dispersions*. International Journal of Pharmaceutics. 329 (2007) 150–157.

[163] V. Luzzati, H. Delacroix, A. Gulik, T. Gulik-Krzywicki, P. Mariani, R Vargas. *The cubic phases of lipids*. Current Topics in Membranes. 44 (1997) 3-24.

[164] C. Nastruzzi, C. Pastesini, R. Cortesi, E. Esposito, R. Gambari, E. Menegatti. *Kinetic of bromocriptine release from microspheres: comparative analysis between different in vitro models*. Journal of Microencapsulation. 11 (1993) 565-574.

[165] Clogston J, Craciun G., Hart DJ., Caffrey M. *Controlling release from the lipidic cubic phase by selective alkylation.* Journal of Controlled Release. 102 (2005) 441–461.

[166] A. Di Stefano, P. Sozio, A. Iannitelli, L.S. Cerasa. *New drug delivery strategies for improved Parkinson's disease therapy.* Expert Opinion on Drug Delivery. 6 (2009) 389-404.

[167] G. Modi, V. Pillay, Y.E. Choonara, V.M. Ndesendo, L.C. du Toit, D. Naidoo. *Nanotechnological applications for the treatment of neurodegenerative disorders.* Progress in Neurobiology. 88 (2009) 272-285.

[168] J.A. Obeso, F. Grandas, M.T. Herrero, R. Horowski. *The role of pulsatile versus continuous dopamine receptor stimulation for functional recovery in Parkinson's disease*. European Journal of Neuroscience. 6 (1994) 889-897.

[169] Y. Sadzuka, R. Hirama, T. Sonobe. *Effects of intraperitoneal administration of liposomes and methods of preparing liposomes for local therapy*. Toxicology Letters. 126 (2002) 83–90.

[170] J. K. Vasir, M. K. Reddy, V. D. Labhasetwar. *Nanosystems in drug targeting: opportunities and challenges*. Current Nanoscience. 1 (2005) 47-64.

[171] T.M. Allen, C.B. Hansen, L.S.S. Guo. *Subcutaneous administration of liposomes: a comparison with the intravenous and intraperitoneal routes of injection*. Biochimica et Biophysica Acta. 1150 (1993) 9-169

[172] L.H. Reddy, R.K. Sharma, K. Chuttani, A.K. Mishra, R.S.R. Murthy. *Influence of administration route on tumour uptake and biodistribution of etoposide loaded solid lipid nanoparticles in Dalton's lymphoma tumour bearing mice*. Journal of Controlled Release. 105 (2005) 185-198.

[173] L.H. Reddy, R.S.R. Murthy. *Pharmacokinetics and biodistribution studies of doxorubicin loaded poly(butyl cyanoacrilate) nanoparticles synthesized by two different techniques*. Biomedical Papers. 148 (2) (2004) 161-166.

[174] E. Tolosa, M.J. Marti, F. Valldeoriola, J.L. Molinuevo. *History of levodopa and dopamine agonists in Parkinson's disease treatment*. Neurology. 50 (1998) S2– S10.

[175] W.C. Koller. *Neuroprotective therapy for Parkinson's disease*. Experimental Neurology. 144 (1997) 24–28.

[176] A. Di Stefano, P. Sozio, A. Cocco, A. Iannitelli, E. Santucci, M. Costa, L. Pecci, C. Nasuti, F. Cantalamessa, F. Pinnen. *L-Dopa- and Dopamine-(R)-r-Lipoic Acid Conjugates as Multifunctional Codrugs with Antioxidant Properties.* Journal of Medicinal Chemistry. 49 (2006) 1486-1493.

[177] J. Ferrer. *Vaginal candidosis: epidemiological and etiological factors*. International Journal of Gynecology & Obstetrics. 71 (2000) S21-S27.

[178] W. Zhu, S.G. Filler. *Interactions of Candida albicans with epithelial cells.* Cellular Microbiology. 12 (2010) 273-82.

[179] I. Olsen. *Oral adhesion of yeasts.* Acta Odontologica Scandinavica. 48 (1990) 45-53.

[180] E. Esposito, F. Bortolotti, E. Menegatti, R. Cortesi. *Amphiphilic association systems for Amphotericin B delivery.* International Journal of Pharmaceutics. 260 (2003) 249–260.

[181] D.L. Brawner, J.E. Cuttler. *Oral Candida albicans isolates from nonhospitalized normal carriers, immunocompetent hospitalized patients, and immunocompromised patients with or without acquired immunodeficiency syndrome.* Journal of Clinical Microbiology. 27 (1989) 1335-1341.

[182] M. Ramos-e-Silva, C.M. Oliveira Lima, R. Casz Schechtman, B. Moritz Trope, S. Carneiro. *Superficial mycoses in immunodepressed patients (AIDS).* Clinics in Dermatology. 28 (2010) 217-225.

[183] J.H. Rex, T.J. Walsh, J.D. Sobel, S.G. Filler, P.G. Pappas, W.E. Dismukes, J.E. Edwards. Practice Guidelines for the Treatment of Candidiasis. Clinical Infectious Diseases. 30 (2000) 662-678.

[184] G.C. Ceschel, P. Maffei, S. Lombardi Borgia, C. Ronchi, S. Rossi. *Development of a mucoadhesive dosage form for vaginal administration.* Drug Development and Industrial Pharmacy. 27 (2001) 541-547.

[185] E. hardly, A.L. Jiménez, K.S. de Pàdua, L.J.D. Zaneveld. *Women's Preferences for Vaginal antimicrobial Contraceptives III: choise of a formulation, applicator and packaging.* Contraception. 58 (1998) 245-249.

[186] E.B. Souto, R.H. Muller. *Investigation of the factors influencing the incorporation of clotrimazole in SLN and NLC prepared by hot high-pressure homogenization.* Journal of Microencapsulation. 23 (2006) 377-388.

[187] E.B. Souto, R.H. Muller. *Rheological and in vitro release behaviour of clotrimazole-containing aqueous SLN dispersions and commercial creams.* Pharmazie. 62 (2007) 505-509.

[188] G. Wei, H. Xu, P.T. Ding, S.M. Li, J.M. Zheng. *Thermosetting gels with modulated gelation temperature for ophthalmic use: the rheological and gamma scintigraphic studies.* Journal of Controlled Release. 83 (2002) 65-74.

[189] C. Roques, K. Bouchemal, G. Ponchel, Y. Fromes, E. Fattal. *Parameters affecting organization and transfection efficiency of amphiphilic copolymer/DNA carriers. Journal of Controlled Release.* 138 (2009) 71-77.

[190] M. Scherlund, A. Brodin, M. Malmsten. *Micellization and gelation in block copolymer systems containing local anesthetics,* International Journal of Pharmaceutics. 211 (2000) 37-49.

[191] E. Hecht, H. Hoffmann. *Kinetic and Calorimetric Investigations on Micelle Formation of Block Copolymers of the Poloxamer Type.* Colloids and Surfaces A: Physicochemical and Engineering Aspects. 96 (1995) 181-197.

[192] D. Tettenborn. Toxicity of Clotrimazole. Postgraduate Medical Journal. 50 (1) (1974) 17-20.

[193] H. Liu, Y. Li, K. Raisch. Clotrimazole induces a late G1 cell cycle arrest and sensitizes glioblastoma cells to radiation in vitro. Anti-Cancer Drugs. 21 (9) (2010) 841-849.

[194] S. Murgia, A.M. Falchi, M. Mano, S. lampis, R. Angius, A.M. Carnerup, J. Schmidt, G. Diaz, M. Giacca, Y. Talmon, M. Monduzzi. *Nanoparticles from Lipid-Based Liquid Crystals: Emulsifier Influence on Morphology and Cytotoxicity.* The Journal of Physical Chemistry B. 114 (2010) 3518-3525.

[195] A.E. Garcia-Bennett. *Synthesis, toxicology and potential of ordered mesoporous materials in nanomedicine.* Nanomedicine. 6 (2001) 867-877.

[196] I. Haller. *Mode of action of clotrimazole: implications for therapy.* American Journal of Obstetrics and Gynecology. 152 (1985) 939-44.

[197] R. Mahajan. *Bromocriptine mesylate: FDA-approved novel treatment for type-2 diabetes.* Indian Journal of Pharmacology. 41 (2009) 197-198.

Acknowledgements

Dopo una serie di soddisfazioni e sacrifici, eccomi arrivata all'ultima pagina di questa tesi. Posso definire questo percorso una vera esperienza di vita, che mi ha permesso di crescere molto, ampliando non solo le mie conoscenze didattiche ma anche quelle personali.

Vorrei innanzi tutto esprimere la mia più sincera riconoscenza alla mia relatrice, Prof.ssa Rita Cortesi e alla mia correlatrice, Dott.ssa Elisabetta Esposito, per avermi accolto nel loro gruppo di ricerca e per avermi permesso di lavorare in un ambiente diventato per me quasi una "seconda famiglia". Le ringrazio per tutto il sostegno che mi hanno dimostrato fin dall'inizio e per avermi permesso una costante crescita professionale.

Ringrazio inoltre tutto il Dipartimento di Scienze Farmaceutiche dell'Università di Ferrara che mi ha vista "nascere" come tesista e poi come dottoranda e nel quale ho avuto modo di instaurare rapporti lavorativi ed umani importanti per il mio percorso di studi e non solo. Un particolare ringraziamento va al Prof. Enea Menegatti, alla Dott.ssa Gaia Colombo e al Dott. Fabrizio Bortolotti.

Desidero ringraziare tutte quelle persone vecchie e nuove con cui ho iniziato e trascorso il mio dottorato, con cui ho scambiato qualche pensiero, qualche idea, qualche risata. In diversi modi hanno contribuito nel mio percorso formativo, aiutandomi a credere in me stessa, suscitando in me nuovi interessi e soprattutto mi hanno suggerito, direttamente o indirettamente, le modalità per poterli raggiungere.

Non posso non menzionare i sei mesi trascorsi presso l'Université Paris Sud e l'ESPCI-Paris Tech. Ringrazio la Prof.ssa Kawthar Bouchmal e la Prof.ssa Madeleine Djabourov, per avermi accolto nei loro rispettivi gruppi di ricerca e tutti i docenti e i ragazzi con cui ho collaborato, anche in minima parte, durante questa mia esperienza. Difficilmente dimenticherò questi mesi trascorsi a Parigi.

Il mio pensiero, ovviamente, va ai miei genitori: senza il loro aiuto non avrei mai raggiunto questa meta. Sono davvero grata per tutto il sostegno che hanno saputo darmi, ma più di ogni

altra cosa di quell’aiuto tacito o esplicito che è venuto dal loro cuore. Mi auguro che tutti i sacrifici spesi siano in questo modo, almeno in parte, ripagati.

L’ultimo grazie, ma non per importanza, va a Leonardo, per dedicarmi la sua presenza e il suo amore in ogni istante. Grazie per tutte quelle volte che hai creduto in me e mi hai incoraggiata vedendomi presa o sconfortata dal mio lavoro, ma soprattutto per la soddisfazione che sai donarmi anche con un solo sguardo.